TURUN YLIOPISTON JULKAISUJA
ANNALES UNIVERSITATIS TURKUENSIS

SARJA - SER. A I OSA - TOM. 436

ASTRONOMICA - CHEMICA - PHYSICA - MATHEMATICA

FREQUENCY-DOMAIN AND WIDE-PULSE TIME-DOMAIN MEASUREMENTS OF LANTHANIDE LUMINESCENCE AND LANTHANIDE-BASED RESONANCE ENERGY TRANSFER

by

Iko Hyppänen

TURUN YLIOPISTO
UNIVERSITY OF TURKU
Turku 2012

From the Department of Chemistry, University of Turku, Turku, Finland and the Graduate School of Chemical Sensors and Microanalytical Systems

Supervised by

Professor Emeritus Jouko Kankare
Department of Chemistry
University of Turku
Turku, Finland

Professor Tero Soukka
Department of Biochemistry and Food Chemistry / Biotechnology
University of Turku
Turku, Finland

Professor Jukka Lukkari
Department of Chemistry
University of Turku
Turku, Finland

Professor Keijo Haapakka
Department of Chemistry
University of Turku
Turku, Finland

Reviewed by

Professor Pekka Hänninen
Department of Cell Biology and Anatomy, Laboratory of Biophysics
University of Turku
Turku, Finland

Professor Hans Tanke
Department of Molecular Cell Biology
Leiden University Medical Center
Leiden, The Netherlands

Opponent

Professor Michael Schäferling
Institute of Analytical Chemistry, Chemo- and Biosensors
University of Regensburg
Regensburg, Germany

ISBN 978-951-29-4875-8 (PRINT)
ISBN 978-951-29-4876-5 (PDF)
ISSN 0082-7002
Painosalama Oy – Turku, Finland 2012

Preface

This work was carried out in the Laboratory of Materials Chemistry and Chemical Analysis at the University of Turku, during the years 2001–2011. Financial support from the Graduate School of Chemical Sensors and Microanalytical Systems (CHEMSEM), the Finnish Funding Agency for Technology and Innovation (Tekes) and the Academy of Finland is gratefully acknowledged.

I wish to express my sincere gratitude and respect to my supervisors, Professor Emeritus Jouko Kankare and Professor Tero Soukka, for their guidance and encouragement. I am extremely grateful to Professor Kankare for the enormous time and effort he has spent on developing the instrumentation and the fitting software for the frequency-domain luminometer which had an essential role in my study. I owe deep gratitude to Professor Soukka for the opportunity to work in the biotechnological luminescence projects and for providing me with a vast supply of filters and other equipment.

I am deeply grateful to Professor Pekka Hänninen and Professor Hans Tanke and for reviewing my thesis, and for their valuable comments. Many thanks to Professor Tanke for an interesting tour in the laboratory of Molecular Cell Biology at Leiden University Medical Center.

I wish to express my warmest thanks to my co-authors Dr. Terhi Rantanen and Johanna Vuojola from the Department of Biotechnology, and to Laura Pihlgren, Docent Mika Lastusaari and Professor Jorma Hölsä from the Department of Chemistry for their invaluable contribution to the publications.

I also wish to thank the present and former staff and students of the Laboratory of the Materials Chemistry and Chemical Analysis for their assistance and a great working atmosphere. Special thanks are due to Kari Loikas and Mauri Nauma for their invaluable help with the instruments and for all the gadgets of high quality which they built for me.

I am most indebted to my mother Tarja and my sister Tuulia for their encouragement and support. Finally, I wish to express my deepest thanks to my beloved Hanna for her love and support and for the enormous time and effort she spent proof-reading my thesis.

Turku, December 2011

Iko Hyppänen

Table of Contents

List of Original Publications

This thesis is based on the following publications, refered to in the text by their Roman numerals (**I**–**V**).

I Hyppänen, I.; Soukka, T.; Kankare, J., Frequency-domain measurement of luminescent lanthanide chelate, *J. Phys. Chem. A* **2010**, *114*, 7856–7867.

II Vuojola, J.; Hyppänen, I.; Nummela, M.; Kankare, J.; Soukka, T., Distance and temperature dependence in non-overlapping and conventional Förster resonance energy-transfer, *J. Phys. Chem. B* **2011**, *115*, 13685–13694.

III Hyppänen, I.; Hölsä, J.; Kankare, J.; Lastusaari, M.; Malkamäki, M.; Pihlgren, L., The effect of Y^{3+} co-doping on the persistent up-conversion luminescence of the ZrO_2:Yb^{3+},Er^{3+} nanomaterials, *J. Lumin.* **2009**, *129*, 1739–1743.

IV Hyppänen, I.; Hölsä, J.; Kankare, J.; Lastusaari, M.; Pihlgren, L.; Soukka, T., Up-conversion luminescence of the NaRF4–NaR´F4 (R: Y, Yb, Er) core–shell nanomaterials, *J. Fluoresc.* **2011**, *21*, 963–969.

V Riuttamäki, T.; Hyppänen, I.; Kankare, J.; Soukka, T., Decrease in luminescence lifetime indicating non-radiative energy transfer from upconverting particles to fluorescent acceptors in aqueous suspensions, *J. Phys. Chem. C* **2011**, *115*, 17736–17742.

Abbreviations

A	Acceptor / activator
A/D	Analog-to-digital
AF	Alexa Fluor
APTE	Addition de Photons par Transfers d'Energie
BPE	B-phycoerythrin
BSA	Bovine serum albumin
CR	Cross-relaxation
CTS	Charge-transfer state
D	Donor
DC	Direct current
DNA	Deoxyribonucleic acid
ESA	Excited state absorption
ETU	Energy transfer up-conversion
Ex1 / Ex2	Excited energy levels of lanthanide ion
FD	Frequency-domain
FRET	Fluorescence resonance energy transfer
FWHM	Full width at half maximum
GFP	Green fluorescent protein
GPIB	General purpose interface bus
GSA	Ground state absorption
GTP	Guanosine triphosphate
H	Host lattice ion
HPLC	High-performance liquid chromatography
IR	Infrared
IC_{50}	half maximal inhibitory concentration
K–K	Kramers–Kronig
LED	Light-emitting diode
Ln	Lanthanide
LRET	Lanthanide-based resonance energy transfer
NIR	Near-infrared
OLED	Organic light-emitting diode
PAH	Poly(allylamine hydrochloride)
PMT	Photomultiplier tube
RET	Resonance energy transfer
S	Sensitizer ion
S.H.G.	Second harmonic generation
S_0	Ground singlet state
S_1	Excited singlet state
SPT	Single-photon timing
T_1	Lowest triplet state
TCSPC	Time-correlated single-photon counting technique
TD	Time-domain
TPA	Two-photon absorption excitation
TRITC	Tetramethylrhodamine isothiocyanate
UCP	Up-converting phosphor
USB	Universal serial bus
UV	Ultraviolet
YFP	Yellow fluorescent protein

Mathematical Symbols

α	Pre-exponential factor in a multiexponential intensity decay
χ^2	Sum of squared deviations
χ_R^2	Reduced chi-squared
ε_A	Molar absorption coefficient of the acceptor
ε_D	Molar absorption coefficient of the donor
κ^2	Orientation factor
λ	Wavelength
λ_A^{em}	Wavelength of acceptor emission
θ	Phase shift
ρ	Relative sum of amplitude factors
τ	Lifetime
τ_{AD}	Sensitized acceptor emission lifetime
τ_D	Donor lifetime
τ_{DA}	Donor lifetime in the presence of the acceptor
τ_{H2O}	Lanthanide chelate lifetime in H_2O
τ_{D2O}	Lanthanide chelate lifetime in D_2O
τ_Φ	Lifetime calculated from the phase shift
τ_M	Lifetime calculated from the modulation ratio
τ_{obs}	Observed lifetime
τ_{rad}	Radiative or natural lifetime
τ_R	Luminescence rise time
A_k	Relative amplitude of frequency-domain component
E	Energy transfer efficiency
E_a	Activation energy
ΔE	Energy difference
f_A	Fraction of the acceptor labelling
f_D	Fraction of the donor labelling
$F_D(\lambda)$	Luminescence intensity of the donor
h_k	Amplitude factor of the frequency-domain signal
I	Luminescence intensity
I_A	Acceptor emission intensity (direct excitation)
I_{AD}	Sensitized acceptor emission intensity
I_D	Donor emission intensity (in the absence of the acceptor)
I_{DA}	Donor emission intensity in the presence of the acceptor
I_{Em}	Emission intensity
I_{Ex}	Excitation intensity
$J(\lambda)$	Overlap integral
$k(T)$	Rate constant of the thermal back-transfer
k_B	Boltzmann constant
k_{ET}	Rate of resonance energy transfer
k_{nr}	Sum of non-radiative rates (excluding k_{ET})
k_{rad}	Radiative decay rate
M	Modulation ratio
n	Refractive index of the medium
$q(H_2O)$	Number of the water molecules on the first coordination sphere of the Ln(III) ion
Q_A	Quantum yield of the acceptor
Q_D	Quantum yield of the donor (in the absence of the acceptor)
Q_{DA}	Quantum yield of the donor in the presence of the acceptor
Q_{et}	Efficiency of the energy transfer between the ligand triplet state and the lanthanide ion
Q_{isc}	Efficiency of the inter-system crossing
Q_{Ln}	Efficiency of the lanthanide luminescence
$Q_{overall}$	Overall quantum yield of the lanthanide chelate

$Q_{transfer}$	Energy transfer efficiency between the antenna and the lanthanide ion
r	Donor–acceptor distance
R_0	Förster distance
S_x	In-phase component of the frequency-domain signal
S_y	Out-of-phase component of the frequency-domain signal
T	Temperature
V_{sig}	Amplitude of the frequency-domain signal

Abstract

Resonance energy transfer (RET) is a non-radiative transfer of the excitation energy from the initially excited luminescent donor to an acceptor. The requirements for the resonance energy transfer are: i) the spectral overlap between the donor emission spectrum and the acceptor absorption spectrum, ii) the close proximity of the donor and the acceptor, and iii) the suitable relative orientations of the donor emission and the acceptor absorption transition dipoles. As a result of the RET process the donor luminescence intensity and the donor lifetime are decreased. If the acceptor is luminescent, a sensitized acceptor emission appears. The rate of RET depends strongly on the donor–acceptor distance (r) and is inversely proportional to r^6. The distance dependence of RET is utilized in binding assays. The proximity requirement and the selective detection of the RET-modified emission signal allow homogeneous separation free assays. The term lanthanide-based RET is used when luminescent lanthanide compounds are used as donors. The long luminescence lifetimes, the large Stokes' shifts and the intense, sharply-spiked emission spectra of the lanthanide donors offer advantages over the conventional organic donor molecules. Both the organic lanthanide chelates and the inorganic up-converting phosphor (UCP) particles have been used as donor labels in the RET based binding assays.

In the present work lanthanide luminescence and lanthanide-based resonance energy transfer phenomena were studied. Luminescence lifetime measurements had an essential role in the research. Modular frequency-domain and time-domain luminometers were assembled and used successfully in the lifetime measurements. The frequency-domain luminometer operated in the low frequency domain (≤ 100 kHz) and utilized a novel dual-phase lock-in detection of the luminescence. One of the studied phenomena was the recently discovered non-overlapping fluorescence resonance energy transfer (nFRET). The studied properties were the distance and temperature dependences of nFRET. The distance dependence was found to deviate from the Förster theory and a clear temperature dependence was observed whereas conventional RET was completely independent of the temperature. Based on the experimental results two thermally activated mechanisms were proposed for the nFRET process. The work with the UCP particles involved the measurement of the luminescence properties of the UCP particles synthesized in our laboratory. The goal of the UCP particle research is to develop UCP donor labels for binding assays. In the present work the effect of the dopant concentrations and the core–shell structure on the total up-conversion luminescence intensity, the red–green emission ratio, and the luminescence lifetime was studied. Also the non-radiative nature of the energy transfer from the UCP particle donors to organic acceptors was demonstrated for the first time in aqueous environment and with a controlled donor–acceptor distance.

Keywords: luminescence, resonance energy transfer, lanthanides, up-conversion, luminescence lifetime, frequency-domain, time-domain, non-overlapping fluorescence resonance energy transfer.

1 Literature Review

1.1 General Background

Lanthanide compounds are known for their unique luminescence properties which include long lifetimes, large Stokes' shifts and sharp emission profiles. Lone lanthanide ions in solutions have a very weak absorbance and a high probability of quenching. Hence, lanthanide ions are commonly used as luminescence centres in organic chelates or inorganic crystals.[1,2] Luminescence applications of the lanthanides are versatile and are found both in everyday life and in scientific field. Applications include fluorescent lamps, cathode-ray and plasma display panels and light-emitting diodes (LEDs),[3–6] fibre amplifiers[7,8] and organic LEDs (OLEDs).[9] Up-converting lanthanide doped phosphors have been utilized in solid state lasers,[10,11] in security documents (copy protecting or authenticity checking),[12–14] and as an active coating on solar cells.[15] A vast application field of the lanthanide compounds is comprised of bioanalytical assays in which lanthanide compounds offer an alternative for radioisotopic labels.[16–19] In heterogeneous assay formats the long luminescence lifetimes of the lanthanides are utilized by time-resolved luminescence detection techniques. Separation free homogeneous assays can be realized by lanthanide-based resonance energy transfer.[20,21] The most utilized lanthanide chelates in assay applications are chelates of Eu(III), Tb(III), Sm(III) and Dy(III) ions due to their high luminescence intensity. However, there is a rising interest towards chelates of Yb(III) and Nd(III) which have their emission at the near-infrared (NIR) region.[22,23] These chelates widen the spectral range of lanthanide labels and increase the possibilities for the simultaneous multiple label analysis. They can be excited by visible radiation which is less harmful for biological material than ultraviolet radiation needed for the excitation of the Eu(III) and Tb(III) chelates. Also, the scattering of the emission at NIR wavelengths is lower than at visible wavelengths. Another new arrival in the field of the lanthanide chelate labels is the non-overlapping FRET phenomenon which offers a high signal-to-background ratio due to an anti-Stokes energy transfer.[24–26] In addition to the lanthanide chelates also up-converting inorganic phosphors doped with optically active lanthanide ions have been used as labels in binding assays.[27–29] The near-infrared excitation and the anti-stokes detection result in a total elimination of the background due to autofluorescence and direct excitation of the acceptors. The emphasis of this thesis is on the study of the luminescence properties of the lanthanide compounds related to their use as the donor labels in homogeneous binding assays and the use of the frequency-domain technique on determining the lifetimes of the lanthanide compounds.

1.2 Transitions in Lanthanide(III) Ions

The lanthanides comprise of fifteen elements with atomic numbers 57 through 71, from lanthanum to lutetium.[30] The lanthanides are f-block elements meaning they have electrons in the f-orbitals, more precisely electrons in the 4f orbitals. The generally accepted electronic configurations of the lanthanide atoms and the trivalent lanthanide ions are presented in Table 1. The presented oxidation

state of +3 is the most common for the lanthanides and is found in both the organic chelates and the solid crystals. Lanthanum does not have 4f electrons and was not originally included in the lanthanide group. However, lanthanum is often included in the discussions of the lanthanide chemistry and is now officially accepted as one of the lanthanides. The lanthanides together with scandium and yttrium are called the rare earth metals.

Table 1. Electronic configurations of lanthanide atoms and trivalent ions.[a]

Atomic number	Name	Symbol	Atom	Ln(III)
57	Lanthanum	La	$5d^1 6s^2$	$4f^0$
58	Cerium	Ce	$4f^1 5d^1 6s^2$	$4f^1$
59	Praseodymium	Pr	$4f^3 6s^2$	$4f^2$
60	Neodymium	Nd	$4f^4 6s^2$	$4f^3$
61	Promethium	Pm	$4f^5 6s^2$	$4f^4$
62	Samarium	Sm	$4f^6 6s^2$	$4f^5$
63	Europium	Eu	$4f^7 6s^2$	$4f^6$
64	Gadolinium	Gd	$4f^7 5d^1 6s^2$	$4f^7$
65	Terbium	Tb	$4f^9 6s^2$	$4f^8$
66	Dysprosium	Dy	$4f^{10} 5d^1 6s^2$	$4f^9$
67	Holmium	Ho	$4f^{11} 6s^2$	$4f^{10}$
68	Erbium	Er	$4f^{12} 6s^2$	$4f^{11}$
69	Thulium	Tm	$4f^{13} 6s^2$	$4f^{12}$
70	Ytterbium	Yb	$4f^{14} 6s^2$	$4f^{13}$
71	Lutetium	Lu	$4f^{14} 5d^1 6s^2$	$4f^{14}$

[a] Only electrons outside the [Xe] shell ($1s^2 2s^2 2p^6 3s^2 3p^6 3d^{10} 4s^2 4p^6 4d^{10} 5s^2 5p^6$) are given.

Lanthanum has an empty and lutetium a full 4f orbital. They do not show absorption bands at wavelengths above 200 nm.[31] The other trivalent lanthanide ions have incompletely filled 4f orbitals (Table 1) and they absorb at wavelengths from near-UV to near-IR. The lanthanides experience three different kinds of absorption bands: the charge transfer transitions between the ion and the ligand, the 4f→5d transitions and the 4f→4f transitions.[32] The first two are broad and strong absorptions in UV region. The charge transfer transitions occur with the lanthanide ions which are easily reduced (Eu(III), Yb(III), Sm(III), Ce(IV), Tb(IV), Pr(IV)) when they are bound to easily oxidized ligands.[2] The spectral position of the charge transfer bands depends on the ligand and the lanthanide ion. The excited charge transfer states may have a resonance with the 4f levels and can feed the 4f emission.[4,5,33] The 4f→5d absorptions are observed for the ions which are easily oxidized (Ce(III), Tb(III), Pr(III), Eu(II), Yb(II), Sm(II)).[2] After the 4f→5d excitation the radiative return to the ground state can occur either by the 5d→4f or 4f→4f transitions.[34,35] The former case results in a broad emission band (due to the splitting of the 5d level) and the peak position is sensitive to the surroundings of the lanthanide ion. In the latter case the characteristic line emission of the corresponding lanthanide ion is observed.

The most interesting transitions of the lanthanides are the intra-configurational 4f→4f electric dipole and magnetic dipole transitions. The characteristic luminescence features of the lanthanides (the line-like emission bands and the long lifetimes) arise especially from the properties of these transitions. The 4f electrons are shielded by the electrons in the 5s and 5p shells which are lower in

energy but spatially located outside the 4f orbital.[36] Therefore, the chemical environment of the lanthanide ions has little effect on the electronic energy levels of the lanthanide $4f^N$ configuration. The splitting of the 4f energy levels by ligand or crystal fields is small, only about 200–300 cm^{-1}.[37] Due to the aforementioned properties, the absorption and emission lines of the 4f→4f transitions are sharp and their spectral positions remain virtually unchanged for a given ion in different compounds and environments. In principle, the intra-4f electric-dipole transitions are parity forbidden. Due to their forbidden nature the probability of the 4f→4f transitions is low. The low probability is observed as the long lifetimes of the lanthanide compounds. The parity selection rule can be partly relaxed by mixing the 4f states with the 5d states which have an opposite parity. This kind of mixing can be induced by the ligand or crystal fields of uneven symmetry.[38] Hence, the lanthanide ions are commonly chelated with organic ligands or doped into inorganic crystals. Energy levels of several lanthanides are presented in Figure 1.

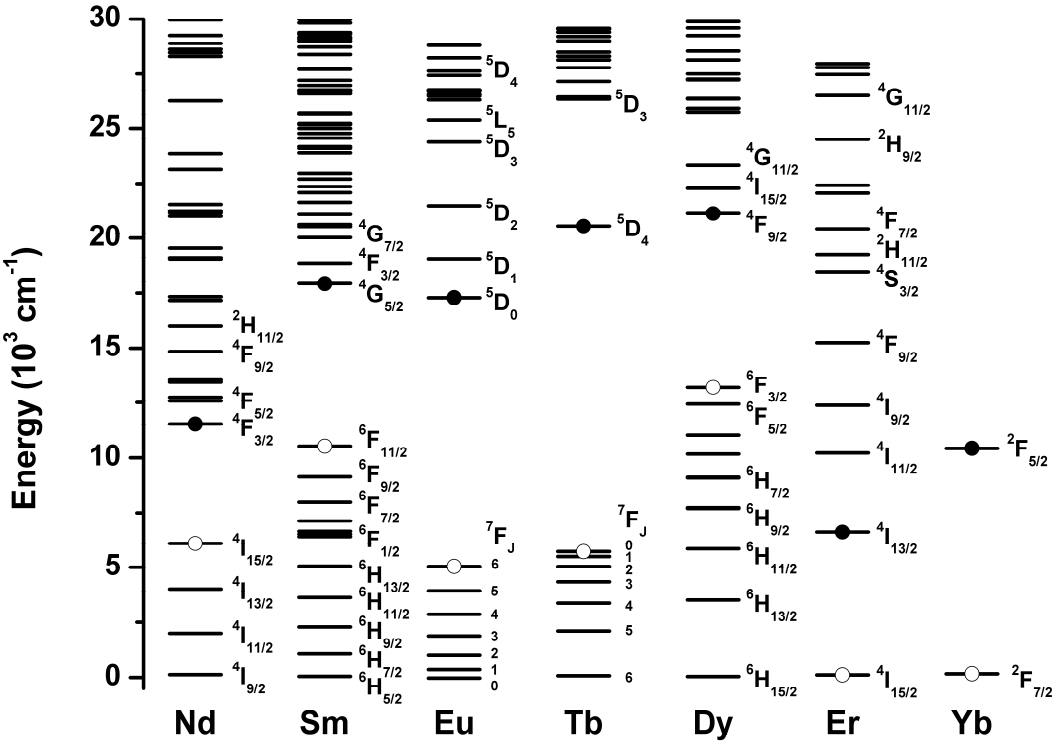

Figure 1. An energy levels scheme of several lanthanide(III) ions. Only levels below 30 000 cm^{-1} are shown. The commonly observed luminescence levels and the next lower-lying levels are marked with filled and open circles, respectively.[37,39–41]

1.3 Lanthanide Chelates

The lanthanide(III) ions in solutions have very low absorption cross sections ($\varepsilon < 10$ $M^{-1}cm^{-1}$).[31] Hence, a high intensity excitation source is needed to produce a sufficient excited-state population for luminescence measurements.[42,43] However, the low absorbance can be circumvented by chelating the lanthanide ions with organic ligands which have a chromophore moiety (Figure 2). The chromophore moiety is commonly called an antenna or a sensitizer.[20] The excitation light is efficiently harvested by the antenna and an excitation source with a considerably lower photon flux is adequate than with free lanthanide(III) ions. After the absorption by the chromophore moiety, the excitation energy is transferred to the lanthanide ion and de-excitation occurs through the characteristic lanthanide emission. Chromophores usually include aromatic groups such as pyridine, bipyridine, terpyridine or quinoline rings substituted with groups containing phenyl groups or five-membered heteroatomic rings.[1,44,45] The nitrogen and oxygen heteroatoms of these chromophores usually serve also as chelating atoms. Hence, the distance between the chromophore and the lanthanide ion is short and the distance dependent energy transfer efficient.[44] Another approach is to separate the chelate and chromophore parts, in which case the chelating and energy-absorbing properties of the ligand can be separately optimized but the distance between the chromophore and the lanthanide ion remains longer. An example of this kind of structure is a 7-amino-4-methyl-2(1H)-quinolinone chromophore coupled to polyaminocarboxylate-based ligands.[46] The symmetry of the ligand affects the strength and the lifetimes of the 4f→4f transitions.[46] The solubility of the chelates in water or in organic solvents have been improved by adding carboxyl and carbohydrate groups or *tert*-butyl groups on the ligand structure, respectively.[1,45]

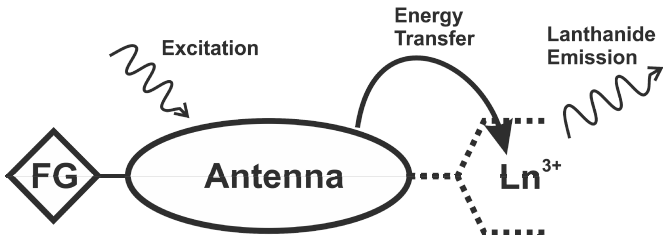

Figure 2. A schematic presentation of lanthanide chelate. The fork in dotted lines represents the ligand part, the ellipse the antenna moiety and the FG-diamond the functional group intended for binding.

The excitation of the lanthanide(III) ions through the intramolecular energy transfer from an organic ligand was first demonstrated by Weissman in 1942.[47] He observed the characteristic Eu(III) line emission when a chelate was irritated with a light absorbed only by the organic ligand. Three mechanisms have been proposed for the intramolecular energy transfer between the organic ligand and the lanthanide(III) ion (Figure 3).[48]

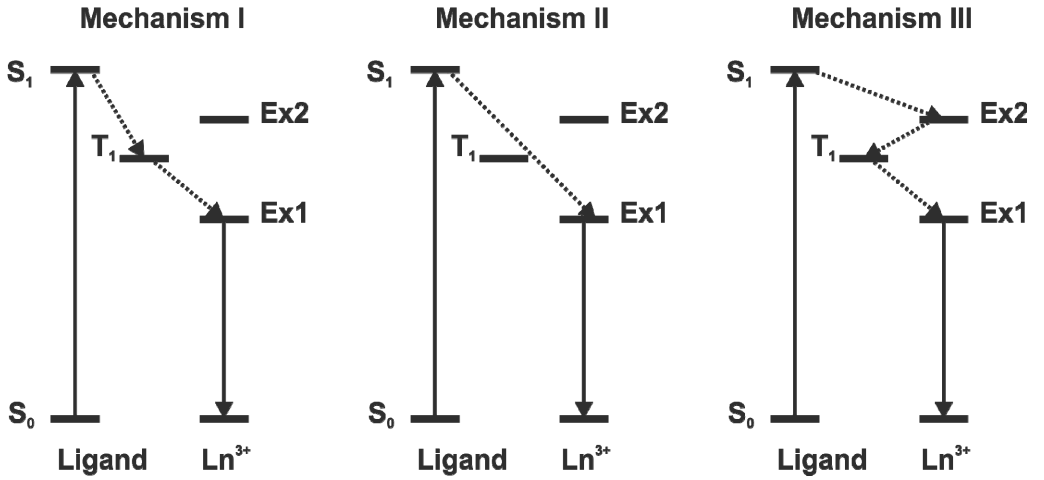

Figure 3. Intramolecular energy transfer mechanisms for lanthanide chelates. S_0 and S_1 are the ground and exited ligand singlet states, respectively. T_1 is the ligand triplet state and Ex1 and Ex2 are the excited energy levels of the Ln(III) ion. Adapted from reference [48].

In all mechanisms the first phase is the absorption of the excitation radiation by the ligand singlet transition ($S_0 \rightarrow S_1$) and the final phase is the lanthanide emission (4f→4f). In *mechanism I* there is an intersystem crossing from the excited ligand singlet state (S_1) to the ligand triplet state (T_1) followed by the energy transfer from T_1 to a lower energy level (Ex1) of the lanthanide(III) ion.[49,50] In *mechanism II* the energy transfer occurs directly from the ligand S_1 state to a lower energy level (Ex1) of the lanthanide(III) ion.[51] In *mechanism III* there is an energy transfer from the ligand S_1 state to an upper intermediate level (Ex2) of the lanthanide(III) ion, back to the ligand (T_1) and finally to a lower energy level (Ex1) of the lanthanide(III) ion.[52] The majority of the experimental results obtained by many research groups support *mechanism I*. The main evidence is the absence of the emission from the lanthanide ion levels above the T_1 level of the ligand.[53–56] Another result on behalf of *mechanism I* and against *mechanism II* is the decrease of the emission originating from the $^5D_1$ and $^5D_0$ levels of the Eu(III) ion in the presence of the triplet quenchers which are not able to quench the ligand singlet states.[52,57] Also the appearance of the europium emission after the excitation of the ligand triplet state of the europium chelate through a triplet–triplet energy transfer from a lanthanum chelate supports the intramolecular energy transfer via the ligand triplet state.[58] Kleinerman who proposed *mechanism II* has pointed out that the absence of the emission from the lanthanide ion energy levels above the ligand T_1 level can also be explained by the ligand T_1 levels quenching the lanthanide ion energy levels above it.[59] Kleinerman also presented experimental evidence in favour of *mechanism II*.[51] Firstly, the terbium $^5D_4$ emission was observed with three Tb(III) complexes in which the ligand T_1 levels lie below the $^5D_4$ level. Secondly, a lower relative quantum yield of the ligand fluorescence ($S_1 \rightarrow S_0$) was observed when ligands were chelated with lanthanide ions which have energy levels adjacent to the ligand S_1 levels, compared to lanthanide ions which have energy levels only above the ligand S_1 levels. In a recent publication Zhang and Li

presented Eu(III) chelates with unusually short lifetimes and explained the result by *mechanism II*.[60] Hayes and Drickamer have shown that under the proper conditions the triplet state can act as an intermediate level for the relaxation between the lanthanide ion levels like in *mechanism III*.[56] Overall, in the light of the experimental results *mechanism I* seems to be prevailing. But there are some results which support the other two mechanisms so they cannot be completely ignored. In the following discussion *mechanism I* is assumed.

The intramolecular energy transfer via the ligand T_1 level in the lanthanide chelates is generally considered to take place by means of the Dexter exchange mechanism.[51,54,61–64] The effect of the ligand triplet state energy on the efficiency of the intramolecular energy transfer has been studied intensively. The majority of the research has been done with the Eu(III) and Tb(III) chelates. The lanthanide emission is obtained only from the energy levels below the ligand triplet state.[50,53] Emission from both the $^5D_1$ and $^5D_0$ levels of the Eu(III) ion has been observed if the ligand triplet state lies above the $^5D_1$ level. Moreover, the $^5D_0$ state is populated by both the fast direct energy transfer to $^5D_0$ (< 50 ns) and the slower internal conversion via $^5D_1$ (≈ 2 μs).[55] The thermal quenching of the lanthanide luminescence by the back-transfer to the ligand triplet state can occur if the energy difference between the lanthanide ion energy level and the ligand triplet state is small.[54,65–67] The equation for the back-transfer probability contains the term $\exp(-\Delta E/k_B T)$, where ΔE is the energy difference between the involved states, k_B is the Boltzmann constant and T is the temperature. The smaller the energy difference ΔE is the more efficient is the thermally induced quenching.[54] However, an excessively large ΔE decreases the transfer probability from the ligand T_1 level to the lanthanide ion. Hence, there exists an optimal energy of the ligand triplet state relative to the lanthanide ion energy levels considering the efficiency of the sensitized lanthanide luminescence.[54,56] The position of the ligand T_1 energy level can be tuned to match the lanthanide energy levels by modifying the chromophore with electron-poor or electron-rich substituents.[68]

The lanthanide ions can be classified into three groups on the basis of the lanthanide luminescence intensity of respective chelates.[48,69,70] The first group consists of the La(III), Lu(III) and Gd(III) ions. The chelates of these ions seldom show lanthanide ion luminescence. Lanthanum has an empty and lutetium a full 4f shell (Table 1). Hence, there are no 4f→4f transitions to receive the energy from the ligand triplet state. Gadolinium has an incompletely filled 4f shell. However, the energy of the lowest excited level of Gd(III) is higher (32 200 cm^{-1})[71] than the energy of the triplet states of typical ligands. As a result, chelates of these ions show no characteristic line emission of lanthanides but strong molecular fluorescence and phosphorescence of the organic ligand. The second group includes the Pr(III), Nd(III), Ho(III), Er(III), Tm(III) and Yb(III) ions. Both the molecular luminescence and the lanthanide line emission of the chelates in this group have low intensity. The low molecular luminescence intensity indicates an efficient energy transfer to the lanthanide ions. The weak lanthanide luminescence is explained by a high probability of the non-radiative de-excitation due to the closely separated energy levels of the lanthanide ions. The Sm(III), Eu(III), Tb(III) and Dy(III) ions of the third group exhibit intense lanthanide

luminescence. The intense luminescence is due to two factors. Firstly, the excited energy levels of the ions are located suitably in relation to the triplet states of the ligands. Thus, the intramolecular energy transfer is efficient. Secondly, the energy gaps between the excited and ground states are relatively large, hence the non-radiative de-excitation probabilities are low. Due to their intense lanthanide luminescence, the ions in the third group (especially Eu(III) and Tb(III)) have been most widely studied. They emit at the visible wavelengths and have been used in many applications especially as luminescent probes in time-resolved binding assays.[16,18] However, the grouping is by no means absolute and the chelates of Nd(III), Er(III) and Yb(III) started to gather interest in the late 1990s.[22,72,73] The interest stems from the potential applications in fluoroimmunoassays and in optical telecommunications utilizing their emission at NIR wavelength region.[7,23]

In addition to the low absorbance, free lanthanide ions have another weakness. Their luminescence is efficiently quenched by solvent X–H oscillators such as O–H, C–H and N–H. The quenching mechanism is a transfer of the electronic excitation energy of the lanthanide ion to high frequency X–H vibrations which are excited to high vibrational states.[74,75] Especially the OH group is an efficient quencher. The efficiency of the quenching depends on three factors. Firstly, each X–H acts independently and the quenching efficiency is directly proportional to the number of the X–H oscillators in the first coordination sphere of the Ln(III) ion.[75–77] Secondly, the quenching efficiency is inversely proportional to the size of the energy gap between the emissive level and the highest vibrational level of the ground state of the lanthanide ion. The number of the vibrational quanta needed for quenching is increased as the size of the energy gap increases.[74,75,78] The quenching probability is reduced by approximately two orders of magnitude with an additional vibrational quantum needed.[78] The third factor is the oscillation energy of the quenching vibration. With large oscillation energy fewer vibrational quanta are needed to fill the energy gap. The effect of the second factor is seen in more efficient quenching of Eu(III) compared to Tb(III) in water solution.[75] The energy gaps for Eu(III) and Tb(III) are about 12200 cm^{-1} and 14800 cm^{-1}, respectively (Figure 1). The gap between the Gd(III) levels is over 32000 cm^{-1} and the quenching due to the O–H vibrations is negligible. The energy of the O–H vibration is 3600 cm^{-1} while energy of the O–D vibration is 2700 cm^{-1}. Twenty times greater intensity and lifetime values have been measured for Eu(III) in D_2O compared to Eu(III) in H_2O.[75] In lanthanide chelates water molecules are displaced from the first coordination sphere of the lanthanide ion by the chelating groups of the ligand. Hence, the quenching efficiency in aqueous solutions is decreased. The number of the replaced water molecules depends on the denticity of the ligand.[43,79] Also the high frequency vibrations of the C–H and N–H groups in the ligands themselves quench the lanthanide luminescence but less efficiently compared to the O–H vibrations of water.[45,80–83] However, the effect of the C–H and N–H vibrations of the ligands or the solvent molecules may be important in the case of lanthanide ions with a relatively small energy gaps like Nd(III), Er(III) and Yb(III) ions (Figure 1, p. 12).[22,84,85] An equation for calculating the number of the water molecules coordinated to the lanthanide ion ($q(H_2O)$) has been published by Horrocks and Sudnick.[43,86] The method is based on measuring the lifetimes of the lanthanide chelate in H_2O and D_2O, τ_{H2O} and τ_{D2O}

respectively. The equation was later refined by the same authors to include the quenching by the X–H oscillators on the ligands and by the water molecules in the second coordinating sphere (Eq. 1 and 2).[87]

$$q(H_2O) = A(\tau_{H_2O}^{-1} - \tau_{D_2O}^{-1} - k_{XH}) \quad (1)$$

$$k_{XH} = \alpha + \beta n_{OH} + \gamma n_{NH} + \delta n_{O=CNH} \quad (2)$$

Here α is the quenching by the second coordination sphere water molecules, n_{OH}, n_{NH} and $n_{O=CNH}$ are the numbers of alcoholic O–H, amine N–H and amide N–H oscillators in the first coordination sphere of the lanthanide ion, A, β, γ, and δ are constants for a given lanthanide ion. For Eu(III) value of A is 1.11, α is 0.31, β is 0.44, γ is 0.99 and δ is 0.075, when lifetimes are given in milliseconds.

In addition to the improved absorbance and the shielding from the solvent quenchers, organic ligands offer still another benefit. Ligands can be equipped with a functional groups which enable binding to biochemical and biological samples and hence utilization of the chelates as labels in bioassays. Functional groups that have been exploited include isothiocyanato, dichlorotriazinyl, iodoacetamido and chlorosulfonyl groups.[79,88–90] The 'ligand' can also be an ion binding site in a macromolecule itself usually with a tryptophan moiety as an antenna moiety.[91] Besides the free chelates in solutions also β-diketone chelates of Eu(III) entrapped inside polystyrene nanoparticles have been used in heterogeneous[92–98] and homogeneous[99,100] immunoassays. The excitation and emission spectra of the free europium chelate and the chelates trapped inside nanoparticles have only insignificant differences. Also, both chelate solutions have the same lifetime (ca. 720 μs).[93] Commercial fluorescent nanoparticles are available in different sizes. The number of the chelated europium(III) ions inside a single 107, 210 or 408 nm diameter particle has been determined to be about 30 000, 250 000 and 2 000 000, respectively.[93] The combination of the high number of the chelates and the lack of the inner-filter effect of the lanthanide luminescence results in a high specific activity of the labels.[88,92,93] The polystyrene shell also creates a hydrophobic environment for the chelates, thus decreasing the quenching by the water molecules and stabilizing the kinetically weak complexes.[93,95] The carboxylic groups on the surface of the particles enable binding to biomolecules. A disadvantage of the particulate labels is the steric hindrance due to the large size.[95] In immunoassay applications utilizing the particulate label, the detection limit is set by the non-specific binding rather than the specific-activity of the label.[96] Hence, smaller nanoparticles could offer advantages without a decrease in detection limit. However, the decrease of the particle size has also disadvantages like increased aggregation. Also, the smaller the particles are the harder it is to sediment them by centrifuging, which is commonly used technique during surface modification of the particles.

1.4 Solid State Luminescence Materials

Solid state luminescent material is often called phosphor. In other words phosphors are solid, inorganic crystalline materials which show luminescence upon excitation. Phosphors consist of a host lattice, activator ions and sensitizer ions.[2] The host lattice is a matrix which holds the optically active sensitizer and activator ions. The host lattice itself does not actively participate in luminescence. The excitation radiation is absorbed by the sensitizer. The excited sensitizer transfers the energy to the activator which is responsible for the luminescence emission. Hence, in analogy to organic lanthanide chelates the host lattice is the chelating part of the ligand, the sensitizer ion is the antenna part of the ligand and the activator ion is the lanthanide ion. A schematic presentation of a phosphor is shown in Figure 4. Sometimes there is no sensitizer ion and the host lattice (e.g., YVO_4:Eu(III))[101] or the activator (e.g., Y_2O_3:Eu(III))[102] are responsible for the absorption of the excitation radiation. The concentrations of the activator and sensitizer ions vary and they can be less than 1 mol-%. Too low a concentration results in a poor absorption whereas too high a concentration can lead to self- quenching. Typically, experimental work must be carried out for finding out best dopant concentrations.[103,104]

The lanthanide ions can be used as sensitizer and activator ions. Applications of lanthanide doped phosphors include fluorescent lamps, cathode-ray and plasma display panels and LEDs.[4,5,6] Depending on the host matrix and the lanthanide ions, the excitation and emission transitions of lanthanides can be due to 4f–4f, 5d–4f, or charge transfer transitions.[4] In the case of the transitions within the 4f levels of the lanthanide ions, the choice of the host matrix is crucial. The lanthanide ions should be situated in a crystallographic site without a centre of symmetry for the electronic dipole transitions to be possible.[38] If the lanthanide ion occupies a lattice-site with a centre of symmetry, only magnetic dipole transitions are allowed.

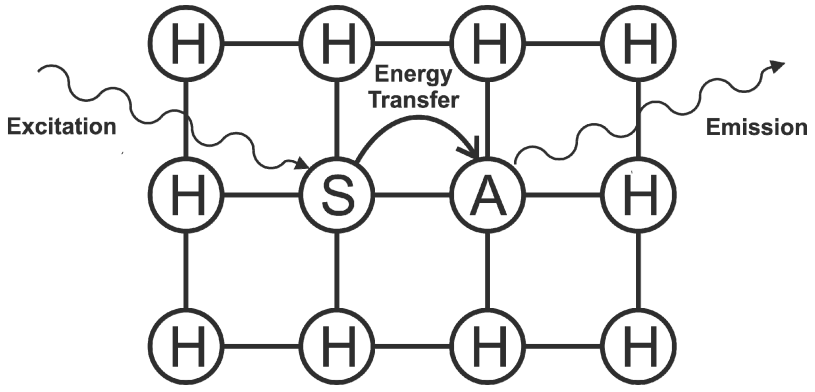

Figure 4. A schematic presentation of the luminescence process in a solid state luminescent material. (H) is a host lattice ion, (S) is a sensitizer ion and (A) is an activator ion. Based on figure by DeLuca.[105]

1.5 Up-Conversion Luminescence

The conventional luminescence is a down-conversion process meaning that the emission wavelength is longer and the respective energy lower compared to the excitation radiation.[106] In the down-conversion process the initial absorption raises the luminescent species into an excited level with energy comparable to the absorbed energy. The energy is then lost in internal conversion, intersystem crossing or energy transfer before the final radiative energy level is reached. Hence, the available emission energy is smaller than the absorbed energy. In the up-conversion luminescence the absorption of a low energy radiation results in the emission of a higher energy photon.[107,108] The up-conversion luminescence is an anti-Stokes process where the emission occurs at a shorter wavelength compared to the excitation radiation. The up-conversion is accomplished by a summation of the energies of two or more low energy photons for the emission of one high energy photon. Due to the unequal number of excitation and emission photons up-conversion is a non-linear process. The emission intensity (I_{Em}) is proportional to a power n of the excitation intensity (I_{Ex}), where n is the number of the summed excitation photons.[109]

$$I_{Em} \propto I_{Ex}^{n} \qquad (3)$$

Because of the non-linearity, the efficiency of the up-conversion process depends linearly on the excitation intensity. For the comparison of the efficiencies they must be normalized for the incident flux and given in $(cm^2W^{-1})^{n-1}$ units for n-photon process.[107] There are several different up-conversion mechanisms.[107,110] A schematic presentation of the mechanisms for two-photon processes is presented in Figure 5. Also examples of up-converting materials are given. The mechanisms for n-photon systems are similar but the number of the subsequent or simultaneous processes is increased. The excitation can also involve two different wavelengths in which case the energy of the successive steps is different.[111]

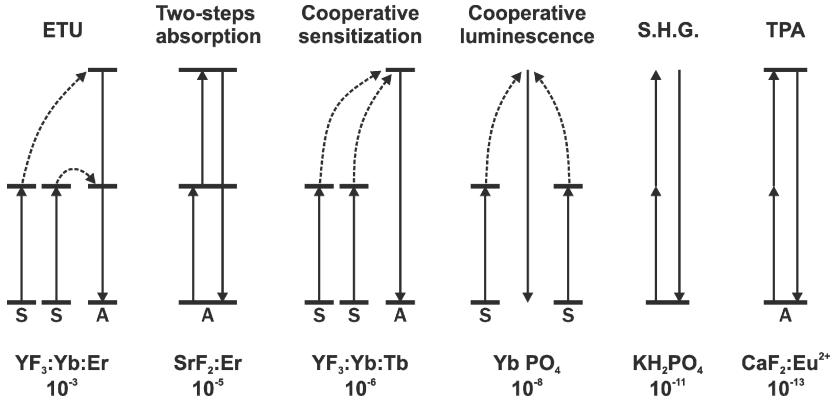

Figure 5. A schematic presentation of the up-conversion mechanisms, examples of the materials and their typical relative efficiencies (cm^2W^{-1}). The efficiencies are normalized for the incident flux. ETU energy transfer up-conversion, S.H.G. second harmonic generation, TPA two-photon absorption excitation. S and A stand for a sensitizer and activator ions, respectively. Based on a figure by Auzel.[110]

The simplest of the up-conversion mechanisms is the *two-steps absorption*, in which a single ion absorbs two sequential photons. The first absorption excites the ion from the ground state into an intermediate energy level (GSA, *ground state absorption*). The second absorption is by the ion in this intermediate state and is termed *excited state absorption* (ESA). The excitation intensity must be high enough for the second absorption to happen within the lifetime of the intermediate excited state. Since the two-steps absorption involves only a single ion, it can occur in materials with low doping levels. The excited state absorption was first proposed in 1959 by Bloembergen for rare earth and other transition ions doped as impurities in host lattices.[112] Bloembergen suggested that ESA could be used in IR quantum counting. The photon avalanche effect is a complex case of ESA.[107,113] In the photon avalanche effect the intermediate energy level is populated by a cross-relaxation process. The build-up of the population leads to an increased probability of ESA followed by an increased probability of the cross-relaxation, hence the term 'avalanche'. The most efficient up-conversion mechanism is the *energy transfer up-conversion* (ETU, also called the APTE effect for *Addition de Photons par Transfers d'Energie*). In ETU the summation of photons is obtained by two sequential resonance energy transfer steps between the sensitizer ion and the activator ion. The same ion can act as a sensitizer in both steps if it is re-excited during the lifetime of the intermediate level, or another nearby sensitizer ion can be involved. As in the two-steps absorption, also in ETU the intermediate energy level of the activator acts as an energy storage reservoir. Higher doping level is required in ETU compared to the two-steps absorption because in ETU at least two ions must be at close proximity. ETU was introduced by Auzel in 1966 for Yb(III)–Er(III) and Yb(III)–Tm(III) sensitizer–activator pairs.[114,115] In the same year Ovsyankin and Feofilov proposed the *cooperative sensitization* mechanism.[116] In the cooperative sensitization the activator does not have an energy level in resonance with the excited level of the sensitizer but the emitting level of the activator is reached by two simultaneous excitation energy transfers from the sensitizer ions to the activator. In the *cooperative luminescence* two sensitizer ions combine their excitation energies for the emission of a high energy photon from a virtual energy level.[117] The *second harmonic generation* (S.H.G. also called frequency doubling) occurs in a non-linear medium without any absorption transitions.[118] The *two-photon absorption excitation* (TPA) resembles the two-steps absorption process but there is no intermediate energy level, hence simultaneous absorption of two photons is required.[119]

The mechanisms in Figure 5 are arranged by their relative efficiencies increasing from left to right. The ETU, two-steps absorption and cooperative sensitization processes have real energy levels which are in resonance with the excitation and the emission radiation. The existence of the intermediate energy levels gives more time for photons to interact with the material. Hence, the probability of the second absorption or energy transfer is increased. The other three mechanisms in Figure 5 do not have resonance levels with both the excitation and emission transitions. Therefore, their up-conversion efficiency is low.

Different up-conversion processes may exist simultaneously,[110,120,121] or the excitation process can be a mixture of two mechanisms.[111] The dominant mechanism may depend on several factors including the composition of the material, the temperature and the excitation power.[122–124] Furthermore, it is not always straightforward to identify which mechanism is in question. The following criteria have be used to distinguish the prevailing mechanism: 1) the positions of the respective energy levels of the sensitizer and activator ions, 2) the power law dependence of the emission versus the excitation power and the sensitizer concentration, 3) the rise and decay times of the emission, 4) the shape of the excitation spectrum.[108,110,125]

The majority of the up-conversion research has involved materials doped with trivalent lanthanide ions, but also actinide and transition-metal ions are capable of up-conversion.[107,125,126] In the case of lanthanide ions, the most studied materials are fluoride, oxide, chloride and bromide compounds doped with Yb(III), Pr(III), Nd(III), Dy(III), Ho(III), Er(III) and Tm(III).[103,108,121,127–130] Generally, the most efficient up-conversion process is obtained with the Yb(III) ion acting as a sensitizer in an ETU process. Ytterbium is an ideal sensitizer. It has a simple energy level structure with only one excited state ($^2F_{5/2}$) (Figure 1), hence there does not exist any ESA mechanism to depopulate the excited state. Furthermore, the energy of the $^2F_{5/2}$ state is about 10 200 – 10 300 cm^{-1} (980–970 nm) and commercial laser diodes are available for this wavelength.[41] The most efficient green and red emitting phosphors are materials co-doped with Yb(III) and Er(III) ions.[103,104,128] The up-conversion mechanism is a two-photon ETU process where the Yb(III) ion acts as a sensitizer and the Er(III) ion as an activator. In theory, also a two-steps absorption process of a single Er(III) ion or a ETU process between two Er(III) ions are possible. However, absorption by the Er(III) ion is usually negligible due to a higher Yb(III) concentration and the larger absorption cross-section of Yb(III) compared to Er(III) at the 974 nm excitation wavelength.[31,108] The low Er(III) concentration is necessary to avoid self-quenching of the green emission.[131]

The energy level scheme of Yb(III)–Er(III) system is presented in Figure 6. The absorption of the excitation radiation at 970–980 nm is by the $^2F_{7/2} \rightarrow {}^2F_{5/2}$ transition of Yb(III). After the absorption the Yb(III) ion can return to the ground state by itself (radiatively or non-radiatively) or alternatively it can transfer the energy to a nearby Er(III) ion. The generally accepted two-photon ETU path to the green emission is presented in Figure 6.[127,128,132] The first Yb(III)→Er(III) energy transfer excites the Er(III) ions into the intermediate $^4I_{11/2}$ level which is at nearly perfect resonance with the Yb(III) $^2F_{5/2}$ level (Figure 6). The lifetime of the $^4I_{11/2}$ energy level is about 10 ms.[108] Hence, there is plenty of time for the second resonance energy transfer step which results in the $^4I_{11/2} \rightarrow {}^4F_{7/2}$ transition. Also this transition is in close resonance with the $^2F_{5/2} \rightarrow {}^2F_{7/2}$ transition of Yb(III). A fast non-radiative multiphonon relaxation of the $^4F_{7/2}$ level of Er(III) leads to the population of $^2H_{11/2}$ and $^4S_{3/2}$ levels. Vetrone et al. have proposed that the $^2H_{11/2}$ level is mainly populated thermally through the $^4S_{3/2}$ level.[131,133] The green emission around 520 nm and 550 nm is due to the $^2H_{11/2} \rightarrow {}^4I_{15/2}$ and $^4S_{3/2} \rightarrow {}^4I_{15/2}$ transitions, respectively.

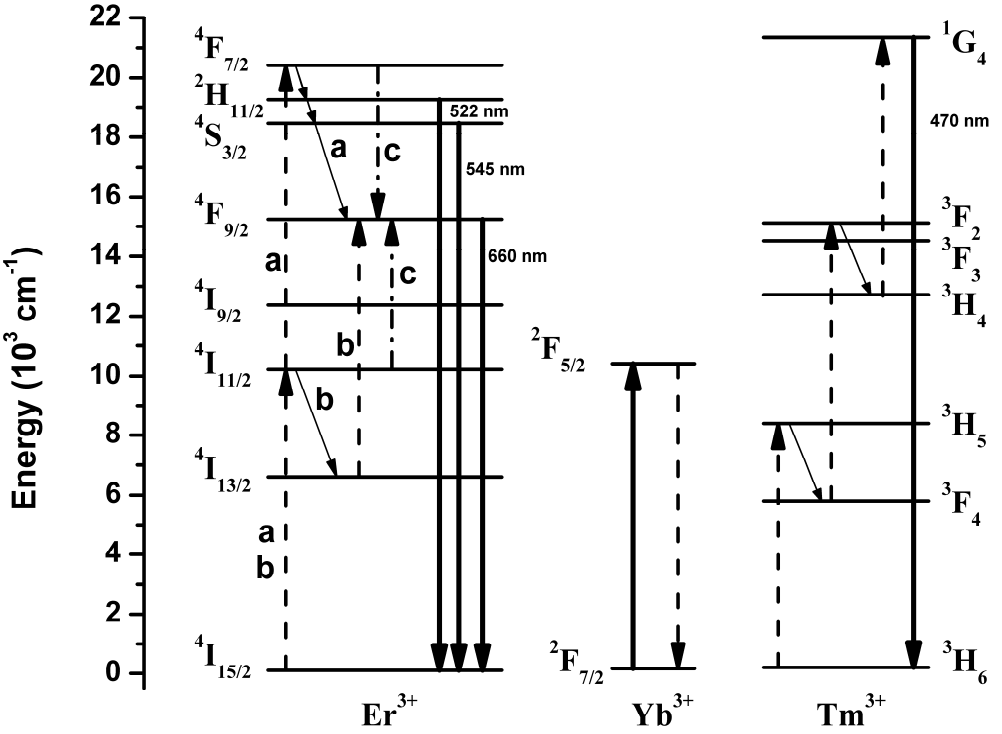

Figure 6. A schematic energy level diagram for the Yb(III)–Er(III) and Yb(III)–Tm(III) ETU systems. Yb(III): the absorption ($^2F_{7/2}\rightarrow{}^2F_{5/2}$) and the return to the ground state by energy transfer ($^2F_{5/2}\rightarrow{}^2F_{7/2}$). The Er(III) route (a): the excitation of the green and red emitting levels, $^4I_{15/2}\rightarrow{}^4I_{11/2}\rightarrow{}^4F_{7/2}\rightarrow(^2H_{11/2}, {}^4S_{3/2})\rightarrow{}^4F_{9/2}$. The Er(III) route (b): the excitation of the red emitting level, $^4I_{15/2}\rightarrow{}^4I_{11/2}\rightarrow{}^4I_{13/2}\rightarrow{}^4F_{9/2}$. The Er(III) route (c): the cross-relaxation between two Er(III) ions leading to the red emitting level, $(^4F_{7/2}, {}^4I_{11/2})\rightarrow(^4F_{9/2}, {}^4F_{9/2})$. Tm(III): the three-photon excitation route to blue emitting level, $^3H_6\rightarrow{}^3H_5\rightarrow{}^3F_4\rightarrow{}^3F_2\rightarrow{}^3H_4\rightarrow{}^1G_4$. Vertical bold solid lines: absorption and emission transitions, vertical dashed lines: resonance energy transfer, tilted thin solid lines: multiphonon relaxation, vertical dash–dot lines: cross-relaxation.[127,129,131,132,136]

The red emission around 650 nm corresponds to the $^4F_{9/2}\rightarrow{}^4I_{15/2}$ transition of Er(III). Several different excitation routes for populating the $^4F_{9/2}$ level have been proposed.[108] The suggested routes involve energy transfer, multiphonon relaxation, back-transfer to Yb(III), direct absorption by ground state Er(III) and cross-relaxation processes. Depending on the route the number of the photons required for reaching the $^4F_{9/2}$ level varies and can be 1.5, 2 or 3. The prevailing route depends on the host lattice, the dopant concentrations, the crystal size and the excitation power.[108,134,135] Three of the routes leading to the population of $^4F_{9/2}$ level are presented in Figure 6. The simplest route (a) follows the path to the green emitting level $^4S_{3/2}$ and concludes by a multiphonon relaxation to $^4F_{9/2}$ level.[127] In the route (b) a multiphonon relaxation of the intermediate Er(III) $^4I_{11/2}$ level populates the $^4I_{13/2}$ level.[136] The lifetime of the $^4I_{13/2}$ is in millisecond range.[135] The last step of the route (b) is $^4I_{13/2}\rightarrow{}^4F_{9/2}$ transition induced by the second energy transfer from Yb(III). The route (c) involves two Er(III) ions which are first excited to $^4I_{11/2}$ and $^4F_{7/2}$ levels by a single and two sequential energy transfers steps, respectively. In a cross-relaxation

process ($^4F_{7/2}$, $^4I_{11/2}$) → ($^4F_{9/2}$, $^4F_{9/2}$) both Er(III) ions end up in red emitting $^4F_{9/2}$ level. [127,131] Hence, three photons are required for the emission of two higher energy photons (n = 1.5 in Eq. 3). An increase in the probability of any route leading to the red emitting level $^4F_{9/2}$ is experimentally observed as an increased red–green emission ratio. In the routes (a) and (b) multiphonon relaxations are needed to dissipate larger energy gaps than in the route to the green emitting levels. Therefore materials with low lattice phonon energies show low red–green ratios.[137] Another source of phonon vibrations are the adsorbed surface contaminants (such as CO_3^{2-} and OH^-) and the red–green ratio is increased with decreasing particle size as the effect of the surface contaminants increases.[138] The cross-relaxation probability is increased with the erbium concentration because the number of the neighbouring Er(III) ions is increased.[132]

In addition to the green and red emissions of the Yb(III)–Er(III) system also weaker up-conversion emissions at 417 nm ($^2H_{9/2}$→$^4I_{15/2}$) and 847 nm ($^4S_{3/2}$→$^4I_{13/2}$) has been observed under NIR excitation.[135] The blue emission at 417 nm is due to a three-photon process.[138] The $^2H_{9/2}$ level is populated by a multiphonon relaxation of the $^4G_{11/2}$ level. The excitation of the $^4G_{11/2}$ level requires three successive resonance energy transfers between the Yb(III) and Er(III) ions. The path follows the route (b) (Figure 6) and concludes by the $^4F_{9/2}$→$^4G_{11/2}$ transition induces by an energy transfer from Yb(III). However, a more effective blue up-conversion emission can be achieved with the Yb(III)–Tm(III) sensitizer–activator system. The up-conversion mechanism is a three-photon ETU and the emission around 470 nm corresponds to the Tm(III) transition $^1G_4$→$^3H_6$ (Figure 6).[103,129] The resonance of the Yb(III) $^2F_{5/2}$→$^2F_{7/2}$ transition with the Tm(III) transitions is poorer than with the Er(III) transitions and the energy transfer steps of the Yb(III)–Tm(III) system are phonon-assisted.

The hexagonal phase $NaYF_4$ has proved to be one of the most efficient host lattices for the Yb(III)–Er(III) up-conversion system.[103,104,128] With the optimized dopant concentrations (18 and 2 mol-% for Yb(III) and Er(III), respectively) normalized efficiency of 10^{-2} cm^2W^{-1} has been obtained with hexagonal $NaYF_4$:Yb,Er material.[103] The high performance of the hexagonal $NaYF_4$ lattice has been attributed to a highly asymmetrical coordination of the Ln(III) ions.[104,128] The asymmetric coordination makes the forbidden electric dipole 4f–4f transitions partly allowed. Ten times stronger green and 4.4 times stronger green plus red emission intensities have been reported for the hexagonal $NaYF_4$ material compared to the cubic phase $NaYF_4$.[104] In the cubic phase $NaYF_4$ the crystal site of lanthanide ions is centrosymmetric.[128] Another factor proposed to explain the high efficiency of the hexagonal $NaYF_4$ material is the low phonon energy of the lattice. The low phonon energy of the host lattice reduces the probability of the non-radiative multiphonon relaxations within the 4f levels of the lanthanides. The phonon energy of the hexagonal $NaYF_4$ material is exceptionally low (350 cm^{-1})[137] compared to other common host materials like $LiYF_4$ (570 cm^{-1})[139], ZrO_2 (470 cm^{-1})[140] or Y_2O_3 (600 cm^{-1}).[138] The theoretically predicted optimal phonon energy for the Yb(III)–Er(III) up-conversion system is about 360 cm^{-1} which is a close match to the phonon energy of the hexagonal $NaYF_4$ material.[107,141]

1.6 Resonance Energy Transfer (RET)

In resonance energy transfer (RET) the electronic excitation energy from an excited luminescent molecule is transferred non-radiatively to another molecule.[106,142] The initially excited molecule is called the donor and the energy receiver is called the acceptor. As a result of the energy transfer the donor is deactivated to its ground state and the acceptor is excited to a higher electronic state. The donor is always luminescent. If the acceptor is luminescent, the acceptor emission due to the resonance energy transfer is called sensitized emission. Besides single molecules, the donor and acceptor can be e.g. lanthanide chelates, fluorescent moieties of macromolecules or dopants in inorganic crystals. In the case of energy transfer within inorganic samples, the donor and the acceptor are usually referred to as the sensitizer and the activator, respectively.[2] As a result of the resonance energy transfer, the donor emission intensity and the donor's lifetime are decreased, and the sensitized emission of the acceptor appears.

The theoretical basis of RET was laid by Förster.[143,144] Sometimes the term FRET for Förster or fluorescence RET is used. The mechanism is a non-radiative long-range induced dipole–dipole interaction between the donor and acceptor transition dipoles.[145,146] The effective range of RET is about 10–100 Å. The maximum distance is limited due to the need of a coupling between the electronic systems of the molecules. Below 10 Å energy transfer by Dexter exchange mechanism is prevailing.[61] The RET efficiency depends on the inverse sixth power of the distance between the donor and the acceptor. The distance dependence and the fact that the effective range of RET is comparable to the size of many biomolecules have inspired many applications.

The rate of the resonance energy transfer (k_{ET}) between a single donor (D) and a single acceptor (A) separated by the distance r is given by Equation 4.[106,144]

$$k_{ET} = \frac{Q_D \kappa^2}{\tau_D r^6}\left(\frac{9000\ln 10}{128\pi^5 n^4 N_A}\right)\int_0^\infty F_D(\lambda)\varepsilon_A(\lambda)\lambda^4 d\lambda \qquad (4)$$

Here Q_D and τ_D are respectively the quantum yield and the lifetime of the donor in the absence of the acceptor, κ^2 is the orientation factor, N_A is Avogadro's number, n is the refractive index of the medium, λ is the wavelength, $F_D(\lambda)$ is the corrected luminescence intensity of the donor with the total intensity normalized to unity and $\varepsilon_A(\lambda)$ is the molar absorption coefficient of the acceptor in units of $M^{-1}cm^{-1}$.

In RET the so called resonance condition must be fulfilled.[144] This means that the energy of the de-excitation of the donor has to be equal to the absorption transition energy of the acceptor. In practice this means that there must be an overlap between the donor emission and acceptor absorption spectra. This requirement is expressed as the integral in Equation 4. The integral is called the overlap integral $J(\lambda)$. The same overlap is required for the trivial radiative energy transfer in which the donor is deactivated by an emission of a photon which is reabsorbed by the

acceptor.[147] However, in RET the energy transfer occurs without the appearance of a photon. There are several differences between the RET and the trivial radiative energy transfer. In the RET process the lifetime of the donor is decreased, the emission spectrum of the donor is unaffected and the efficiency of the energy transfer is independent of the volume of the sample solution. In the RET process the donor's lifetime in the presence of the acceptor (τ_{DA}) is shortened due to a new deactivation pathway with the rate k_{ET}. This is mathematically expressed in Equation 5 in which τ_{DA} is the lifetime of the donor in the presence of the acceptor, k_{rad} is the radiative decay rate of the donor and k_{nr} is the sum of all non-radiative rates of the donor except the k_{ET} (Figure 7).[145]

$$\tau_{DA} = \frac{1}{k_{rad} + k_{nr} + k_{ET}} = \frac{1}{\tau_D^{-1} + k_{ET}} \qquad (5)$$

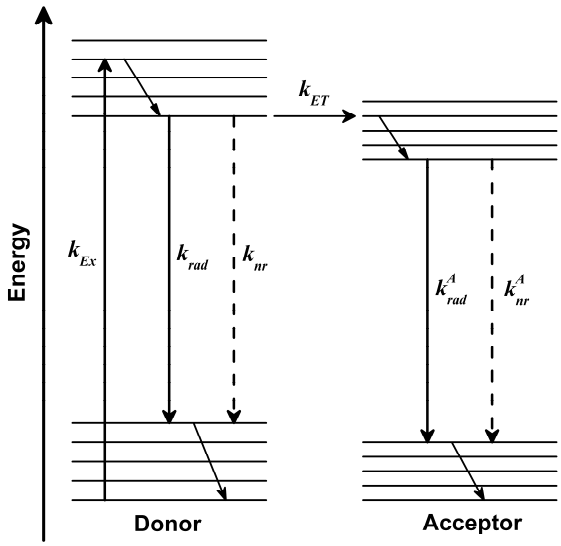

Figure 7. A Jablonski diagram representing resonance energy transfer. Vertical solid arrows are absorption (k_{Ex}) and emission (k_{rad} and $k_{rad}{}^A$) transitions, vertical dashed arrows are non-radiative transitions (k_{nr} and $k_{nr}{}^A$), tilted solid arrows represent internal conversion of energy and the horizontal arrow is the resonance energy transfer (k_{ET}). The superscript *A* refers to the acceptor.

The values of k_{rad} and k_{nr} are generally considered to be constant and unaffected by the presence of the acceptor. On the contrary, the value of k_{ET} depends on the distance between the donor and the acceptor. The dependence of k_{ET} on the inverse sixth power of the distance between the donor and the acceptor is displayed in Equation 4. The origin of the sixth power is in the dipole–dipole transfer mechanism. The energy of dipole–dipole interaction decreases as the third power of the distance between the dipoles ($\propto r^{-3}$). The probability of the energy transfer (i.e., the rate k_{ET}) is proportional to the square of the dipole–dipole interaction. Hence, the result is dependence on the sixth power.[148]

Equation 4 can be written as

$$k_{ET} = \frac{1}{\tau_D}\left(\frac{R_0}{r}\right)^6 \tag{6}$$

$$R_0 = \left(\frac{9000\ln 10}{128\pi^5 N}\frac{Q_D\kappa^2}{n^4}J(\lambda)\right)^{\frac{1}{6}} = 0.211\left(Q_D\kappa^2 n^{-4}J(\lambda)\right)^{\frac{1}{6}} \tag{7}$$

R_0 is called the Förster distance or the critical distance. When the distance between the donor and the acceptor is R_0 the rate of RET is equal to the decay rate of the donor in the absence of the acceptor and the efficiency of RET is 50%. This can be noted by substituting R_0 for r in Equation 6. The right side of Equation 7 is obtained by combining the constant terms. The value of the numerical constant depends on the units of the wavelength and R_0. The value presented in Equation 7 is valid if the wavelength is expressed in nanometers and gives R_0 in angstroms. The efficiency of RET (E) is the fraction of donor molecules that are deactivated through the energy transfer to the acceptor (Eq. 8).

$$E = \frac{k_{ET}}{k_{rad} + k_{nr} + k_{ET}} = \frac{k_{ET}}{\tau_D^{-1} + k_{ET}} \tag{8}$$

By combining Equations 5 and 8, E can be expressed by the donor lifetimes in the presence and in the absence of the acceptor (Eq. 9). If the natural lifetime of the acceptor is substantially short compared to the lifetime of the donor, the lifetime of the sensitized acceptor emission (τ_{AD}) is virtually the same as the lifetime of the donor in the presence of the acceptor.[149] This kind of situation is true for the lanthanide chelate donor and organic fluorophore acceptor pairs (Chapter 1.6.3).[150,151]

$$E = 1 - \frac{\tau_{DA}}{\tau_D} = 1 - \frac{\tau_{AD}}{\tau_D} \tag{9}$$

The efficiency of the energy transfer can also be expressed by the quantum yields of the donor luminescence in the presence (Q_{DA}) and in the absence (Q_D) of the acceptor (Eq. 10). Equation 10 is valid only if the absorption and emission spectra of the donor are not affected by the presence of the acceptor.[148] If the donor concentrations and the number of the photons absorbed by the donor are equal in both samples the quantum yields can be replaced by the donor emission intensities (I_{DA} and I_D) of the two samples.

$$E = 1 - \frac{Q_{DA}}{Q_D} = 1 - \frac{I_{DA}}{I_D} \tag{10}$$

Equation 11 is obtained by inserting Equation 6 into Equation 8. The energy transfer efficiency is strongly dependent on the donor–acceptor distance when the distance is close to the value of R_0. However, just a two-fold decrease or increase in the donor–acceptor distance results in E values close to unity or zero, respectively. Hence, the donor–acceptor pair should be chosen so that the value of R_0 is close to the expected donor–acceptor distance.

$$E = \frac{R_0^6}{R_0^6 + r^6} \qquad (11)$$

1.6.1 Quantum Yield

The rate of the resonance energy transfer is directly related to the quantum yield of the donor (Eq. 4, p. 24). The quantum yield is the measure of how well the donor converts the absorbed energy into an electric field.[145] In conventional organic fluorophores, the luminescence quantum yield is unambiguous and can be measured by comparative methods. This involves the use of a scatterer or a compound of a known quantum yield as a standard.[152–154] With lanthanide chelates the system is more complex.[150,151] The antenna part of the ligand absorbs a photon and transfers the energy to the lanthanide ion that may emit a photon. After the initial absorption the excitation energy can be lost at two states. The energy transfer from the antenna to the lanthanide ion may fail or the excited lanthanide may relax through a non-radiative path. The overall quantum yield ($Q_{overall}$) of the lanthanide chelate is the probability that the lanthanide ion will emit a photon after the excitation photon is absorbed by the antenna. This is basically the conventional quantum efficiency and can be measured by the comparative techniques. The overall process can be divided into two parts: $Q_{transfer}$ and Q_{Ln}.[151] The efficiency of the energy transfer from the antenna to the lanthanide ion ($Q_{transfer}$) is the probability that the lanthanide ion is excited by the energy transfer after the antenna has been excited. $Q_{transfer}$ can be divided to the inter-system crossing efficiency (Q_{isc}) and the energy transfer efficiency between the ligand triplet state and the lanthanide ion (Q_{et}).[155] The efficiency of the lanthanide luminescence (Q_{Ln}) is the probability that the excited lanthanide ion will deactivate via a radiative path, i.e. Q_{Ln} is the ratio of the radiative rate to the sum of the radiative and non-radiative rates of the lanthanide ion. The overall quantum yield is the product of $Q_{transfer}$ and Q_{Ln} (Eq. 12). In the case of the lanthanide chelate being used as a donor in a RET process, the Q_{Ln} is the donor's quantum yield to be used in Equations 4, 7 and 10.[150]

$$Q_{overall} = Q_{transfer} Q_{Ln} = Q_{isc} Q_{et} Q_{Ln} \qquad (12)$$

The relation of Q_{Ln} to the radiative (k_{rad}) and non-radiative (k_{nr}) rates of the lanthanide ion is presented in Equation 13.[151] Where τ_{obs} is the observed lifetime and τ_{rad} is the radiative or natural lifetime ($\tau_{rad} = k_{rad}^{-1}$). The term τ_D is the lifetime of the lanthanide chelate in H_2O (or H_2O–D_2O mixture) and $\tau_{D(D2O)}$ is the lifetime in 100% D_2O. The right-hand side of Equation 13 is based on

the assumption that the quantum yield of the lanthanide chelate in D_2O is unity ($k_{nr} = 0$). However, the assumption is not completely correct. This is because the N–H and C–H groups of the ligand molecule cause non-radiative decay.[45,80–83]

$$Q_{Ln} = \frac{k_{rad}}{k_{rad} + k_{nr}} = \frac{\tau_{obs}}{\tau_{rad}} \approx \frac{\tau_D}{\tau_{D(D_2O)}} \qquad (13)$$

Xiao and Selvin have developed a method to measure the lanthanide quantum yield and the radiative and non-radiative decay rates of lanthanide chelates.[151] The method is based on the diffusion-enhanced resonance energy transfer between a lanthanide chelate and an organic fluorophore of a known quantum yield.[156] The efficiency of the resonance energy transfer (E) between the donor and acceptor pair can be calculated from the lifetimes (Eq. 9) or from the emission intensities (Eq. 14).[157] The values of E measured by the two methods must be equal. Equation 15 is obtained by combining Equations 9 and 14. In Equations 14 and 15 τ_{DA} and τ_D are the lifetimes of the donor in the presence and in the absence of the acceptor, I_{AD} is the intensity of the sensitized emission, I_{DA} is the residue donor emission in the presence of the acceptor, Q_A and Q_{Ln} are the quantum yields of the acceptor and the lanthanide donor.

$$E = \frac{\left(I_{AD}/Q_A\right)}{\left(I_{DA}/Q_{Ln} + I_{AD}/Q_A\right)} \qquad (14)$$

$$Q_{Ln} = Q_A \frac{I_{DA}}{I_{AD}} \frac{\left(\tau_D - \tau_{DA}\right)}{\tau_{DA}} \qquad (15)$$

$$Q_{Ln} = \frac{k_{rad}}{k_{rad} + k_{nr}} = \tau_D k_{rad} \qquad (16)$$

Parameters I_{DA}, I_{AD}, τ_D and τ_{DA} can be measured. In Equation 15, τ_{DA} can be replaced with τ_{AD} if the lifetime of the acceptor is more conveniently determined. If an organic fluorophore of a known quantum yield is used as an acceptor, Q_{Ln} can be calculated. After the value of Q_{Ln} has been obtained, the Q_A of an acceptor with an unknown quantum yield can be determined by rearranging Equation 15. Also k_{rad} and k_{nr} of the lanthanide ion can be determined by Equation 16. Finally, $Q_{transfer}$ can be calculated from Equation 12 if $Q_{overall}$ is measured by standard techniques. The method has several advantages. Only two samples are needed: a donor sample to measure the value of τ_D and a donor–acceptor sample to measure the values of τ_{DA} and the ratio I_{DA}/I_{AD}. With the diffusion-enhanced technique, the donor–acceptor distance is easily adjusted to an optimal range by the acceptor concentration, and the acceptor is easily changed. Because of the long lifetimes of the lanthanide chelates, the rapid diffusion limit is achieved with relatively low concentrations.[156] Therefore, the lifetimes are single exponential and can be accurately measured. Another method for the determination of Q_{Ln} has been presented by Lemmetyinen et al.[155] They have calculated Q_{Ln}

from the values of $Q_{overall}$, Q_{isc} and Q_{et} (Eq. 12). The value of Q_{isc} is calculated from the fluorescence lifetimes of the ligand in the absence and in the presence of the lanthanide ion. The value of Q_{et} is calculated from the triplet state lifetimes of the Gd(III) chelate and another lanthanide chelate (Eu or Tb). Hence, three samples and four lifetime measurements are needed.

1.6.2 Orientation Factor

The orientation factor κ^2 describes the relative orientations of the emission and absorption transition dipoles of the donor and the acceptor, respectively. The orientation factor is defined by Equation 17 in which ϕ_{DA} is the angle between the transition dipole vectors of the molecules, ϕ_D and ϕ_A are the angles between the vector joining the two molecules and the transition dipole vectors of the donor and the acceptor, respectively.[106,142]

$$\kappa^2 = \left(\cos\phi_{DA} - 3\cos\phi_D \cdot \cos\phi_A\right)^2 \qquad (17)$$

The value of the orientation factor cannot be measured experimentally and it is considered to be the major source of uncertainty in the determination of the molecular distance by RET. The orientation factor can get values between 0 and 4.[158] If both the donor and the acceptor rotate freely and fast compared to the lifetime of the donor, the orientations of the transition dipole moments are random. The average value of κ^2 for a random directional distribution is 2/3. The values of κ^2 have been calculated for special cases. In the case of random but fixed orientations, the value of 0.476 has been used for κ^2.[159] However, it has been argued that this value is valid only for cases in which also the donor–acceptor distance is a random distribution.[160] The range of the possible κ^2 values is 1/3 to 4/3 if the donor is free to rotate and the acceptor is fixed.[161] The most unfavourable situation is when the orientations are fixed, non-random and unknown. In this case the value of κ^2 cannot be estimated. However, this is rarely the case. The range of the possible values of κ^2 is limited by partial rotational freedom.[158] The limits for the value of κ^2 can be calculated if the extent of the rotational freedom of both molecules is known. The extent of the rotational freedom of molecules has been estimated by fluorescence anisotropy experiments.[162–164] The range of κ^2 is also limited by degenerate transitions polarized along orthogonal directions.[158,165] Metal ions (such as Co(II), Eu(III) and Tb(III)) which have a three-fold or higher degeneracy are equivalent to rapidly and randomly rotating chromophores, even when ions are stationary.[20,91,157] Multiple donor–acceptor pairs and the statistical interpretation of the results have been used to evaluate the validity of the used κ^2 value.[161,166,167] The uncertainty of the orientation factor have also been estimated through an apparent distance distribution of the donor–acceptor pair.[168] Due to the difficult estimation of the dipole angles in real samples, commonly free rotation of the donor and acceptor is assumed and the value 2/3 is used for κ^2. Usually, the flexibility of the probe linkers provides enough dynamic averaging, and the orientation factor does not significantly affect the accuracy of an average distance measurement.

1.6.3 Lanthanide-Based Resonance Energy Transfer (LRET)

The resonance energy transfer with a lanthanide compound as a donor is called *lanthanide-based* or *luminescence resonance energy transfer* (LRET).[20,150,157] The name was introduced to distinguish LRET from FRET (fluorescence RET). Firstly, the lanthanide emission is technically not fluorescence which is by definition a singlet–singlet transition. Secondly, although the mechanism of the energy transfer is the same in both FRET and LRET the use of lanthanide donors offers several advantages. The advantages of LRET arise from the intrinsic properties of the lanthanides including the sharply spiked emission spectra, the long single exponential lifetimes, the unpolarized emission and the large Stokes' shifts. Eu(III) and Tb(III) chelates have commonly been used as donors and fluorescent organic dyes as acceptors in LRET research and applications.[169–172] More recently, also lanthanide doped up-converting particles (UCPs) have been used as LRET donors. UCPs have their own specific advantages in LRET application (Chapter 4.4).[173,174]

The emission spectra of the lanthanides consist of intense sharp emission peaks and dark regions with low emission intensity. Europium and terbium have excellent spectral overlaps ($J(\lambda) = 10^{15}$–10^{16} $M^{-1}cm^{-1}nm^4$) with several acceptor dyes.[20] A high value of the overlap integral leads to a high R_0 value (Eq. 7, p. 26). Critical distances as great as 70 Å have been obtained when a large $J(\lambda)$ is combined with a high Q_{Ln} value.[20,169] The nature of the transitions should be considered when calculating $J(\lambda)$. The resonance energy transfer arises from the electric dipole transitions, whereas the magnetic dipole and the electric quadrupole transitions are ineffective in the resonance energy transfer.[61] Some lanthanide transitions are fully or partially due to magnetic dipole transitions and should be excluded from the spectral overlap integral.[157] The $^5D_0 \rightarrow {}^7F_1$ transition of Eu(III) is acknowledged to be a magnetic dipole and can be relatively easily excluded from the calculation of $J(\lambda)$. The case of Tb(III) is more complex as the exact nature of its transitions is not well known. It is possible that the main transition $^5D_4 \rightarrow {}^7F_5$ contains some amount of magnetic dipole character. The extent of the electric dipole character can be enhanced by the use of asymmetric chelates.[46] In general, the sensitized acceptor emission has at least a moderate intensity over the dark regions of the lanthanide spectra. Hence, the sensitized emission can be measured against a very low background. The background is further decreased by an effective exclusion of the scattered excitation light due to the large Stokes' shift of the lanthanide chelates. Signal-to-background ratios of 50–100 for the sensitized acceptor emission have been measured with Eu(III) and Tb(III) chelate donors.[169,170] A high signal-to-background ratio facilitates the detection of small signals and the sensitized acceptor emission at distances much greater than R_0 is measurable. Together with a large R_0 this enables measurements of long distances and assays involving binding of large molecules.

The lifetimes of the lanthanide chelates range from hundreds of microseconds to milliseconds and can be measured with a high precision even with a basic instrumentation like a standard spectrofluorometer capable for time-resolved measurements. The measurement of the nanosecond lifetimes of the conventional fluorophores requires more sophisticated instruments. The long

lifetimes are a benefit also in the characterisation of the energy transfer. The donor and acceptor labels have more time to rotate during the lifetime of the donor and the transition dipole orientations are randomized.[158] Hence, the range of the possible κ^2 values is limited and the error in the value of R_0 induced by the use of the average value 2/3 is reduced. In the case of the donor's lifetime being notably longer than the acceptor's lifetime, the lifetime of the sensitized acceptor emission follows the lifetime of the donor engaged in the energy transfer.[149,150] The millisecond lifetime of the lanthanide donors is decreased due to the energy transfer process. However, when the donor–acceptor distances are close to R_0, the lifetimes of the lanthanide donors are still in the range of a hundred microseconds, i.e. a substantially longer time than the nanosecond lifetimes of the organic fluorophores. Hence, the energy transfer process is the rate limiting step in the sensitized acceptor emission because after the energy transfer, the acceptor decays in nanoseconds. An excellent agreement between the lifetime of the sensitized acceptor emission and the lifetime of the quenched donor emission has been obtained with lanthanide chelate donors and organic fluorophore acceptors.[169,170] Since the lifetime of the sensitized acceptor emission is virtually the same as the decreased lifetime of the donor, the lifetime of the sensitized acceptor emission (τ_{AD}) can be used in the place of the donor's lifetime (τ_{DA}) in Equation 9 (p. 26).[20] The possibility to use the value of τ_{AD} offers an advantage in detection if the emission at the donor's wavelength has a strong contribution from lone donors (I_D). Such a case occurs for example in the case of an incomplete acceptor labelling or an incomplete binding reaction between labelled biomolecules. The result is a biexponential decay of the donor emission as the lone donors decay with their normal lifetime (τ_D) and the donors in the close proximity of the acceptors with a decreased lifetime (τ_{DA}). In a severe case of the incomplete labelling or binding the τ_{DA} component of the donor emission may be buried under intense emission from the lone donors. The situation is worse if the decrease of the donor's lifetime is small for example due to a long donor–acceptor distance. A pure sensitized acceptor emission signal and lifetime (τ_{AD}) can be measured by a spectral discrimination of the donor emission and a temporal discrimination of the directly exited acceptor fluorescence and autofluorescence.

In one respect the sensitized acceptor decay diverges from the donor decay. In the case of multiple donor–acceptor distances the pre-exponential amplitude factors of the donor decay are proportional to the populations of different donor–acceptor pairs. However, the amplitudes of the sensitized acceptor emission are proportional to the populations and the energy transfer rates.[175] Hence, the amplitudes of the donor–acceptor pairs with high rates of the resonance energy transfer (i.e. short donor–acceptor distance) are overemphasized. The observed amplitudes of the sensitized emission should be corrected for their dependence on the energy transfer rates before using them to analyze the populations.

When lanthanide chelates are used as donors in RET, the donor quantum yield that should be used in calculations (Eq. 4, 7 and 10, pp. 24 and 26) is the lanthanide luminescence quantum yield (Q_{Ln}) not the overall quantum yield of the chelate (Chapter 1.6.1).[151,157] However, also a high overall

quantum yield is beneficial because it affects the brightness of the chelate. The quantum yield of the lanthanide chelates can be adjusted with the H_2O–D_2O ratio of solution.[170] Hence, the R_0 value can be tuned by varying the H_2O–D_2O ratio of the solvent. This offers a unique way to optimize the energy transfer properties for a particular application. The amount of the H_2O–D_2O effect can be controlled by the denticity of the chelate.

The emission of the lanthanides is generally considered to be nearly isotropic due to the multiple transition dipole moments.[91,157] Three-fold or higher degeneracy of either level of a transition means that the corresponding emission is unpolarized. The Tb(III) emission arises from the $^5D_4 \rightarrow {}^7F_J$ transitions. The $^5D_4$ level and the most important ^7F_J levels (J = 5, 6, 4, 3, 2) are highly degenerate. The number of the dipole orientations of the Eu(III) emission is less since the main emitting level $^5D_0$ is non-degenerate. However, the ground levels ^7F_J (except $^7F_0$) are degenerate and the number of transition dipoles is fairly high. Polarized Eu(III) emission has been observed with $Zn_3Eu_2(NO_3)_{12}{\cdot}24H_2O$ single crystals at 77 K and crystallized polyaminocarboxylate-based chelates of Eu(III).[176,177] Reifenberger et al. have shown that the polarization of the Eu(III) emission depends on whether the $^5D_0$ level is excited directly or through an antenna.[178] They studied polyaminocarboxylate-based chelates of Eu(III) and Tb(III) frozen in amorphous glass. The anisotropy of the directly excited Eu(III) emission was high but nearly isotropic emission was observed when the excitation proceeded via the antenna moiety. The emission of the Tb(III) chelates was nearly isotropic irrespective of the excitation method. As a result of the isotropic donor emission, the value of κ^2 is constrained within the range 1/3 to 4/3 even if the donor and the acceptor are completely immobilized.[157] In such a case, the error in the calculated donor–acceptor distance is at worst 12% if the average value 2/3 is used. The error is usually less than 12% because the donor and acceptor moieties have plenty of time to rotate and randomize the dipole orientations during the long lifetime of the lanthanides.

1.6.4 Non-Overlapping Fluorescence Resonance Energy Transfer (nFRET)

One of the basic requirements of the resonance energy transfer (in both FRET and LRET) is the resonance condition which in practice means a spectral overlap between the emission spectrum of the donor and the absorption spectrum of the acceptor.[144] In 2005 Laitala and Hemmilä introduced a lanthanide-based resonance energy transfer in which the absorption of the organic acceptor molecules was at shorter wavelengths than the main emission transitions of the Eu(III) ($^5D_0 \rightarrow {}^7F_J$) or Sm(III) ($^4G_{5/2} \rightarrow {}^6H_J$) chelate donors.[24,25] They termed the phenomenon as *non-overlapping FRET* (nFRET) to emphasize the lack of the spectral overlap. The mechanism of nFRET has not been established but the term FRET was kept because some characteristics of the conventional FRET are maintained. The most important being the requirement of the close proximity between the donor and the acceptor. However, the nFRET process does not strictly follow the Förster theory. Especially the experimental lifetime properties differ from the theoretical values calculated with the

Förster equations. Since the acceptor absorption is at shorter wavelengths than the donor emission, nFRET is an anti-Stokes' energy transfer process.

Laitala and Hemmilä used terpyridine chelates of Eu(III) and Sm(III) as donors and applied six different organic fluorophores (Alexa Fluors 488, 514, 532, 546, 555 and 647) as acceptors.[24,25] Alexa Fluor 647 was a reference acceptor with a strong spectral overlap with the donor emission. The other acceptor fluorophores had at best a minor spectral overlap with the $^5D_0 \rightarrow {}^7F_0$ transition of Eu(III) or the $^4G_{5/2} \rightarrow {}^6H_{5/2}$ transition of Sm(III). The close proximity of the donor and the acceptor was realized by the donor and acceptor labelled oligonucleotide probes hybridized to a common complementary oligonucleotide target. The hybridization reaction resulted in a donor–acceptor distance of ca. 20 Å. The negative control samples were mixtures of the donor and acceptor probes without the complementary DNA target. Depending on the nFRET acceptor, the sensitized acceptor emission was detected at 530, 545 or 572 nm, i.e. below the donor emission wavelength.

The requirement of the close proximity of the labels in nFRET is a property inherited from conventional FRET. The main deviations of nFRET from the Förster theory are the length and the number of the lifetimes observed for the sensitized acceptor emission. In the case of the europium donor all five nFRET acceptors showed a strong and fast decaying lifetime component with a lifetime of ca. 0.64 μs.[24] In addition, three nFRET acceptors with absorption maximums at the longest wavelengths of the studied nFRET acceptors (AF532, AF546, AF555) had a second longer (31.3–54.0 μs) lifetime component. The regular FRET acceptor probe and the free donor probe had single lifetimes of 1.9 μs and 1169 μs, respectively. In the case of the samarium donor all acceptors showed a single exponential decay profile. Lifetimes ranged from 6.6 to 8.5 μs with the nFRET acceptors and a clearly different 1.3 μs lifetime was obtained for the regular FRET acceptor.[25] The lifetime of the free samarium donor probe was 13.7 μs. The experimental lifetimes were compared with the theoretical Förster-type lifetimes calculated according to the conventional RET equations (Eq. 9 and 11, pp. 26 and 27). In the case of the europium donor the theoretical lifetimes were significantly longer (309–1169 μs) compared to the experimental ones. Hence, a clear deviation from the Förster theory was noticed. With the samarium donor the difference between the theoretical and the experimental lifetimes was less pronounced but undeniable with the nFRET acceptors (AF514 and AF532). With the AF546 and the AF555 acceptors the experimental and theoretical lifetimes correlated fairly well. These two acceptors have a minor overlap with the Sm(III) $^4G_{5/2} \rightarrow {}^6H_{5/2}$ transition. Thus, the energy transfer may be at least partly due to the conventional FRET process.

Assays based on the nFRET phenomenon showed very low picomolar detection limits for a DNA-target with both the europium and samarium donors.[24,25] The detection limit of ca. 1 nM for the respective time-resolved fluorescence quenching assay with the same Eu(III) chelate has been reported.[179] The quantum yield of the terpyridine Sm(III) chelate is approximately 90-fold lower compared to the quantum yield of the respective terpyridine Eu(III) chelate. However, the

difference in detection limits was only five to ten-folds depending on the method of calculation. Hence, the quantum yield of the donor does not seem to be a critical property in nFRET assays. This is another deviation from the Förster theory where the efficiency of the energy transfer is linked to the donor quantum yield through R_0 (Eq. 7 and 11, pp. 26 and 27).

The experimental lifetimes suggest a deviation from the Förster theory. However, the donor–acceptor distance of 20 Å is within the range where the non-radiative dipole–dipole interaction dominates over the multipole and exchange interactions. Laitala and Hemmilä proposed the nFRET energy transfer to proceed through the $^5D_1$ and $^5D_2$ energy levels of the Eu(III) ion.[24] Based on the absorption maximums, all the nFRET acceptors had their absorption energy above the main radiative energy level $^5D_0$ and below the $^5D_2$ energy level of the Eu(III) ion. The nFRET acceptors (AF488 and AF514) which had a single lifetime were energetically between the $^5D_2$ and $^5D_1$ levels. Other three nFRET acceptors (AF532, AF546 and AF555) were energetically below the $^5D_1$ level and showed biexponential decay profiles. Based on these observations Laitala and Hemmilä concluded that the nFRET acceptors accepted energy only from the $^5D_2$ level or from both the $^5D_2$ and the $^5D_1$ levels depending on the position of their absorption maximum relative to the energy levels of the Eu(III) donor. The short lifetime component was associated with the energy transfer from the $^5D_2$ level and the long lifetime component with the energy transfer from the $^5D_1$ level. The energy levels above the $^5D_2$ level were not considered as potential energy-donating states since they were energetically above the lowest triplet state of the used ligand. In the case of the Sm(III) donor Laitala and Hemmilä proposed that nFRET energy transfer occurs from the $^4G_{7/2}$ level of Sm(III).[25] However, further experimental work is required to establish the proposed energy transfer mechanism.

In addition to the two initial papers[24,25] also Vuojola et al. have published a report on nFRET.[26] Vuojola et al. utilized the nFRET phenomenon in a homogeneous competitive assay for GTP (guanosine triphosphate). A Eu(III) chelate labelled GTP and an analyte GTP competed for the binding with Rab21 (a small guanosine triphosphatase) labelled with the yellow fluorescent protein (YFP). The binding reaction was initiated with the addition of $MgCl_2$. A conventional FRET reference assay was realized with a Tb(III) chelate donor and the green fluorescent protein (GFP) acceptor. The decay profiles of both the Eu(III) and Tb(III) chelates alone and the Tb(III)–GFP pair were all single exponential with lifetimes 1040, 940 and 60 μs, respectively. The nFRET donor–acceptor pair Eu(III)–YFP had a biexponential decay profile (τ_1 = 1080 μs and τ_2 = 8 μs) not explicable by the normal Förster-type energy transfer. The excitation band of YFP overlaps with the $^5D_1$ energy level of the Eu(III). Hence, the biexponential decay can be explained by the energy transfer from the $^5D_2$ and $^5D_1$ levels to YFP. For the GTP detection, the dynamic range over two orders of magnitude and the IC_{50} value (ca. 100 nM) were about the same for the nFRET and FRET assays. The signal strength of the sensitized acceptor emission was lower for the nFRET assay. However, due to the complete absence of the donor emission at the detection wavelength the

signal-to-background ratio was five-fold higher for the nFRET assay compared to the conventional FRET assay.

The advantage of nFRET in assay applications is that the sensitized acceptor emission can be measured at wavelengths shorter than the donor emission. Hence, the background signal level due to the donor emission is very low. In addition, the radiative energy transfer by the reabsorption of the donor emission by the acceptor is absent. The similar range of the detection limits obtained with the Eu(III) and Sm(III) chelate donors suggests that in the nFRET process the high quantum yield of the donor is not essential. Thus, in addition to samarium, other low intensity or even non-fluorescent lanthanide chelates may be useful as nFRET donors. However, for the time being the nFRET technology has not been widely utilized in homogeneous assay applications. This may be due to the discouraging fact that the nFRET mechanism is still not fully established. Another disadvantage is that nFRET does not strictly follow the Förster distance dependence. This means less predictable energy transfer efficiency for a certain donor–acceptor distance. Also, as discussed in Chapter 4.2, the effective range of nFRET is shorter than the range of FRET. Hence, the distances measurable with nFRET are shorter than with FRET. This sets limitations also for binding assays since the binding of the labelled molecules should result in a relative short distance between the donor and acceptor labels.

1.6.5 Donor–Acceptor Distance

The power of RET is based on its distance dependence. The effective RET distance (10–100 Å) is comparable to the size of common macromolecules. Hence, RET offers a possibility to measure the size and the structure of macromolecules as well as the dynamic changes of the structure.[180–182] The term *spectroscopic ruler* was introduced by Stryer and Haugland.[183] RET has also been used in bioanalytical assay and high-throughput screening applications.[99,100,170,172,184] In these applications RET is a result of some binding reaction which brings the donor and the acceptor into a close proximity. The power of RET in binding assays stems from the fact that the signal is detected only from those molecules that are binding. Hence, fast and easily automated homogeneous separation-free assays can be realized. The distance dependence of RET has also been used to study the level of interpenetration between polyelectrolyte layers[185,186] and polyelectrolyte multilayers adsorbed on particles.[187] In binding assays the measured RET signal is usually compared to the calibration curve of standard samples. Hence, the exact knowledge of the donor–acceptor distance, R_0 or κ^2 is not critical. Certainly, some knowledge of the properties of the donor and the acceptor is needed for an educated selection of suitable labels for a specific assay. However, when RET is used to measure distances, the accuracy of the measurements depends on the correctness of the used parameter values. If these values are incorrect, only relative distances can be obtained. Hence, a calibration system for donor–acceptor pairs is needed.

The first fixed donor–acceptor distances were realized with rigid molecules. Latt et al. used a rigid decacyclic molecular system.[188] The molecule provided a fixed separation (ca. 18.5 Å) of two

hydroxyl groups for the donor and acceptor labelling. Some uncertainty of the exact separation of the donor and the acceptor was introduced due to the possible rotation of labels. Later Stryer and Haugland used oligomers of poly-L-proline as rigid spacers.[183] They controlled the donor–acceptor distance (12–46 Å) by the number of the monomer units in the oligomer.

Fluorescein (donor) and rhodamine B (acceptor) or rhodamine B (donor) and Texas Red (acceptor) pairs have been used to study resonance energy transfer between self-assembled multilayers.[189,190] Poly(allylamine hydrochloride) (PAH) polyelectrolyte layers labelled with the fluorophores were separated by optically inactive layers of α-zirconium phosphate (α-$Zr(HPO_4)_2$). According to the energy transfer results, multilayers were almost ideally flat layers without interlayer penetration. Hence, multilayers constructed of alternating α-$Zr(HPO_4)_2$ and PAH layers could be used for the calibration of the donor–acceptor pairs in parallel planes geometry. Another parallel plane system is the Langmuir–Blodgett films. In Langmuir–Blodgett films the distance is controlled by the number of the inert fatty acid layers and by the length of the carbon chain in the layers.[191,192]

Thermolysin (a metalloendopeptidase) has been used to calibrate Tb(III)–Co(II) donor–acceptor pair.[91] Thermolysin contains one Zn(II) ion and four Ca(II) ion binding sites. The Zn(II) ion can be replaced by a Co(II) ion and three Ca(II) ions can be replaced by trivalent lanthanide ions. The three-dimensional structure of thermolysin has been established by X-ray structure analysis. The distance between the Ca site most readily occupied by lanthanide ions and the Zn site is 13.7 Å. In the case of the Tb(III) ion, a tryptophan residue serves as an antenna moiety and a decrease in the Tb(III) emission intensity is observed due to the resonance energy transfer to the Co(II) ion. The R_0 value of 19.6 Å obtained with the known donor–acceptor distance can be used to measure unknown distances and to monitor conformational changes in other systems which have suitable binding sites for the Tb(III) and Co(II) ions.

DNA strands labelled with the donor and the acceptor have been used to set the donor–acceptor distance.[193–195] The donor–acceptor distance is controlled by the number of the base pairs between the labels. The close proximity of the labels is achieved by a hybridization reaction. Different strategies have been used to fix the donor–acceptor distance. In one strategy complementary DNA strands are labelled with the donor and the acceptor, respectively. Either the lengths of the DNA strands are varied with the labels at the 5′ends or the length is kept unchanged but the labelling site of one of the labels is varied.[193,195] Alternatively, two non-complementary oligonucleotides are labelled at the 5′ end and at the 3′ end, respectively. The labelled oligonucleotides are complementary to closely separated sequences of a longer unlabelled target oligonucleotide. The donor–acceptor distance is controlled by the number of the bases separating the complementary sequences.[193,194] In both strategies the structure should be fully double-stranded because single-stranded sequences are flexible and can induce uncertainty in the donor–acceptor distance.[196] Commonly the donor–acceptor distance is calculated simply by a linear model, i.e. adding 3.4 Å for a base pair. However, for a more accurate calculation of the donor–acceptor distance also the three-dimensional helical geometry of the DNA double-strand, the length of the label linkers and the

orientation of the label linkers relative to the double-strand should be taken into account.[148,193,197] It has been reported that the hybridization of the donor labelled DNA strand with an unlabelled complementary strand has a quenching effect on the donor luminescence.[193,198] Also the base sequence near to the fluorescent labels may have an effect on the efficiency of the energy transfer.[198]

One source of uncertainty in the donor–acceptor distance is the molecular linkers used to attach the donor and acceptor labels. Linkers may allow some diffusional freedom and make the calculated donor–acceptor distance inaccurate.[148] On the other hand, the probe linker arms may be flexible enough to cause rotational averaging of the transition dipole moments and therefore decrease the uncertainty caused by the orientation factor.[199] Macromolecule structures have also been determined by a series of relative distance measurements as an alternative for the measurement of absolute distances.[180]

1.7 Characterization of RET efficiency

The distance between the donor and the acceptor can be calculated from the energy transfer efficiency if the Förster distance is known (Eq. 11, p. 27). The energy transfer efficiency can be determined from: (i) the quenching of the donor emission intensity, (ii) the intensity of the sensitized acceptor emission, (iii) the change in the luminescence anisotropy of the donor or the acceptor, (iv) the decrease in the donor's lifetime.[148,158]

The measurement of the decrease of the donor emission intensity due to the energy transfer is in principle a simple method. The donor emission intensity is measured in the presence and in the absence of the acceptor and the energy transfer efficiency can be calculated from Equation 10 (p. 26). The samples are excited at the wavelength of the donor absorption and the donor emission is detected at a wavelength with a negligible acceptor emission. If the donor and acceptor emissions overlap, the use of a spectral range and curve fitting instead of a single wavelength can improve the accuracy of the measurement.[199] The problem of the method is that the concentrations of the donor–acceptor sample and the donor–only sample should be equal or at least known so that the emission intensities can be normalized to the same concentration. This may be difficult to achieve experimentally. The acceptor labelling is assumed to be 100% in Equation 10. In the case of incomplete labelling, Equation 18 can be used if the degree of the acceptor labelling (f_A) is known.[106]

$$E = 1 - \frac{I_{DA} - I_D(1 - f_A)}{I_D f_A} = \left(1 - \frac{I_{DA}}{I_D}\right)\frac{1}{f_A} \qquad (18)$$

A luminescent acceptor is required if the sensitized acceptor emission is used to calculate the energy transfer efficiency. The acceptor emission intensities are measured in the presence ($I_{AD}(\lambda_A^{em})$) and in the absence ($I_A(\lambda_A^{em})$) of the donor. The energy transfer efficiency can be

calculated from Equation 19.[106] The molar absorption coefficients of the acceptor ($\varepsilon_A(\lambda_D^{ex})$) and the donor ($\varepsilon_D(\lambda_D^{ex})$) at the donor excitation wavelength and the fraction of the donor labelling (f_D) must be known. In Equation 19 it is assumed that the donor does not emit at the acceptor emission wavelength (λ_A^{em}). If this is not the case, the donor's contribution must be compensated or the obtained value of E is too large. As the method of the donor intensities, also this method requires two samples of equal concentrations.

$$E = \frac{\varepsilon_A(\lambda_D^{ex})}{\varepsilon_D(\lambda_D^{ex})}\left[\frac{I_{AD}(\lambda_A^{em})}{I_A(\lambda_A^{em})} - 1\right]\left(\frac{1}{f_D}\right) \qquad (19)$$

Epe et al. have developed a method in which the donor–acceptor sample is treated in a way that the donor and the acceptor become separated and the energy transfer is omitted.[200–202] Hence, the concentrations of the donor–acceptor sample and the donor–only (or the acceptor-only) sample are equal. They used enzymatic digestion of protein samples to separate the originally proximate donor and acceptor labels. The authors also proposed other methods of separation, including acidic or alkaline hydrolysis, induced dissociation of the subunits, and denaturation by urea or dodecyl sulfate.[200] However, the separation method is not suitable for all samples.

Clegg et al. have developed steady-state fluorescence methods in which the energy transfer efficiency is calculated from the results of two fluorescence measurements performed with a single sample.[148,180,197] These methods are called $(\text{ratio})_A$ and $(\text{ratio})_D$. In both methods only a single sample and a single instrument are needed. In the $(\text{ratio})_A$ method the energy transfer efficiency is determined from the emission and excitation spectra of the acceptor.[148] The advantage of the method is that since the measurements are done with a single sample, the problem of the equal sample concentrations is eliminated. In the $(\text{ratio})_A$ method the percentage of the acceptor labelling is not required but the percentage of the donor labelling must be known. The $(\text{ratio})_D$ method is similar to the $(\text{ratio})_A$ method but the emission spectrum of the donor is used.[148,180] The advantage of the $(\text{ratio})_D$ method is that the acceptor does not have to be fluorescent. However, the $(\text{ratio})_D$ method has some disadvantages compared to the $(\text{ratio})_A$ method. In the $(\text{ratio})_D$ method the percentage of both the donor and the acceptor labelling are needed and an uncertainty in the labelling percentages may lead into a greater error than in the $(\text{ratio})_A$ method. Also the variations in the quantum yields of the donor and the acceptor are not cancelled. In both methods the molar absorption coefficients of the labels are needed. The fluorescence spectra of the donor-only sample and the acceptor-only sample are needed to extract the donor and acceptor contributions from the spectra of the donor–acceptor sample. The inconvenience of these methods is a complicated data analysis. Liu and Lu have extended the $(\text{ratio})_A$ method to a trifluorophore system.[182]

Both the donor and the acceptor emission anisotropy can be used to measure the resonance energy transfer efficiency.[148] The anisotropy of a molecule depends on the extent of the rotational diffusion the excited molecule undergoes before it emits a photon. As the lifetime of the donor becomes

shorter due to the resonance energy transfer, the molecule has less time to rotate. Hence, the fluorescent anisotropy of the donor emission is increased in the presence of the acceptor. The anisotropy of the sensitized acceptor emission is lower than that of the directly excited acceptors. In the RET process the excitation energy is passed to the transition dipoles of the acceptor which are orientated differently compared to the dipoles of the donor originally photo-selected by the polarized excitation light.

The energy transfer efficiency can be calculated from the lifetimes of the donor in the presence (τ_{DA}) and in the absence (τ_D) of the acceptor (Eq. 9, p. 26). The basic requirement is that the difference between the values of τ_{DA} and τ_D is large enough so that they can be reliably determined from the lifetime data. The measurement of the energy transfer efficiency by lifetimes has several advantages compared to the steady-state intensity methods.[142,148,199] Firstly, the lifetimes are unaffected by the concentration of the sample. Secondly, the method is unaffected by non-stoichiometric labelling. Hence, 100% labelling is not necessary and the labelling percentage can be unknown. These facts are remarkable advantages considering the sample preparation. Thirdly, lifetimes are generally very reproducible, and extensive spectral data analysis is not necessary. The interpretation of the lifetime data becomes more complex if more than a single donor–acceptor distance is present, but so does the interpretation of the steady-state data. A disadvantage of the lifetime method is the more complex instrumentation compared to the steady-state system. If the lifetime of the donor is notably longer than the lifetime of the acceptor, the lifetime of the sensitized acceptor emission (τ_{AD}) is virtually equal with the decreased lifetime of the donor (τ_{DA}).[149] Hence, τ_{DA} can be replaced by τ_{AD} in Equation 9 (p. 26). The advantage of τ_{AD} is that a pure energy transfer signal can be detected by spectral and temporal discrimination of the donor emission and the directly exited acceptor emission, respectively. This is one of the advantages of the lanthanide-based RET (Chapter 1.6.3).

Lifetime measurement techniques

Two different techniques are used to measure lifetimes: the time-domain (TD) and the frequency-domain (FD) methods, also called the pulse fluorometry and the phase-modulation methods, respectively.[106,203] Their basic principles are presented in Figure 8.

.

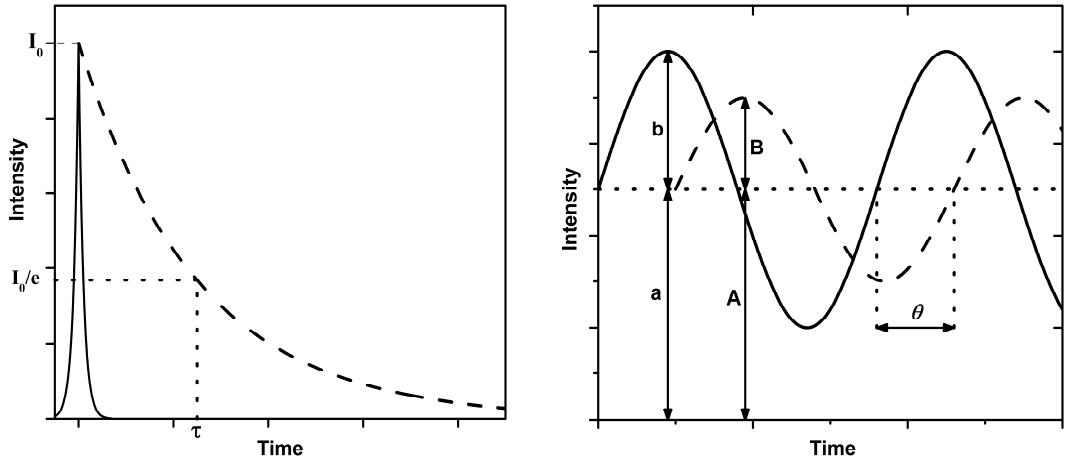

Figure 8. Excitation (solid lines) and emission response (dashed lines) curves of the time-domain (left) and the frequency-domain (right) fluorometry.

The main difference between the two techniques is the form of the excitation signal. In the time-domain measurement the sample is excited with a short pulse of light and the luminescence response of the sample is monitored as a function of time. The sample luminescence decays exponentially. In Equation 20 $I(t)$ is the luminescence intensity at the time t after the excitation pulse, α_i and τ_i are the amplitude and the decay time of the ith component.[106] If the length of the excitation pulse is long in respect to the lifetime of the sample, it overlaps with the sample decay. In this case a deconvolution of the luminescence signal with the instrument response function is required. The time profile of the excitation pulse can be measured with a scattering sample.

$$I(t) = \sum_i \alpha_i \exp(-t/\tau_i) \qquad (20)$$

Different techniques are used in the TD measurements.[106,204] The most commonly used techniques are the time-gated detection and the time-correlated single-photon counting technique (TCSPC) also called the single-photon timing (SPT). The gated detection is an older technique of the two. The principle is to sample the intensity decay with a short time gate which is moved forward on the time axis after each pulse. In TCSPC the time between the excitation pulse and the arrival of the first emission photon to the detector is measured. The probability of the arrival of the first photon at time t is proportional to $I(t)$. The TCSPC experiment consists of a high number (10^9) of excitations and of recording a histogram of photon counts versus time which equals the decay profile of the sample. Compared to the gated detection the TCSPC offers better time resolution and accuracy. A time resolution of 50–100 ps is available with commercial TCSPC instruments.[204] An even better time resolution can be achieved with streak cameras (few picoseconds) and with the non-linear optical gating method (about 100 fs).[106,204] An advantage of the streak cameras is the ability to record the wavelength dependence simultaneously with the time decay. However, the streak cameras have a low dynamic range and a low signal-to-noise ratio compared to the TCSPC method.

The disadvantages of the non-linear optical gating method are complexity, low sensitivity and high cost. Also, the non-linear optical gating method is unpractical for the measurement of the long decay times of the lanthanide luminescence. In the case of the long-lived lanthanide luminescence, the gated detection usually provides an adequate time resolution, and deconvolution is unnecessary.

In the frequency-domain method the excitation signal is intensity-modulated light. Commonly a sine wave modulation is used. The intensity of the emission signal follows the excitation modulation at the same frequency. However, due to the lifetime of the sample, the emission is delayed in time relative to the excitation. The delay is observed as a phase shift (θ) and a modulation ratio (M) (Figure 8 and Eq. 21). For a single exponential decay the phase shift and the modulation ratio are related to the decay time by Equations 22 and 23, where τ_Φ and τ_M are the lifetimes and ω is the angular frequency of the excitation.[106] For a single exponential decay the lifetime can be calculated by either equation and the result is independent of the excitation frequency. The best accuracy is obtained if the excitation frequency is close to the reciprocal of the lifetime of the sample i.e. $\omega \approx \tau^{-1}$. In the case of a more complex than a single exponential decay profile Equations 22 and 23 give only apparent values of the lifetimes. For more accurate results the phase shift and modulation ratio values must be measured as a function of the excitation frequencies and the values of α_i and τ_i are determined by finding the best fit between the calculated and experimental values of the phase shift and the modulation ratio, usually by a least-squares analysis. Decay times on picosecond time scale have been obtained with 10 GHz FD fluorometer.[205]

$$M = \frac{B/A}{b/a} \tag{21}$$

$$\tau_\phi = \frac{1}{\omega}\tan\theta \tag{22}$$

$$\tau_M = \frac{1}{\omega}\left(\frac{1}{M^2} - 1\right)^{\frac{1}{2}} \tag{23}$$

The periodic excitation and the intensity-modulated emission signal are the foundation of the FD methods. However, the phase shift and the modulation ratio are not necessarily the signals measured. The measured parameters can be any quantities that can be related to the lifetimes and the corresponding amplitudes of the luminescence signal. We have assembled a modular FD luminometer based on the dual-phase lock-in detection of the emission. The recorded quantities are the in-phase and out-of-phase signals of the lock-in amplifier. The decay times and their amplitudes are obtained after a fitting process. A measurement consists of recording the signal at 200 frequencies between 10 Hz and 100 kHz. The frequency range corresponds to a decay time range from 16 ms to 1.6 μs which is quite befitting for studying the lanthanide luminescence and the

lanthanide-based resonance energy transfer. The instrument and related mathematical theory have been presented in publication **I** and in the reference [206] and are reviewed in Chapters 3.1 and 4.1.

The TD and FD techniques are theoretically equivalent but have different strengths.[203] The TD method allows more intuitive visualization of the luminescence decay (Figure 8). The sensitivity of the TD method is better mainly because the luminescence is measured against a dark background, whereas in the FD measurements the excitation source is always on. In the FD method no deconvolution is necessary. In TD (especially with the TCSPC technique) the assignment of the standard deviations is straightforward. This is an advantage in the data analysis.[106] In FD the estimation of the standard deviations of the phase shift and the modulation ratio is more difficult. Time-resolved spectra are more easily recorded with the TD method, while the lifetime-based decomposition of the emission spectra into components is simpler in FD. In the lifetime-imaging spectroscopy the short acquisition time of the FD technique for the phase shift and the modulation ratio at a single frequency is a distinct advantage. The FD method is generally considered to offer better accuracy in the determination of multiple lifetimes.[207–209] The TD and FD methods have different advantages and disadvantages and are complementary techniques.

2 Aims of the Thesis

The overall aim of this thesis was to study lanthanide luminescence and lanthanide-based resonance energy transfer. An important part of the research was the assembly of two modular luminometers, a frequency-domain luminometer operating in the low-frequency domain (i.e. below 100 kHz) and a time-domain luminometer with an adjustable duration wide-pulse excitation.

The aim of publication **I** was to present the mathematical and instrumental techniques of the frequency-domain measurements in the low-frequency range. The emphasis of the mathematical part was in deriving the equations which link the frequency-domain instrument signal to the luminescence intensity and the lifetime information. The instrumental part of publication **I** describes the details of the modular frequency-domain luminometer assembled in our laboratory and the measurement strategy. The goal of the experimental results presented was to demonstrate the operation and the strengths of the luminometer.

In publication **II** the distance and temperature dependence in the non-overlapping and the conventional resonance energy transfer were studied. The aim was to establish the mechanism of the nFRET phenomenon. The temperature dependence was studied using the modular FD luminometer.

In publications **III** and **IV** the luminescence properties of up-converting nanoparticles based on the Yb–Er system were studied. The underlying aim was to develop up-converting phosphor nanoparticles with suitable properties to be used as donor labels in resonance energy transfer based assays. In these publications the frequency-domain methods were not used but the excitation was done by using relatively wide laser pulses in order to demonstrate the low rise time of the emission. In publication **III** phosphors with a ZrO2 host matrix were synthesized by the combustion method. The concentrations of the Yb(III), Er(III) and Y(III) dopants were varied and the effect on the intensity, on the wavelength and on the lifetime of the up-conversion luminescence was studied. In publication **IV** phosphors with a $NaYF_4$ host matrix and core–shell structure were synthesized by the co-precipitation method. The difference between the phosphors was the composition of the core and the shell i.e. the distribution of the Y(III), Yb(III) and Er(III) ions between the core and the shell. The goal was to prepare phosphor nanoparticles with the activator ion (erbium) in the shell layer combined with a high up-conversion luminescence intensity. Donor particles with the emitting ions located only in the shell layer would be advantageous because all donor emission would originate within the Förster distance to the acceptor labels.

The aim of publication **V** was to provide conclusive evidence concerning the non-radiative nature of the energy transfer with up-converting particle donors. The plan was to detect a decrease of the donor lifetime which would indicate the presence of the resonance energy transfer. For the measurements a sample configuration with a controlled proximity of the donor and acceptor fluorophores in aqueous solution was designed. The lifetime measurements were performed with the modular frequency-domain luminometer.

3 Experimental

3.1 Instruments

In the experimental work a modular FD luminometer, a modular TD luminometer and a modular up-conversion spectrometer were used. The optical part of all three modular systems was based on the same basic configuration presented inside the dashed box in Figure 9. The optical part consisted of the tubular excitation and emission chambers (Thorlabs, Inc., Newton, NJ) in the right-angle configuration. In the excitation chamber a shortpass or a longpass filter was used to ensure pure UV or NIR excitation, respectively. Likewise in the emission chamber a longpass or a shortpass filter was used to exclude the scattered UV or NIR excitation radiation, respectively. In the emission chamber also an interference filter with a suitable bandpass was used to select the emission wavelength. In both chambers lenses were used to focus the light. The sample chamber was an aluminium cube (Thorlabs). Three different sample holders were able to accommodate a short-cut NMR tube, a conventional cuvette or a capillary tube. NMR tubes and cuvettes were used with liquid samples and capillary tubes with powder samples. The NMR tube holder was made of aluminium and was equipped with a Peltier element for thermoelectric cooling/heating of the samples.

Frequency-Domain Luminometer

The frequency-domain luminometer was an essential part of the studies presented in publications **I**, **II** and **V**. A schematic representation of the constructed modular FD luminometer is shown in Figure 9. The heart of the system is a digital dual-phase lock-in amplifier (SR850, Stanford Research Systems, CA). The sine-wave modulation between 10 Hz and 100 kHz was generated by the internal frequency oscillator and the amplified signal was recorded by the phase-sensitive detector of the lock-in amplifier. For the modulation of the excitation source a DC bias was added to the sine-wave and the sum signal was fed into the excitation-source driver. In the case of the UV-LED excitation the driver was a simple operation amplifier circuit. With a NIR laser diode a commercial laser driver (WLD3343, Wavelength Electronics, Inc., Bozeman, MT) was used. The excitation source was either a UV-LED (T9H34C, Seoul Optodevice Co., Ltd) with a peak wavelength at 345 nm (15 nm FWHM) and a maximum optical power output ca. 0.2 mW (publications **I** and **II**) or a NIR laser diode (L9418-04, Hamamatsu Photonics, Hamamatsu City, Japan) providing a maximum of 1.2 W at 976 nm (1.5 nm FWHM) (publication **V**). The detector was a head-on type photomultiplier tube (R1464, Hamamatsu) with the spectral response extending to 850 nm. The photomultiplier signal was amplified in a high-speed current amplifier (DHPCA-100, Femto Messtechnik GmbH, Germany). The in-phase and out-of-phase components of the amplified signal were recorded with the phase-sensitive detector of the lock-in amplifier. The lock-in amplifier was connected to a personal computer with a GPIB interface for controlling the

instrument and collecting data by a program written in LabVIEW (National Instruments, Austin, TX).

A single measurement consisted of collecting the in-phase and out-of-phase signals at 200 frequencies divided equidistantly in the logarithmic scale between 10 Hz and 100 kHz. The used frequency range corresponds to the lifetime range from 16 ms to 1.6 μs. The range is appropriate for the studied lanthanide luminescence. The 200 modulation frequencies used offered a statistically satisfactory number of data points for a reliable fitting. The choice of the time constant and the time used to measure the signal of a single frequency were based on the signal strength and the noise level. The time constant and the delay values together with the number of the frequencies determined the total measurement time which typically was 15 to 30 minutes. The preliminary data processing and the actual fitting were performed with a computer program written in Visual Fortran 90 equipped with a DISLIN graphics package (www.dislin.de). The fitting theory and practice are discussed in Chapter 4.1. The theory and the instrumentation are also discussed in a chapter of a recently published volume of Springer Series on Fluorescence.[206]

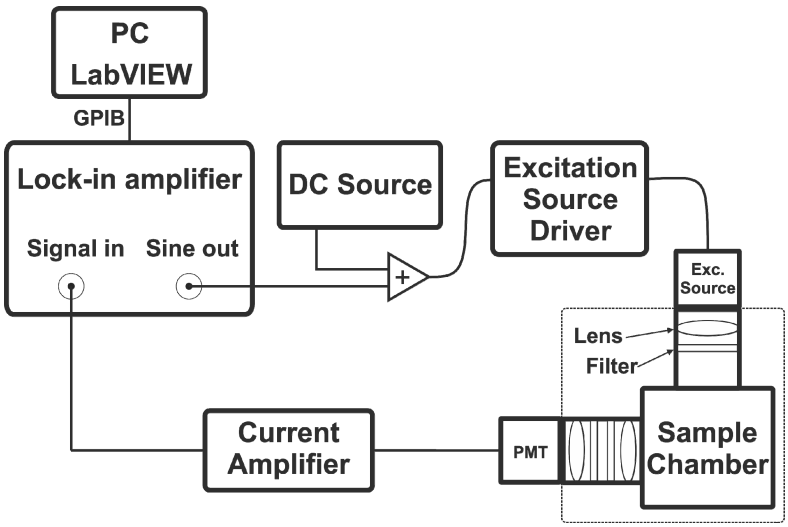

Figure 9. A schematic representation of the frequency-domain luminometer. The optical part of the system inside the dashed box was used also with the time-domain luminometer and the up-conversion spectroluminometer systems. PMT, photomultiplier tube; GPIB, general purpose interface bus.

Time-Domain Luminometer

In publications **III** and **IV** the luminescence lifetimes were measured with the modular wide-pulse time-domain luminometer. The excitation source of the TD luminometer was a fibre-coupled NIR laser diode providing a maximum of 1.3 W at 970 nm (FLMM-0980-711-1300m, Hi-Tech optoelectronic Co., Ltd., Beijing, China). The laser driver (WLD3343) and the photomultiplier tube (R928) were the same as in the FD luminometer. An analog-to-digital converter (NI USB-6251,

National Instruments, Austin, TX) was used to generate the square-wave excitation pulse for the laser driver and to record the output of the preamplified photomultiplier signal. The A/D converter was connected to a personal computer via USB and a computer program written in LabVIEW (National Instruments) was used to control the A/D converter. A LabVIEW program was also used to create the excitation pulse profile. The form and the duration of the excitation pulse were unrestricted. A typical pulse profile was a single excitation pulse (e.g. 5 ms) of constant height followed by a delay period (e.g. 95 ms). The pulse height in volts determined the laser diode current and hence the optical output power. The excitation power was kept low to avoid the saturation of the intermediate state and to ensure the luminescence rise time to be independent of the excitation power.[210] The adjustable length of the pulse and the measurement of the luminescence intensity during the pulse allowed studies of the luminescence rise time. The instrument recorded the full emission profile during every pulse. Hence, the measurements were fast and thousands of pulse-delay cycles could be collected within several minutes to improve the signal-to-noise ratio. The luminescence profiles were analyzed with the exponential decay fitting in Origin 8.0 (Originlab Corboration, Northampton, MA).

Up-Conversion Spectroluminometer

The up-conversion emission spectra were measured with the PC2000-CCD optical fibre spectrometer (Ocean Optics, Inc., Dunedin, FL). Bandpass filters were not used in emission chamber but the whole spectral range (300–870 nm) was recorded. The photomultiplier tube used with the FD and TD luminometers was replaced with an optical fibre connected to the spectrometer. The excitation source was the same fibre-coupled NIR laser diode (Hi-Tech optoelectronic Co.) as used in the TD luminometer. The laser diode was used in the constant current mode and the current was set manually from the panel of the laser driver (WLD3343). The OOIIrrad software (Ocean Optics, Inc.) was used to record the up-conversion emission spectra. The spectral response of the system was calibrated with the LS-1-CAL Calibrated Tungsten Halogen Light Source (Ocean Optics, Inc.).

3.2 Europium Chelates

The europium chelates used in the experimental work related to this thesis were the Eu(III) chelate of 2,2′,2′′,2′′′-{[4-[(4-isothiocyanatophenyl)ethynyl]pyridine-2,6-diyl]bis(methylene-nitrilo)}tetrakis(acetate)[88,211] (**1**), the Eu(III) chelate of 2,2′,2′′,2′′′-{[2-(4-isothiocyanatophenyl)-ethylimino]-bis(methylene)bis{4-{[4-(α-galactopyranoxy)phenyl]ethynyl}-pyridine-2,6-diyl}bis(methylenenitrilo)}tetrakis(acetate)[79] (**2**) and the Eu(III) chelate of 2,2′,2′′,2′′′-{{4′-{4′′′-[(4,6-dichloro-1,3,5-triazin-2-yl)amino]phenyl}-2,2′:6′,2′′-terpyridine-6,6′′-diyl}-bis(methylenenitrilo)}tetrakis(acetate)[90] (**3**). The molecular structures of the Eu(III) chelates are shown in Figure 10. Dashed lines are drawn between the liganding atoms and the central Eu(III) ion. Compound **1** is a heptadentate and compounds **2** and **3** are nonadentate chelates. The energy-absorbing chromophore(s) in compounds

1 and **2** is a 4-(phenylethynyl)pyridine moiety and a terpyridine moiety in compound **3**. The functional group intended for binding the chelates to target molecules is an isothiocyanato group in compounds **1** and **2** and a dichlorotriazine group in compound **3**. The lanthanide quantum yields (Q_{Ln})[151] were determined for the three europium chelates in aqueous solution. The obtained values of Q_{Ln} were 0.184 ± 0.004, 0.603 ± 0.003 and 0.854 ± 0.026 for compounds **1**, **2** and **3**, respectively (publication **II**).

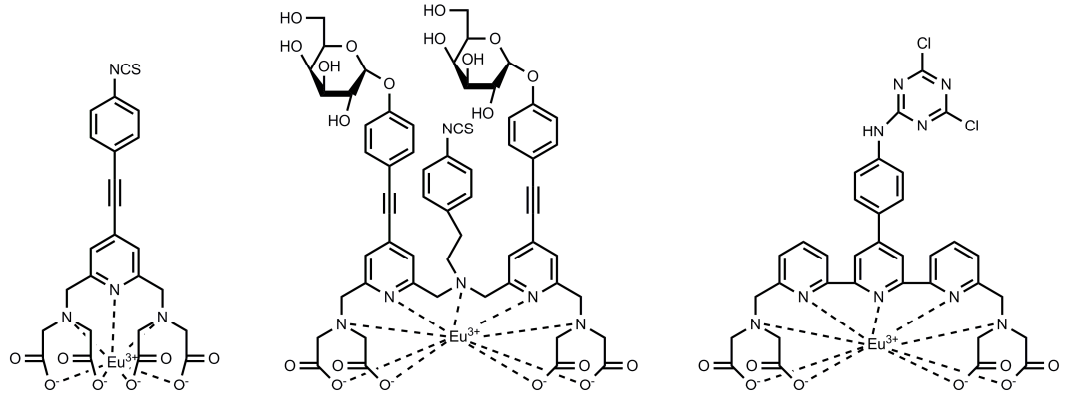

Figure 10. The molecular structures of the Eu(III) chelates.

3.3 Up-Converting Phosphors

The up-converting phosphors used in the experimental work were synthesized within the research projects. The phosphors based on the ZrO_2 host matrix doped with Yb(III), Er(III) and Y(III) (publication **III**) were synthesized by the combustion method.[132] The precursor materials were aqueous solutions of zirconyl, ytterbium, erbium and yttrium nitrates. Semicarbazide was used as a fuel and ammonium nitrate as an oxidizer. The molar concentrations of the dopants were controlled by the volumes of the respective lanthanide nitrates used in the combustion reaction. The phosphors based on the $NaYF_4$ host matrix doped with Yb(III) and Er(III) (publication **IV**) were synthesized by the co-precipitation method.[212] The precursor materials were aqueous solutions of sodium fluoride and yttrium, ytterbium and erbium chlorides. The volumes of the lanthanide chloride solutions determined the molar concentrations of the lanthanides in the particles. Five different $NaRF_4$–$NaR'F_4$ (R: Y, Yb, Er) core–shell combinations were prepared. The shell layer was prepared by mixing the core particles into a second co-precipitation solution. The core–shell particles were annealed at 600 °C for five hours under a static $N_2 + H_2$ (90:10) gas sphere.

4 Results and Discussion

4.1 Frequency-Domain Measurements of LRET

Both the frequency-domain methods as well as the time-domain methods are commonly used to measure the prompt fluorescence of organic and biological compounds. However, in the case of the long-lived lanthanide luminescence the TD methods prevail. The scarce utilization of the FD methods in the field of the lanthanide luminescence stems from the lack of suitable instruments. In the FD methods the modulation frequency of the excitation source must correspond to the time scale of the measured lifetimes. The frequency range of the majority of the commercial FD instruments is optimized for the nanosecond to picosecond timescale of the organic and biological compounds. The basic principle of the FD methods was presented in Chapter 1.7. The suitable frequency range for the nanosecond lifetimes is from tens to hundreds of megahertz. The cross-correlation technique is used to shift the detection frequency to a lower frequency (10–100 Hz) at which the accurate measurement of the phase-shift and the modulation ratio is easier.[106] The measurement range of the long-lived lanthanide luminescence should extend to at least 10 Hz at the low frequency end. This is not within the measurement range of the majority of the commercial FD instruments. Furthermore, the cross-correlation technique would result in a detection frequency below 10 Hz. At frequencies below 10 Hz long time constants are needed and the time required for a single measurement would be overly long. The lifetimes of the lanthanide compounds generally fall within the range of 16 ms to 1.6 μs which in FD corresponds to the frequency range of 10 Hz to 100 kHz. This frequency range can be accurately detected by inexpensive digital lock-in amplifiers and there is no need for the cross-correlation technique. We have constructed a modular FD luminometer for the measurements in the low-frequency domain below 100 kHz. The luminometer is based on the FD principle of the sine-wave modulated excitation and the detection of the emission signal that follows the frequency of the excitation modulation (Figure 8, p. 40). The FD principle was discussed in Chapter 1.7. However, instead of the phase-shift and the modulation ration, the in-phase and out-of-phase signals of the dual-phase lock-in amplifier are measured. Also the equations used for the fitting are different from the common FD equations presented in Chapter 1.7. The instrument and the mathematical derivation of the equations linking the in-phase and out-of-phase signals of the lock-in amplifier to the luminescence intensity and the decay times have been presented in publication **I** and in reference [206]. The components of the instrument are described in detail in Chapter 1. The theory of the method, the measurement strategy and the experimental results of the system are reviewed in this chapter.

The heart of the system is a digital dual-phase lock-in amplifier. The sine-wave modulation between 10 Hz and 100 kHz is generated by the internal oscillator and the amplified emission signal is recorded by the phase-sensitive detector of the lock-in amplifier. The excitation source is a light emitting diode in the ultraviolet wavelength or a laser diode in the near-infrared range. The intensity of these excitation sources is conveniently modulated by modulating the current of the

diodes. The optical part of the instrument consists of the tubular excitation and emission chambers equipped with suitable filters. A photomultiplier tube is used as a detector. The preamplified signal from the photomultiplier is taken directly into the lock-in amplifier input without a cross-correlation process. The signals recorded by the dual-phase lock-in amplifier at a single frequency are the in-phase (S_x) and the out-of-phase (S_y) components of the signal.

$$S_x = V_{sig} \cos\theta \tag{24}$$

$$S_y = V_{sig} \sin\theta \tag{25}$$

In Equations 24 and 25 V_{sig} is the signal amplitude and θ is the phase shift between the signal and the reference oscillator. For a sinusoidal modulation the equations linking the in-phase and out-of-phase signals to the luminescence lifetimes and the relative amplitudes were derived in publication **I.**

$$S_x(\omega) = \sum_{k=1}^{N} \frac{h_k \tau_k}{1+\omega^2 \tau_k^2} \tag{26}$$

$$S_y(\omega) = -\sum_{k=1}^{N} \frac{h_k \omega \tau_k^2}{1+\omega^2 \tau_k^2} \tag{27}$$

Here $S_x(\omega)$ and $S_y(\omega)$ are the in-phase and out-of-phase signals as the functions of the angular reference frequency (ω), respectively. N is the number of discrete lifetimes, h_k is the amplitude factor and τ_k is the corresponding lifetime. The values of h_k and τ_k are obtained by minimizing the sum of squares written as

$$\chi^2 = \sum_{k=1}^{N} \left\{ \frac{1}{\sigma_{x,k}^2} \left[S_x^{obs}(\omega_k) - S_x^{calc}(\omega_k) \right]^2 + \frac{1}{\sigma_{y,k}^2} \left[S_y^{obs}(\omega_k) - S_y^{calc}(\omega_k) \right]^2 \right\} \tag{28}$$

Here ${\sigma_{x,k}}^2$ and ${\sigma_{y,k}}^2$ are the variances, ${S_x}^{obs}$ and ${S_y}^{obs}$ the observed and ${S_x}^{calc}$ and ${S_y}^{calc}$ the calculated signals respectively. As discussed later, in many cases only the out-of-phase signals are included in the sum. The variances for each data point are obtained by smoothing the observed data by the second-order Savitzky–Golay method and estimating the deviations between the observed and the smoothed data within the neighbouring 22 points. The figure-of-merit function χ^2 is minimized by finding the best parameters for $S^{calc}(\omega)$. The observed signals ($S^{obs}(\omega)$) used in the calculation are not the in-phase ($S_x^{raw}(\omega)$) and the out-of-phase ($S_y^{raw}(\omega)$) signals recorded by the lock-in amplifier but the signals compensated for the instrumental deviations. Systematic deviations in the gain and the phase shift may be induced into the data depending on the frequency range and the quality of the instrument. These instrumental deviations can be compensated by measuring the signals

($S_x^{comp}(\omega)$ and $S_y^{comp}(\omega)$) for a sample which does not induce phase shifts within the measurement range. In practice this means a fluorescent sample with a notably short lifetime compared to the frequency range of the measurement or a non-fluorescent colloidal sample in which case the scattered excitation radiation is measured. We have used fluorescein or colloidal silica. The compensation is easily accomplished by a complex division of the unprocessed signal (S^{raw}) by normalized compensation signal (S^{comp}) (Eq. 29). The normalization factor is the quadratic mean (root mean square) of S^{comp} within the frequency range. This is a simpler process than the deconvolution of the decay profile of the time-domain measurement.

$$S_x^{obs}(\omega_k) + jS_y^{obs}(\omega_k) = \frac{S_x^{raw}(\omega_k) + jS_y^{raw}(\omega_k)}{S_x^{comp}(\omega_k) + jS_y^{comp}(\omega_k)} \qquad (29)$$

In the lanthanide luminescence experiments also prompt fluorescence may be present due to the autofluorescence and the direct excitation of the organic acceptor fluorophores. Then the emission signal is a sum of two sine waves. The prompt fluorescence in the nanosecond time scale has a negligible phase shift below 100 kHz. Therefore, the out-of-phase signal (Eq. 25) of the prompt fluorescence with the term $sin\theta$ tends to zero, and the prompt fluorescence contribution is observed only in the in-phase signal. Hence, by fitting only the out-of-phase signal the influence of the prompt fluorescence can be eliminated. Also electrical interference can have a non-negligible influence in the in-phase signal which likewise is eliminated by using only the out-of-phase signal. The decision of using only the out-of-phase signal is based on the Kramers–Kronig relation (Eq. 30).[213]

$$S_x^{K-K}(\omega) = -\frac{2}{\pi} P\int_0^{\infty} \frac{\omega' S_y^{obs}(\omega')}{\omega'^2 - \omega^2} d\omega' \qquad (30)$$

In Equation 30 P is the Cauchy principal value of the integral which has a singularity at $\omega' = \omega$ and ω' is a real-valued integration variable (see the supporting information of publication **I**). The $S_x^{K-K}(\omega)$ signal calculated from the $S_y^{obs}(\omega)$ signal is graphically compared to the $S_x^{obs}(\omega)$ signal. If the $S_x^{obs}(\omega)$ and $S_x^{K-K}(\omega)$ curves overlap, both the $S_x^{obs}(\omega)$ signal and the $S_y^{obs}(\omega)$ signal can be used for the fitting. Otherwise only $S_y^{obs}(\omega)$ should be used. Examples of the K–K transforms are presented in Figure 11. In the case of the sample containing only the Eu(III) chelate the observed in-phase data and the K–K transformed data overlap almost perfectly. In the case of the sample containing the Eu(III) chelate and the organic acceptor the discrepancy between the curves is immense and only the out-of-phase data should be used in the fitting. The reason is the direct excitation of the organic acceptor which results in the acceptor emission with a nanosecond lifetime contributing only to the in-phase signal in the frequency range of the measurement. According to Equation 30 the in-phase and out-of-phase signals are not independent. Hence, in principle no information is lost if only the out-of-phase signal is used for fitting. However, the additional data

points of the in-phase signal offer statistical advantage and should be used in the absence of the in-phase interference. The use of the Kramers–Kronig relation requires a reasonably high density of data points. Also for an accurate determination of the lifetimes, it is statistically advantageous to measure the sample signal at as many modulation frequencies as possible within the relevant frequency range and a realistic time period. We have used a set of 200 frequencies between 10 Hz and 100 kHz distributed equidistantly in the logarithmic scale. Depending on the choice of the time constants and the delay times the measurement of the whole frequency range takes from 15 to 30 minutes.

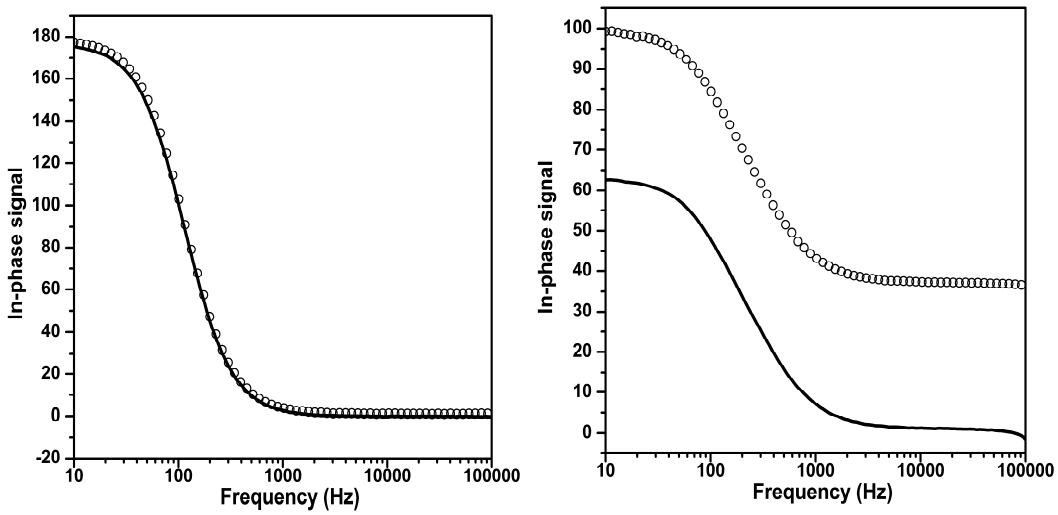

Figure 11. The observed in-phase signals (open circles) and the Kramers-Kronig transforms of the corresponding out-of-phase signals (solid lines) of the donor-only (left) and the donor–acceptor (right) samples. For visual clarity, only every third data point of the observed signal is shown. Emission detected at 615 nm with the excitation at 345 nm. The donor is a Eu(III) chelate (compound **3** in Figure 10, p. 47) and the acceptor is AF532. The samples were based on a DNA-hybridization reaction between the donor labelled capture oligonucleotides and the unlabelled (donor-only sample) or the acceptor labelled (donor–acceptor sample) tracer oligonucleotides. A more detailed description of the samples is given in Chapter 4.2 and in publication **II**.

A five-state Eu(III) chelate system was used as an experimental example in publication **I**. The energy levels included were the ^7F_J, $^5D_2$, $^5D_1$ and $^5D_0$ states of the Eu(III) ion and the triplet state of the ligand. An extensive mathematical derivation was presented. The starting point was a set of linear differential equations of the excited-state processes of the Eu(III) chelate. As a result equations for the photochemical rate processes of the system were obtained. The experimental results demonstrated the capability of the FD technique as a powerful method for the accurate determination of the lifetimes and the intensity of the lanthanide luminescence. The Eu(III) chelates used in the experiments were compounds **1** and **2** presented in Figure 10 (p. 47).

In the case of a single lifetime the S_y signal (Eq. 27) has a maximum at $\omega = \tau^{-1}$. In the logarithmic frequency scale the shape of the S_y signal is symmetrical and the width at the half-maximum is

$\log(7+4\sqrt{3}) \approx 1.144$. The out-of-phase signal of the luminescence of 10^{-7} M aqueous solution of compound **2** at 615 nm is presented in Figure 12. An excellent fitting was obtained with a single lifetime giving τ = 1023 μs. The symmetrical shape, the FWHM value and the position of the maximum predicted by the theory are all present.

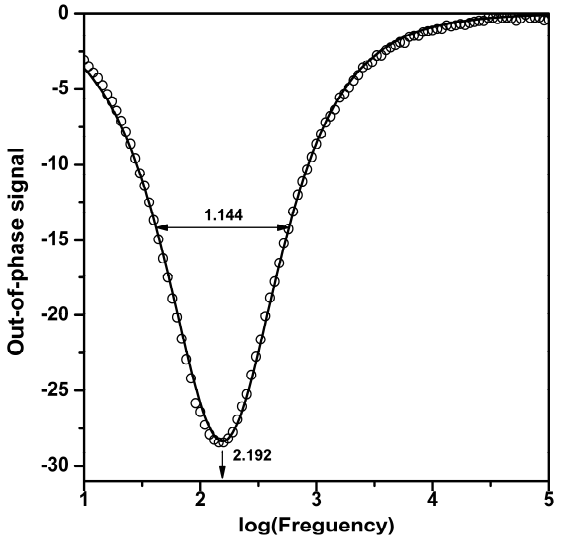

Figure 12. The out-of-phase signal of the luminescence of 10^{-7} M aqueous solution of compound **2** at 615 nm. The circles are experimental data points and the solid line is the calculated fitting giving a lifetime of 1023 μs. For visual clarity, only every second data point of the observed signal is shown. The width at the half-height is 1.144. The position of the maximum is 2.192 $\rightarrow f$ = 155.6 Hz $\rightarrow \omega$ = 977.6 $\rightarrow \tau$ = 1023 μs. These values are consistent with the theory.

The power of the FD method in determining the lifetimes of the lanthanide compounds was demonstrated by calculating the number of the water molecules in the first coordinating sphere of the Eu(III) ion. The FD signals of compounds **1** and **2** in H_2O and in D_2O were measured. From the obtained lifetimes the number of the water molecules was calculated with Equations 1 and 2 (p. 17) with $k_{XH} = \alpha$ (Table 2).[87] The values obtained for compounds **1** and **2** were 2.04 and -0.03, respectively. These values are in an excellent agreement with the known denticities of seven and nine for compounds **1** and **2**, respectively.

Table 2. The luminescence lifetimes in H_2O and D_2O and the calculated number of the coordinated water molecules in H_2O for compounds **1** and **2**.

Compound	$\tau(H_2O)$ (ms)	$\tau(D_2O)$ (ms)	$q(H_2O)$
1	0.378	2.017	2.04
2	1.023	1.436	-0.03

In publication **I** a special interest was focused on the rate constants of the non-radiative relaxation $^5D_1 \rightarrow {}^5D_0$ and the thermally induced back-transfer $^5D_0 \rightarrow {}^5D_1$ assigned respectively by k_{21} and k_{12}. The connection between the rate constants and the amplitudes of emission lifetimes was derived.

$$\alpha \cong \frac{h_1^{(2)}}{h_2^{(2)}} \cong \frac{k_{12}}{k_{21}} = 3\exp\left(-\Delta E/k_B T\right) \qquad (31)$$

Here $h_1^{(2)}$ and $h_2^{(2)}$ are the amplitudes of the two lifetimes and the superscript (*2*) denotes the radiative transition from the $^5D_1$ state. Due to the thermal non-radiative nature of the process, the ratio of the rate constants can be written as the Boltzmann distribution (the right hand site of Equation 31).[54] The term ΔE is the energy difference between the states $^5D_0$ and $^5D_1$, k_B is the Boltzmann constant and T is the temperature. The factor 3 comes from the degeneracy of the state $^5D_1$ compared to the degeneracy of the state $^5D_0$. Hence, ΔE can be calculated from the results of the FD measurement. We measured the emission of the 10^{-4} M solution of compound **2** in H_2O. The emission wavelength was 540 nm corresponding to the $^5D_1 \rightarrow {}^7F_1$ transition and the luminescence was measured at seven temperatures ranging from 3°C to 63°C. The S_y^{obs} and S_y^{calc} signals of these measurements are shown in Figure 13.

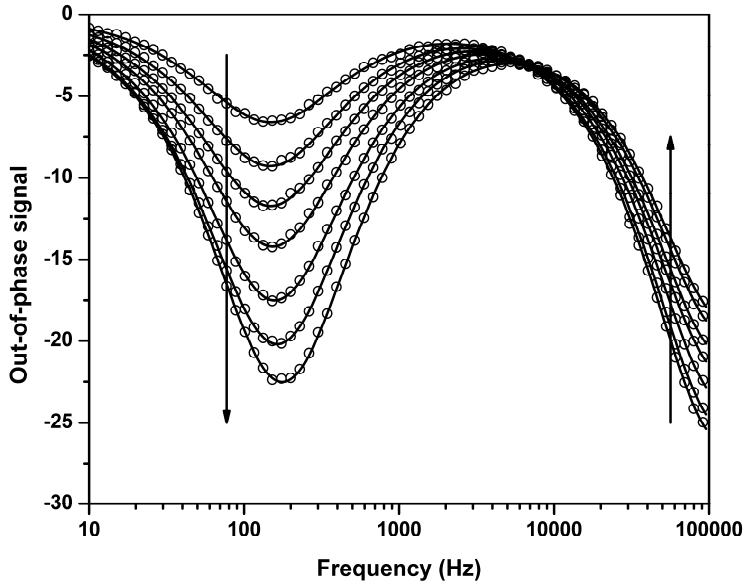

Figure 13. The effect of the temperature on the out-of-phase signal of compound **2** in 10^{-4} M aqueous solution. Emission wavelength 540 nm. The temperatures are given in Table 3. The arrows indicate the direction of the increasing temperature. The circles are the compensated experimental points (S_y^{obs}) and the solid lines the calculated fitting for two lifetimes (S_y^{calc}). For visual clarity, only every third data point of the observed signals is shown.

The S_y^{calc} signals were calculated for two lifetimes (Table 3). By rearranging Equation 31, a linear relation for $k_B\ln(\alpha/3)$ vs. $1/T$ with ΔE as the slope is obtained. The data from Table 3 is plotted in Figure 14. The line is a linear regression fit through the origin. The slope of the line, i.e. ΔE, is 1760 ± 5 cm^{-1} (95% confidence). The same energy difference can be estimated from the emission spectrum as the separation between the $^5D_1 \rightarrow {}^7F_1$ and $^5D_0 \rightarrow {}^7F_1$ transitions. The value ΔE = 1758 cm^{-1}

was calculated from the emission spectrum of compound **2** (Figure 15). The accurate value of ΔE has been known for decades.[40] However, the way we obtained this value is a display of the power of the FD method. The data were obtained with a single sample at a single wavelength. This would be difficult with the TD methods because the different relation of the intensity to the amplitude factors and the lifetimes. In the TD methods the signal strength is determined by the amplitude factors whereas in the FD methods it is determined by the product of the amplitude and the lifetime. The value of the ratio $h_1^{(2)}/h_2^{(2)}$ is very small for the luminescence of compound **2** at 540nm (Table 3). Considering the low intensity of the $^5D_1 \rightarrow {}^7F_1$ emission the decay curve corresponding to the lifetime τ_1 will be buried in noise. However, the magnitude of the ratio $(h_1^{(2)} \cdot \tau_1)/(h_2^{(2)} \cdot \tau_2)$ allows the measurement of both lifetimes with the FD method.

Table 3. The fitting results of the out-of-phase signals of compound **2** in 10^{-4} M aqueous solution presented in Figure 13. Emission wavelength 540 nm.

Temperature (K)	τ_1 (μs)	τ_2 (μs)	$\alpha = h_1^{(2)}/h_2^{(2)}$	$(h_1^{(2)} \cdot \tau_1)/(h_2^{(2)} \cdot \tau_2)$
276.8	1078 ± 3	1.32 ± 0.01	$3.06 \cdot 10^{-4}$	0.25
287.2	1087 ± 2	1.30 ± 0.01	$4.40 \cdot 10^{-4}$	0.37
297.2	1076 ± 2	1.28 ± 0.01	$5.90 \cdot 10^{-4}$	0.50
307.1	1045 ± 2	1.28 ± 0.01	$7.90 \cdot 10^{-4}$	0.64
316.8	1012 ± 1	1.26 ± 0.01	$10.40 \cdot 10^{-4}$	0.84
326.2	976 ± 1	1.23 ± 0.01	$13.10 \cdot 10^{-4}$	1.02
335.8	904 ± 1	1.22 ± 0.01	$16.20 \cdot 10^{-4}$	1.20

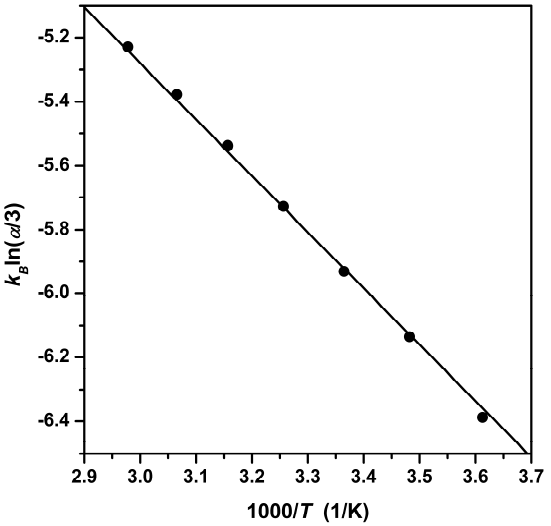

Figure 14. The linear regression fit of $k_B \ln(\alpha/3)$ vs. $1/T$ forced through the origin. The parameter α is defined in Equation 31. The units of k_B and T are cm^{-1}/K and K, respectively. The slope of the line is 1760 ± 5 (95% confidence) and is equal to ΔE.

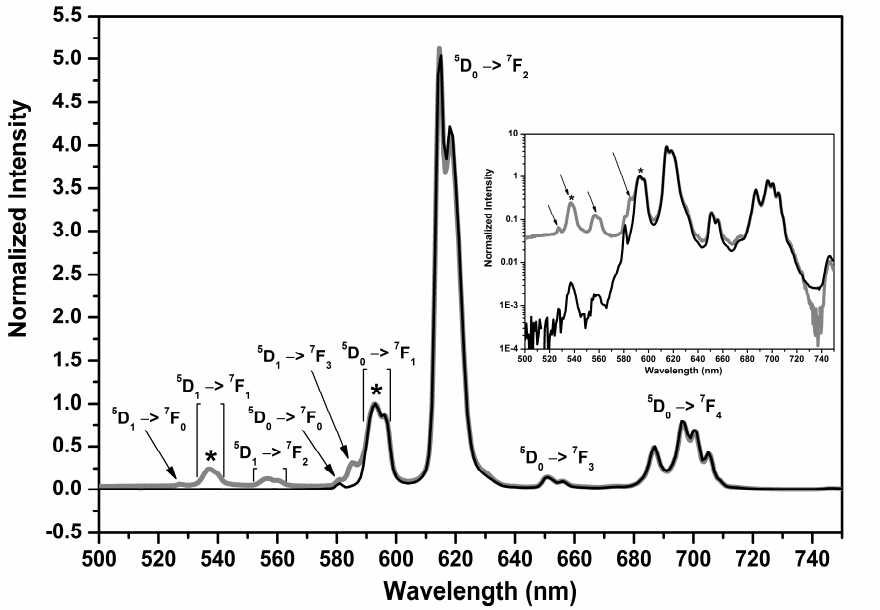

Figure 15. The fluorescence spectrum (thick grey line) and the time-resolved fluorescent spectrum (thin black line, delay 100 μs, gate 10 ms) of compound **2**. The stars indicate the $^5D_1 \rightarrow {}^7F_1$ (537 nm) and $^5D_0 \rightarrow {}^7F_1$ (593 nm) transitions giving $\Delta E(^5D_1 - {}^5D_0) = 1758$ cm^{-1}. Inset: the same spectra in the logarithmic intensity scale with arrows indicating the $^5D_1 \rightarrow {}^7F_J$ transitions. The assignment of the transitions according to reference [40].

The main purpose of publication **I** was to present the FD instrumentation and the mathematic treatment of the FD data. Hence, the aim of the experimental results presented above was not to offer new chemical information, but to demonstrate the capabilities of the FD luminometer as a tool in lanthanide luminescence research. The comparison of the FD and TD methods reveals that the two methods have their strengths in different application areas (Chapter 1.7). We have used both the FD method and the TD method in lanthanide luminescence research. Instruments were assembled in our laboratory and aimed particularly for the measurements in the lifetime range of the lanthanide luminescence. The main advantage of the TD instrument was the measurement of the emission signal against a dark background allowing the detection of very low emission signals. Another benefit of the TD instrument was a shorter measurement time compared to the FD instrument. The adjustable duration of the excitation pulse allowed the detection of the slow rise time of the UCP emission. The TD method was used to measure the luminescence lifetimes of the UCP particles (publications **III** and **IV**) and the results are discussed in Chapter 4.3. The FD instrument was designed for the measuring of the lanthanide luminescence lifetimes between 1.6 μs and 16 ms. In the FD method the rise time of the emission was observed as a lifetime component with a negative amplitude. The attraction of the FD methods stems from the good resolution of multiexponential intensity decays.[207–209] Hence, the FD method was our choice in the LRET research, since multiple lifetimes were expected (publications **II** and **V**). The developed measurement strategy and the data analysis of the FD method provided a facile elimination of the

instrumental interference and the background due to the prompt fluorescence. The weighting of the experimental data is different in the FD and TD methods as discussed above in the context of the $^5D_1 \rightarrow {}^7F_1$ transition emission. The conclusion is that neither of the methods is superior but the two methods are complementary and the method of choice depends on the studied system.

4.2 Distance and Temperature Dependency of nFRET

The non-overlapping FRET (nFRET) phenomenon has been reported with europium and samarium chelate donors.[24–26] The term non-overlapping refers to the absence of the spectral overlap between the acceptor absorbance spectrum and the main emittive transitions of the lanthanide chelates. The absence of the spectral overlap in nFRET is a notable difference compared to the conventional FRET in which a high spectral overlap is a prerequisite. The different mechanism is manifested in the experimental lifetimes of the nFRET samples. The experimental lifetimes differ from the theoretical lifetimes calculated with the Förster equations. Also the efficiency of the Sm(III) donor based nFRET is significantly higher than expected for this low quantum yield donor by the FRET theory. The proposed mechanism of nFRET involves excited energy levels above the main emitting level of the trivalent lanthanide ions. The $^5D_2$ and $^5D_1$ levels in the case of Eu(III) and the $^4G_{7/2}$ level in the case of Sm(III). The conclusive proof of the mechanism is still lacking. In the previous reports it was established that nFRET requires a close proximity between the donor and acceptor species. The nFRET operating distance of 20 Å suggested an energy transfer process based on the dipole–dipole interactions. Preliminary tests with varying D–A distances were also referred but the data was not published.[25] According to these unpublished results the effective range of nFRET is shorter than the range of FRET.

In publication **II** we conducted systematic studies on the distance and temperature dependencies of both the nFRET and the conventional FRET processes. We controlled the D–A distance by a homogeneous DNA-hybridization reaction between the complementary capture and tracer oligonucleotides labelled with an Eu(III) chelate donor and an organic fluorophore acceptor, respectively. The seven different donor–acceptor distances were obtained by varying the conjugation position of the acceptor label on the tracer oligonucleotide. The used donor–acceptor distances were 1.4, 4.1, 4.7, 6.7, 7.9, 9.8 and 12.0 nm. The helical structure of the DNA was taken into account on the calculation of the donor–acceptor distances.[193] The hybridization reaction between an unlabelled oligonucleotide and complementary labelled capture or tracer oligonucleotides was used to prepare the donor-only or the acceptor-only samples, respectively. For the background measurements radiative energy transfer samples were realized by a mixture of the labelled capture, the labelled tracer and a 30-fold molar excess of the unlabelled tracer oligonucleotides. The donor–acceptor pair with the longest donor–acceptor distance (12.0 nm) was used in the background sample to minimize the non-radiative signal. Due to the low concentrations (< 20 nM) used, the amount of the diffusion-enhanced non-radiative energy transfer was negligible and the radiative background could be determined. Since the europium chelates, the acceptor dyes

and the oligonucleotide chains are all negatively charged, the close proximity due to diffusion was further minimized by the charge repulsion. Three europium chelates (compounds **1**, **2** and **3**, Figure 10, p. 47) were used as the donor labels. Three Alexa Fluor dyes (AF) were chosen to represent pure nFRET (AF532), pure FRET (AF680) and mixed nFRET–FRET (AF546) acceptors. The classification of the acceptors was based on the extent of the spectral overlap of the acceptor absorbance with the $^5D_0 \rightarrow {}^7F_J$ transitions of the europium chelates (Figure 2. in publication **II**). The overlap with the AF546 was very minor and for the sake of simplicity in text it is referred to as an nFRET acceptor. This is justified also on the basis of the results which were similar to the results obtained with pure the nFRET acceptor, the AF532.

The energy transfer efficiency as a function of the donor–acceptor distance was measured by a Victor 1420 Multilabel Counter (Wallac Oy). The triplicate measurements were made in microtitration wells. In all cases the excitation wavelength was 340 nm. The Eu(III) chelate emission was measured at 615 nm with a 400 μs delay and a 400 μs gate time. The sensitized emission of the AF532 and the AF546 was measured at 560 nm and the AF680 at 730 nm. In the sensitized acceptor emission measurements a 60 μs delay and a 50 μs gate time were used with all the acceptors. In the absence of a mathematical model for the nFRET mechanism, the Förster equations were used to calculate the energy transfer efficiencies for both the nFRET and FRET samples. The theoretical efficiencies were calculated from the experimental spectral overlap including all $^5D_1/^5D_0 \rightarrow {}^7F_J$ transitions of europium by using Equations 7 and 11 (pp. 26 and 27). The experimental efficiencies were calculated from the measured emission intensity of the Eu(III) chelate donor in the absence and in the presence of the acceptor by using Equation 10 (p. 26). The experimental Förster distances were calculated from the experimental efficiency values by fitting the experimental results to Equation 11. The total energy transfer efficiencies (Q_{tot}) representing the maximal donor quenching as a result of the energy transfer were determined from the same fit. The maximum signal-to-background ratio was determined by comparing the sensitized acceptor emission signals of the positive sample (hybridization reaction of the labelled oligonucleotides only) and the background sample (hybridization reaction with the excess of the unlabelled tracer oligonucleotide). The results for compound **3** are presented in Table 4 and Figure 16. The results with the two other donors were similar (Table 2 and Figure 3 in publication **II**). The small differences between the used donor oligonucleotides is partly explained by variation in the small amount of the free europium chelate remaining in the fractions after HPLC-purification.

Table 4. The experimental and theoretical results of the non-radiative energy transfer between the chelate **3** and different acceptors. The experimental (exp. R_0) and theoretical (theor. R_0) Förster distances, the spectral overlap (J), the maximum signal-to-background ratio (max S/B) and the total energy transfer efficiency (exp. Q_{tot}).

Acceptor	exp. R_0 (nm)	theor. R_0 (nm)	J ($M^{-1}cm^{-1}nm^4$)	max S/B	exp. Q_{tot} (%)
AF532	4.3	2.5	1.57×10^{13}	126	87
AF546	4.6	3.4	1.02×10^{14}	1123	83
AF680	7.7	7.6	1.15×10^{16}	125	79

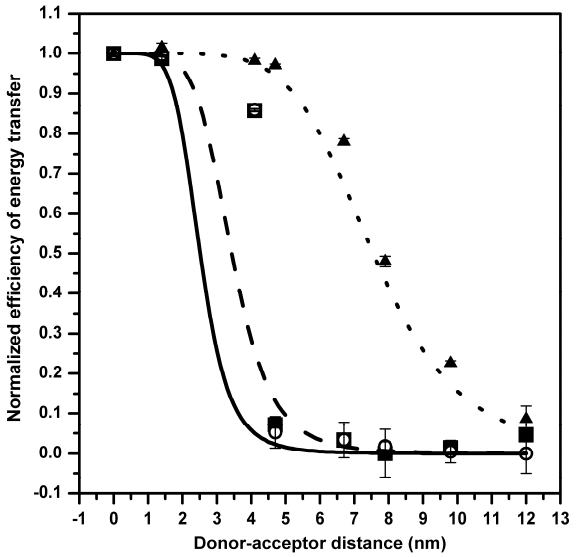

Figure 16. The theoretical (lines) and the experimental (symbols) energy transfer efficiencies as a function of the donor–acceptor distance for the energy transfer between compound **3** and different acceptors. The acceptors were AF532 (solid line, square), AF546 (dashed line, circle) and AF680 (dotted line, triangle). The error bars represent the standard deviation between three replicate reactions.

In Table 4 the order of the theoretical R_0 values follows the order of the spectral overlaps. The order of the experimental R_0 values is the same. The agreement between the theoretical and the experimental values is fairly good for the conventional FRET acceptor (AF680). But for the two other acceptors the experimental R_0 values are notably higher than the corresponding theoretical R_0 values. The results indicate that the efficiency of the nFRET process is greater than estimated by the Förster model. The same conclusion can be reached by comparing the theoretical curves and the experimental points in Figure 16. The experimental efficiency with the AF532 and the AF546 acceptors at the distance of 4.1 nm is far above the theoretical curve. The shorter effective distance of the nFRET process compared to the conventional FRET process is evident in Figure 16. Unfortunately the donor–acceptor distance range obtained by the used tracer oligonucleotides was designed for the conventional FRET pairs and was not optimal for the AF532 and AF546. None of the experimental distances was close to the R_0 value of the AF532 or the AF546.

The advantage of the low background signal of the nFRET assay is manifested in the difference of the maximum signal-to-background ratios of the AF546 and the AF680 (Table 4). The low signal-to-background ratio of the AF532 is a result of the used measurement parameters. The short lifetime component with a high relative amplitude of the sensitized AF532 emission (τ_1 in Table 5) decays mainly during the used delay time of 60 μs.

The FD method was used to study the temperature dependence of the lifetimes of the nFRET and FRET processes. The FD luminescence response was measured at 200 frequencies divided equidistantly in the logarithmic scale between 10 Hz and 100 kHz. The hybridization reactions

contained 100 nM of the labelled capture oligonucleotide and 150 nM of the labelled or unlabelled tracer oligonucleotide. Compound **3** was selected to act as the donor label based on the highest luminescence intensity of the three chelates. The tracer oligonucleotides used were selected so that the induced donor–acceptor distance would result in a high intensity of the sensitized acceptor emission and that the sensitized acceptor emission lifetimes would be in the measurement range. With the nFRET acceptors (AF532 and AF546) the donor–acceptor distance was 4.1 nm and with the FRET acceptor (AF680) the distance was 6.7 nm. The excitation wavelength was 345 nm and the luminescence was measured at 560 nm (AF532 and AF546), 730 nm (AF680) or 615 nm (unlabelled tracer oligonucleotide). In Figure 17 the experimental out-of-phase signals and the calculated fitting of the luminescence from the hybridization reactions at different temperatures are shown as a function of the modulation frequency. The corresponding calculated lifetimes are shown in Table 5. The FD data was best fitted with two lifetimes, except in the case of the AF546 for which the best fit was obtained with three lifetimes. It is possible that also the AF532 had a third lifetime which was buried in the noise due to the low signal level and not distinguished in the fitting. The donor-only sample had a second very minor lifetime component (604–156 μs, relative amplitude of 0.3–4 %) not shown in Table 5. The origin of this lifetime component is probably some minor impurity in the sample.

Table 5. The fitted lifetimes for the luminescence of the hybridization reactions. The donor label was compound **3** in all reactions. The excitation wavelength was 345 nm and emission was detected at 560 nm (AF532/AF546), at 730 nm (AF680) or at 615 nm (donor-only sample with unlabelled tracer oligonucleotide). The donor–acceptor distance was 4.1 nm with the AF532 and AF546 acceptors and 6.7 nm with the AF680 acceptor. The corresponding experimental and fitted data are shown in Figure 17.

T (°C)	AF532[a]		AF546[b]			AF680[c]		D-only[d]
	τ_1 (μs)	τ_2 (μs)	τ_1 (μs)	τ_2 (μs)	τ_3 (μs)	τ_1 (μs)	τ_2 (μs)	τ_1 (μs)
5	0.65±0.03	719±6.4	0.52±0.02	138±4.4	482±3.4	81±6.9	366±2.4	1441±1.9
15	0.67±0.02	466±4.4	0.59±0.04	97±2.5	352±2.1	84±5.4	366±2.4	1423±2.1
25	0.69±0.03	270±3.5	0.56±0.05	68±1.5	244±1.5	87±7.5	365±3.4	1382±1.4
35	0.65±0.03	160±2.5	0.70±0.05	49±1.4	164±1.4	72±6.1	356±2.6	1331±0.9
45	0.76±0.03	97±1.6	0.66±0.05	35±1.0	109±1.1	81±5.9	347±3.0	1256±0.7
55	0.65±0.05	56±1.0	0.57±0.10	26±0.8	72±1.0	73±7.3	333±4.2	1154±1.2

[a] the relative amplitudes for τ_1 and τ_2 were approximately 80% and 20%, respectively
[b] the relative amplitudes for τ_1, τ_2 and τ_3 were approximately 30%, 15% and 55%, respectively
[c] the relative amplitudes for τ_1 and τ_2 were approximately 10% and 90%, respectively
[d] there was also a minor second lifetime component (604–156 μs, relative amplitude 0.3–4%)

In Figure 17 a clear shift of the out-of-phase signal maximum towards higher frequencies (shorter lifetimes) is observed with the nFRET acceptors (AF532 and AF546), whereas no such shift is seen with the conventional FRET acceptor (AF680) or with the donor-only sample. The same effect is seen in the calculated lifetimes in Table 5. The decrease of the signal intensity with all the samples is suspected to be a result of the increased vibrational quenching by OH-groups. The replacement of the ligand coordination sites by water molecules is increased with the rising temperature. The melting temperature of the oligonucleotides is so high (approximately 90°C) that melting is not suspected to have any effect in the results.

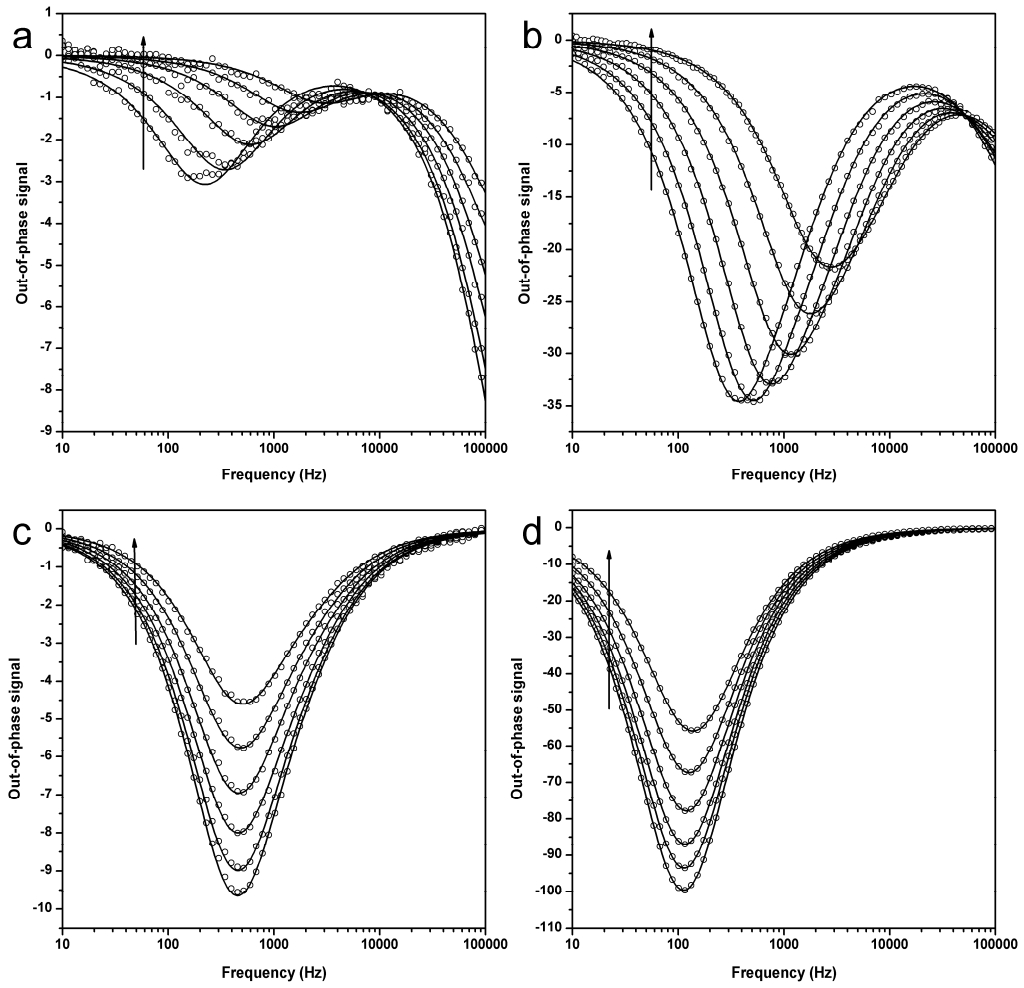

Figure 17. The out-of-phase signals of the luminescence from the hybridization reactions between the capture and tracer oligonucleotides in different temperatures as a function of the modulation frequency. In all reactions the donor label was compound **3**. The acceptor labels and the emission wavelengths were (a) AF532 and 560 nm, (b) AF546 and 560 nm, (c) AF680 and 730 nm, and (d) no acceptor and 615 nm, respectively. The donor–acceptor distance was 4.1 nm with the AF532 and AF546 acceptors (a and b), and 6.7 nm with the AF680 acceptor (c). The experimental points are marked by the circles. For visual clarity, only every third data point of the observed signal is shown. The lines are the fitted signals with two (a, c and d) or three (b) lifetimes (see Table 5). The temperature ranged from 5°C to 55°C with ten degree intervals. The arrows indicate the increasing temperature.

We proposed that the shift in the lifetimes of the AF532 and the AF546 acceptors is due to a thermally induced back-transfer of energy. The back-transfer increases the probability of the nFRET process. The rate constant ($k(T)$) for the thermal back-transfer is given by

$$\ln\left(k(T)\right) = \ln\left(\frac{1}{\tau_{AD}} - \frac{1}{\tau_{D}}\right) = -\frac{E_a}{k_B}\frac{1}{T} + \ln A \qquad (32)$$

Here E_a is the activation energy of the thermal back-transfer, k_B is the Boltzmann constant, T is the temperature and A is the pre-exponential factor. The lifetimes τ_{AD} and τ_D are the temperature dependent lifetime of the sensitized acceptor emission and the temperature independent lifetime of the donor emission in the absence of the acceptor, respectively. The values of $k(T)$ were calculated with the lifetimes presented in Table 5. The lifetime of the donor-only sample was used for τ_D and the lifetime of the sensitized acceptor emission (τ_2 or τ_3) was used for τ_{AD}. The Arrhenius plot of $\ln(k(T))$ plotted against the inversed temperature ($1/T$) is presented in Figure 18. Again no temperature effect is observed with the conventional FRET acceptor (AF680). With the nFRET acceptors (AF532 and AF546) there is a clear linear dependency of $k(T)$ on the temperature. The values of the activation energy and the pre-exponential factor were calculated from the slopes and the intercepts of the lines in Figure 18, respectively. The obtained values of the activation energy were 4045 ± 35 cm^{-1} (correlation coefficient R = 0.9999) for the AF532 and 2228 ± 20 cm^{-1} (R = 0.9998) or 2861 ± 77 cm^{-1} (R = 0.9986) for the AF546 (calculations based on the τ_2 and τ_3 lifetime estimates respectively) with 95% confidence. The values of the pre-exponential factor were 8.7E+11, 3.5E+9 and 6.6E+8, respectively.

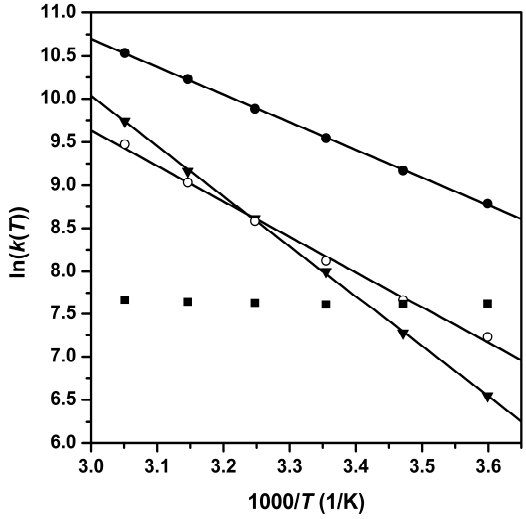

Figure 18. The natural logarithm of $k(T)$ plotted against the inverse temperature for the hybridization reactions between the capture oligonucleotide labelled with compound **3** and the tracer oligonucleotide labelled with AF532 (triangle), AF546 (circle) or AF680 (square). The values of $k(T)$ were calculated by Equation 32 from the lifetimes presented in Table 5. The lifetime of the sensitized acceptor emission (τ_{AD}) was τ_2 (solid symbols) or τ_3 (open circle).

The experimental results of the nFRET process as a function of the donor–acceptor distance presented above (Table 4 and Figure 16) demonstrated a shorter effective distance range of the nFRET process compared to the conventional FRET process. In this short range the energy transfer was more efficient than the theoretical estimate based on the Förster equations. A clear temperature dependence was observed with the nFRET acceptors but not with the conventional FRET acceptor

(Table 5, Figure 17 and Figure 18). These observations together with the absence of the spectral overlap between the nFRET acceptor absorption spectra and the donor emission spectrum indicate that the nFRET mechanism is different compared to the conventional FRET process. The difference between the nFRET acceptors (AF532, AF564) and the conventional FRET acceptor (AF680) is the position of the excitation spectrum relative to the excited energy levels of the Eu(III) ion. The relative positions of the related energy levels of the Eu(III) ion[40] together with the lowest triplet states of the light-harvesting ligands and the excitation bands of the Alexa Fluor dyes used in our studies are presented in Figure 19. The energies of the lowest triplet states were 21 950, 21 740 and 22 250 cm^{-1} for the ligands of compounds **1**, **2** and **3** respectively.[44] The exact values may differ slightly from the referenced values due to small differences in the chelate structures. The triplet states lie just above the $^5D_2$ level of Eu(III). Hence the energy transfer from the ligand to the Eu(III) ion is supposed to proceed through the $^5D_2$ level followed by a non-radiative relaxation to the $^5D_0$ level.[50,53] The energy levels of the Alexa Fluor dyes are presented as the excitation maxima (square) together with the half-widths of the excitation spectra (error bars).

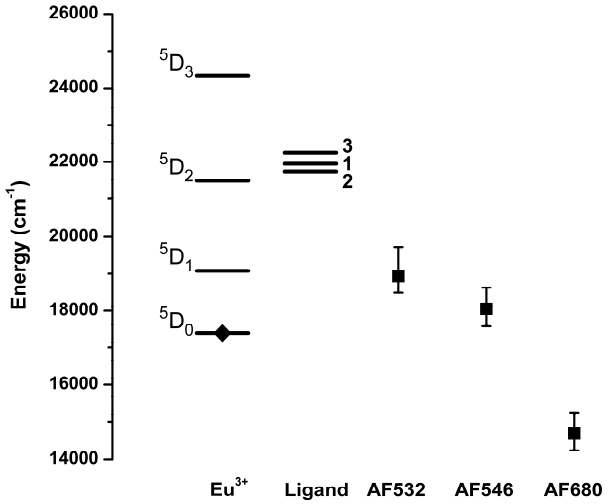

Figure 19. A simplified diagram showing the selected excited energy levels of the Eu(III) ion,[40] the lowest triplet states of the light-harvesting ligands of compounds **1**, **2** and **3**[44] and the excitation bands of the Alexa Fluor dyes (AF532, AF546 and AF680). The diamond indicates the main emitting level of the Eu(III) ion. The squares mark the excitation maxima of the dyes and the error bars the half-widths of the excitation spectrum.

The excitation band of the AF680 lies below the main emitting level ($^5D_0$) of the Eu(III) ion and allows the conventional downstream FRET. The excitation bands of the two other acceptors lie above the $^5D_0$ level but below the $^5D_1$ and $^5D_2$ levels. Laitala and Hemmilä proposed that in the nFRET process the relevant energy levels are the $^5D_1$ and $^5D_2$ levels of Eu(III) or in the case of the Sm(III) donor the $^4G_{7/2}$ level.[24,25] This hypothesis denotes that the nFRET process is essentially a property of the lanthanide ion and independent of the ligand or the acceptor. The observed thermal dependence of the nFRET process can be explained by the population of the $^5D_1$ level by thermal excitation from $^5D_0$ to $^5D_1$. The activation energies obtained by us for the AF546 (2861 cm^{-1} or

2228 cm^{-1}) were greater than the energy separation (1700 cm^{-1})[40] between $^5D_1$ and $^5D_0$. However, slightly greater activation energies for the thermal transition $^5D_0 \rightarrow {}^5D_1$ compared the energy separation between the two levels have been obtained also by others. Kropp and Dawson obtained an activation energy value of 2000 cm^{-1} for uncomplexed Eu(III) in methanol and Haas and Stein a value of 2500 cm^{-1} for uncomplexed Eu(III) in acetonitrile.[214,215] The activation energy obtained for the AF532 (4045 cm^{-1}) is approximately the width of the energy separation (4098 cm^{-1}) between $^5D_0$ and $^5D_2$ levels.[40]

An alternative explanation for the nFRET process could be the energy transfer through a ligand-to-metal charge-transfer state (CTS). The Eu(III) and Sm(III) ions can be reduced to the oxidation state +2. The temperature dependent quenching of the $^5D_0$ and $^5D_1$ levels via a crossover from the respective Eu(III) ion energy level to a ligand-to-metal CTS has been reported.[216,217] In this case the nFRET process would be a joint property of the lanthanide ion and the ligand. The open question in this hypothesis is why the activation energies of the two hybridization reactions containing the AF532 or the AF546 were not equal even though the same lanthanide ion and ligand were used in both experiments.

In conclusion, we have demonstrated a difference in the distance and the temperature dependences between the conventional and non-overlapping FRET processes. The efficient nFRET energy transfer cannot be explained solely by the conventional FRET theory. Two alternative temperature dependent routes for the nFRET phenomenon were proposed utilizing either the high excited states of the lanthanide ion ($^5D_1$ and $^5D_2$ for europium) or a ligand-to-metal charge-transfer state. The exact mechanism is still uncertain and demands further studies. Applying FD methods on a donor–acceptor distance series optimized for the short distance range of the nFRET phenomenon could provide a more accurate estimate of the R_0 value for the nFRET donor–acceptor pairs. Also experiments with a Tb(III) donor and a suitable acceptor would be interesting. The energy separation between the lowest radiative energy level ($^5D_4$) and the next excited level ($^5D_3$) of the Tb(III) ion is considerably larger (5800 cm^{-1}) than with the Eu(III) or Sm(III) ions (Figure 1, p. 12). Hence, thermal back-transfer to the higher excited levels is unlikely. Furthermore, the Tb(III) ion cannot be reduced to the oxidation state of +2 like the Eu(III) and Sm(III) ions. Hence, both the thermal back-transfer and the ligand-to-metal charge-transfer state explanations proposed for the nFRET process would be invalid in the case of a terbium donor. Thus, indirect support for the proposed routes could be obtained if the nFRET phenomenon was not observed with a terbium donor and an acceptor with the excitation band above the $^5D_4$ level of the Tb(III) ion. So far no positive or negative reports of the nFRET phenomenon with a terbium donor have been reported. In every case the nFRET phenomenon has proved to offer some distinct advances for assay applications.[26] The detection sensitivity is improved due to the low background of the donor emission at the wavelength of the sensitized emission of the nFRET acceptor. The choice of the acceptor fluorophores is widened and even low quantum yield lanthanide chelates (such as samarium) can be utilized.

4.3 Lanthanide UCP Particles

Up-converting phosphors (UCP) based on the ZrO_2 (publication **III**) and the $NaYF_4$ (publication **IV**) host materials were synthesized and characterized. The ZrO_2 phosphor was synthesized by the combustion[132] method and the $NaYF_4$ material by the co-precipitation[212] method. In both cases Yb(III) was used as a sensitizer and Er(III) as an activator. The materials were aimed to be used as donors in RET assays. Hence, for an optimal performance the particle size should be in nanoscale and the luminescence intensity high. In the following chapters the effects of the dopant concentration and the core–shell structure on the luminescence properties of the materials are reviewed.

4.3.1 Effect of Dopant Concentrations (ZrO_2 Host)

In the case of the ZrO_2 host material the effect of the dopant concentrations on the luminescence intensity and the lifetimes was studied. The mole fractions of the ytterbium and erbium ions were 10% and 4%, respectively. The mole fraction of Y(III) was varied and was 0, 14, 28 or 42%. In one sample the mole fractions were 5% Yb(III), 2% Er(III) and 0% Y(III). The mole fractions are based on the amounts of zirconyl, yttrium, ytterbium and erbium nitrates used in the synthesis. The crystal structure of the ZrO_2:Y,Yb,Er materials was cubic. Small amounts of monoclinic and tetragonal phases were present in the sample with the lowest dopant concentrations. Evidently the concentrations were too low to completely stabilize the cubic phase.[218] The crystallite sizes were ca. 30 nm (estimated from X-ray powder diffraction patterns with the Scherrer equation).[219] The up-conversion emission spectra and decay curves of the five ZrO_2:(Y),Yb,Er samples are shown in Figures 20 and 21, respectively.

The up-conversion spectra were measured with the modular up-conversion spectrometer described in Chapter 3.1. The excitation source was a fibre-coupled NIR-laser emitting at 970 nm. The two-photon excitation mechanism of the Yb–Er system is presented in detail in Chapter 1.5. A common feature of the spectra in Figure 20 is broad emission bands without a well-resolved fine structure. The reason is the existence of multisite positions of the lanthanide dopants in the zirconia host. Different site symmetries and crystal fields result in an inhomogeneous broadening of the emission lines.[218] The multisite positions are due to the oxygen vacancies (Kröger–Vink notation: $V_o^{\bullet\bullet}$) which are formed when trivalent ions occupy tetravalent Zr(IV) sites. The different positioning of the oxygen vacancies around the trivalent ions results in different immediate environments around the lanthanide ions.[218,220] Also, ions near the surface have a more disordered environment compared to the ions in the particle core and the inhomogeneous broadening is induced.[131] Especially with nanoparticles the surface effects cannot be ignored due to the large surface area. Defects have a tendency to form aggregates, hence Yb(III)–$V_o^{\bullet\bullet}$–Yb(III) and Yb(III)–$V_o^{\bullet\bullet}$–Er(III) pairs are formed. These pairs can enhance the energy migration and the energy transfer efficiency between the Yb(III) and Er(III) ions.

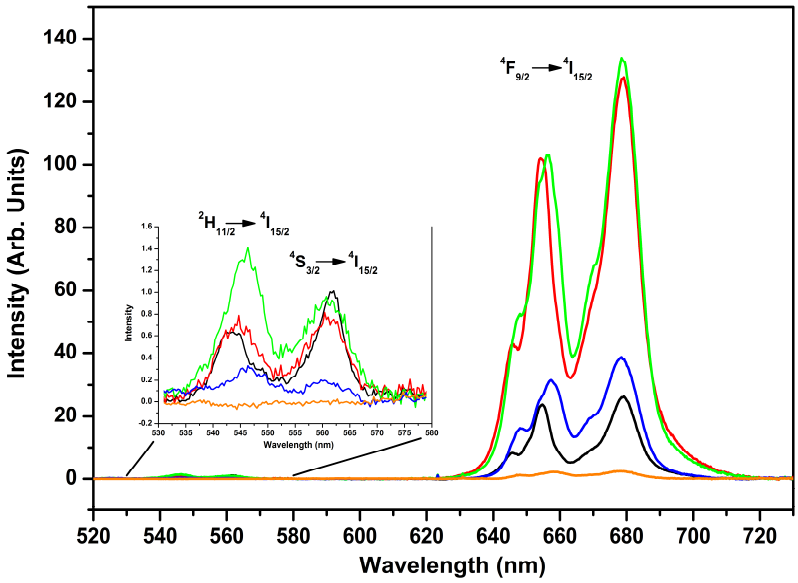

Figure 20. The up-conversion emission spectra of the ZrO_2:(Y,)Yb,Er materials. The excitation wavelength 970 nm. The mole fractions of Y/Yb/Er: Sample **1** 0/0.05/0.02 (black curve), **2** 0/0.10/0.04 (red), **3** 0.14/0.10/0.04 (green), **4** 0.28/0.10/0.04 (blue) and **5** 0.42/0.10/0.04 (orange).

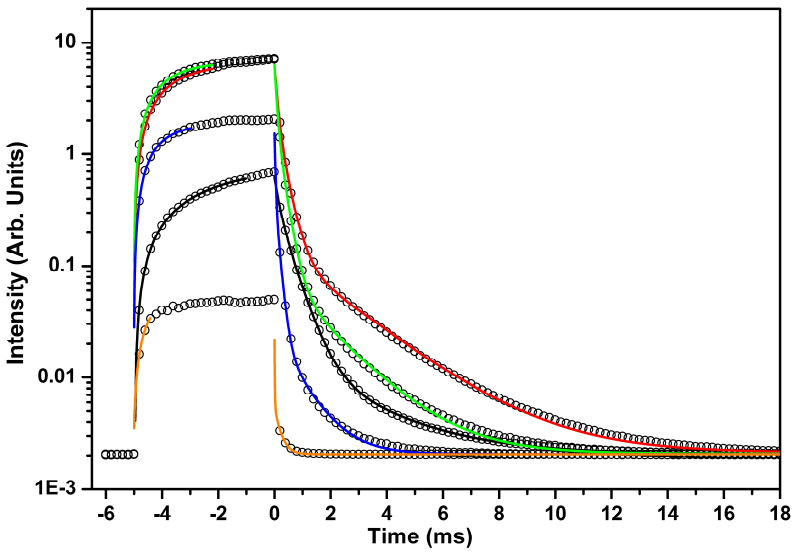

Figure 21. The up-conversion luminescence decay curves of the ZrO_2:(Y),Yb,Er materials. The experimental results presented with open circles and the exponential fitting results with colored solid lines. For visual clarity, only every twentieth point of the experimental data is shown. The mole fractions of Y/Yb/Er: Sample **1** 0/0.05/0.02 (black curve), **2** 0/0.10/0.04 (red), **3** 0.14/0.10/0.04 (green), **4** 0.28/0.10/0.04 (blue) and **5** 0.42/0.10/0.04 (orange). The excitation wavelength 970 nm, the emission wavelength 650 nm. Excitation cycle profile: 1 ms wait period, 5 ms pulse and 95 ms wait period. A single measurement consists of 10 000 cycles. The rise period of all sample curves fitted with one exponential time constant. The decay period of the sample curves 1–4 fitted with three exponential time constants and the sample curve 5 with two exponential time constants.

Another common feature for the spectra in Figure 20 is the low intensity of the green luminescence compared to the intensity of the red luminescence. We propose that this is due to cross-relaxation (CR) processes. Three possible CR processes that could explain the increase of the red–green emission ratio are presented in Figure 22. The first two CR processes involve the Er(III) $^2H_{11/2}$ energy state which is relaxed to a lower state ($^4I_{13/2}$ or $^4I_{9/2}$).[221,222] Simultaneously an adjacent Er(III) ion is excited from the ground state $^4I_{15/2}$ to a higher state ($^4I_{9/2}$ or $^4I_{13/2}$, respectively). Hence, the green emitting $^2H_{11/2}$ level is non-radiatively de-excited. Indirectly these CR processes also decrease the intensity of the green luminescence from the $^4S_{3/2}$ level because the $^4S_{3/2}$ level is quenched via thermally induced energy transfer to the $^2H_{11/2}$ level.[131,133] These CR processes also decrease the population of the red emitting $^4F_{9/2}$ level by a multiphonon relaxation of the $^4S_{3/2}$ level. However, these CR processes end up with one ion in the $^4I_{13/2}$ level which can be excited to the red emitting $^4F_{9/2}$ level by resonance energy transfer from Yb(III) (Figure 6, p. 22). The third CR process ($^4F_{7/2}\rightarrow{}^4F_{9/2}$, $^4I_{11/2}\rightarrow{}^4F_{9/2}$) in Figure 22 is actually the last phase of the route (c) presented in Figure 6. In this CR process the green emitting levels are completely bypassed as the $^4F_{7/2}$ level relaxes straight to the red emitting $^4F_{9/2}$ level. The red emission is particularly favoured as both ions end up in the $^4F_{9/2}$ level. As discussed in the context of Figure 6, this CR process can produce two red photons with just three NIR photons. The inter-ion cross-relaxation probability is increased by a high erbium concentration.[132] The concentration effect can be seen in Figure 20 by comparing the spectra of the samples **1** and **2**. The intensity of the green emission is about the same for the two samples. But the intensity of the red emission is notably stronger for the sample **2** which has a higher Er(III) concentration. We assumed this to be due to the enhanced quenching of the green emission through a cross-relaxation process. The overall emission intensity is increased as the Yb(III) and Er(III) concentrations are doubled (samples **1** and **2** in Figure 20). The reason is the increased absorption by the ytterbium ions and the more efficient energy transfer between the Yb(III) and Er(III) ions due to the decreased distance between the dopants. Another factor may be a lower structural purity of the material **1** with lower dopant concentrations.[218] The addition of the yttrium mole fraction up to 14% had no effect on the up-conversion luminescence intensity but the higher amount of yttrium cause a significant decrease in the luminescence intensity. A high yttrium concentration causes a formation of the Yb(III)–$V_o^{\bullet\bullet}$–Y(III) pairs which can cut the energy migration before reaching the Er(III) ions.

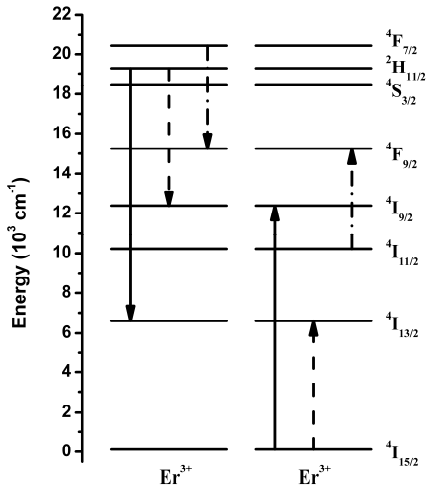

Figure 22. Possible cross-relaxation processes of Er(III).[127,131,221,222] The $^2H_{11/2}\rightarrow{}^4I_{13/2}$ relaxation and the $^4I_{15/2}\rightarrow{}^4I_{9/2}$ excitation (solid lines), the $^2H_{11/2}\rightarrow{}^4I_{9/2}$ relaxation and the $^4I_{15/2}\rightarrow{}^4I_{13/2}$ excitation (dashed lines), the $^4F_{7/2}\rightarrow{}^4F_{9/2}$ relaxation and the $^4I_{11/2}\rightarrow{}^4F_{9/2}$ excitation (dash–dot lines).

The up-conversion luminescence decay curves of the ZrO_2 based UCP materials were measured with the wide-pulse time-domain luminometer described in Chapter 3.1. The excitation and emission wavelengths were 970 nm and 650 nm, respectively. The excitation cycle consisted of a 1 ms waiting period, a 5 ms excitation pulse and a 95 ms waiting period after the pulse. The excitation source power was kept low enough to avoid the saturation of the intermediate states. A single measurement was an averaging result of 10 000 cycles. The experimental data and the fitting curves are presented in Figure 21. The fitting results are collected in Table 6.

Table 6. The luminescence properties of the ZrO_2:(Y),Yb,Er up-converting materials.

Sample [a]	Mole fractions			Red/Green ratio[b]	Decay times (ms)[c,d]			Rise times (ms)
	Y	Yb	Er		τ_1	τ_2	τ_3	τ_R
1	0.00	0.05	0.02	43	0.15 (37)	0.51 (61)	2.43 (2)	2.99
2	0.00	0.10	0.04	198	0.10 (60)	0.31 (38)	2.27 (2)	1.31
3	0.14	0.10	0.04	141	0.08 (65)	0.25 (34)	1.65 (1)	1.02
4	0.28	0.10	0.04	137	0.03 (71)	0.14 (28)	0.88 (1)	0.89
5	0.42	0.10	0.04	906	0.01 (83)	0.22 (17)	-	0.72

[a] Sample numbering used in Figure 20 and Figure 21.
[b] The ratio of the integrated intensity of the red (620–720 nm) and the green (510–590 nm) emissions of the up-conversion emission spectra (Figure 20).
[c] Excitation wavelength 970 nm and emission wavelength 650 nm.
[d] In parenthesis the relative percentage of the decay time components.

The advantage of the adjustable excitation pulse length and the recording of the full excitation–decay cycle is that the rise of the up-conversion luminescence can be observed. With the low excitation intensity used, the luminescence rise time is independent of the excitation power.[210] Due to the inverted logarithmic scale of the rise period in Figure 21 it is not visually evident but the rise

of the up-conversion luminescence was single exponential with all the samples. The rise time (τ_R) was in the millisecond range with all samples (Table 6). The absorption by the ytterbium ion and the relaxation of the excited erbium ion to the emitting level ($^4F_{9/2}$) occur in much shorter time than 1 millisecond. Hence, the energy transfer between the Yb(III) and Er(III) ions is probably the rate-limiting step in the excitation process. The rise time of the luminescence was the longest (2.99 ms) for the sample with the lowest Yb(III) and Er(III) concentrations (5% and 2% respectively). The result can be explained by the long distances between the lanthanide ions in the host matrix and the consequently low efficiency of the energy transfer between the Yb(III) and Er(III) ions. The doubling of the dopant concentrations (10% Yb(III) and 4% Er(III)) caused a distinct decrease in the rise time (1.31 ms) which was attributed to the increased energy transfer efficiency. The rise time decreased further as the yttrium concentration was increased. As discussed above the increase of the yttrium concentration causes an increase in the number of the Yb(III)–$V_o^{\bullet\bullet}$–Y(III) pairs which can cut off the energy migration before reaching the distant Er(III) ions. Hence, only the Er(III) ions close to the Yb(III) ions with an efficient and fast energy transfer are excited resulting in a short rise time.

The best fitting for the decay part of the curves was obtained with three time constants. With the exception of the sample with the highest yttrium concentration which was best fit with a two component fit (Figure 21, Table 6). Multi-exponential decay profiles of the lanthanide-doped inorganic nanoparticles have been presented in literature.[223–225] One explanation is a different probability of the non-radiative decay for the ions at or near the surface and for the ions in the core of the particles. Adsorbed contaminants with high energy vibrations, e.g. the CO_3^{2-} (1500 cm^{-1}) and OH^- (3350 cm^{-1}) groups, are present at the surface.[131] These groups can quench the excited states of the lanthanides more efficiently than the low phonon energies of the host matrix. We concluded that the shortest lifetime of our samples was probably due to the emission from the Er(III) ions near the particle surface. The intermediate lifetime component again was associated with the Er(III) ions in the core of the particle unaffected by the surface contaminants. The longest lifetime component ranged from 0.88 to 2.43 milliseconds. The relative amplitude of the longest component was very small, only 1–2 %. However, the fitting result with two time constants was decidedly worse compared to the fitting result with three components. A possible explanation for the longest lifetime is that the energy is temporarily trapped in the host material and recovered later. The energy traps can be created by doping trivalent ions into the tetravalent Zr(IV) sites in the host matrix. At the moment this "persistent up-conversion" is far too weak and short-lived for any applications. The fitting with three time constants was the best but not perfect. However, increasing the number of the time constants did not improve the fitting result and there probably are several closely matched lifetimes undistinguishable by the exponential fitting. The explanation is that the individual Er(III) ions have somewhat different immediate environments as indicated by the broad emission bands (Figure 20, p. 65). Differences in the crystal sites and in the local Er(III) concentration can cause slightly different lifetimes.[223,225] Hence, instead of three distinct lifetimes there is a distribution of lifetimes centred on the apparent lifetimes obtained as fitting results. The

lifetimes are decreased as the concentrations of the dopants are increased (Table 6). The reason for the decreasing of the lifetimes as the mole fraction of Er(III) is increased from 2% to 4% is most probably the increased inter-ion cross-relaxation rate. The decrease of the decay times as the yttrium concentration is increased may be due to an increased non-radiative deactivation by the defects in crystal structure. The amount of the defects is increased as a higher number of the Zr(IV) ions is replaced with Y(III) because of size and charge mismatch.

4.3.2 Core–Shell Nanoparticles ($NaYF_4$ Host)

The luminescence of the phosphor materials can be non-radiatively quenched by surface defects and high energy vibrations of organic groups adsorbed on the surface.[138,225] The effect is stronger the smaller the particles are because the surface area is increased. Alongside with the decrease of the total luminescence intensity, an increase in the red–green emission ratio of the Yb(III)–Er(III) system is observed. This occurs because the excitation routes leading to the red emitting level $^4F_{9/2}$ are dominating at the surface due to high multiphonon relaxation rates (Figure 6, p. 22). A significant enhancement of both the down- and up-conversion luminescence of the phosphor nanoparticles has been achieved by coating the optically active core material with an optically inactive shell layer.[226–229] The shell layer separates the luminescent lanthanide ions from the surface defects and the quenching groups on the surface. If phosphor nanoparticles are used as single labels, the protection of the optically active core with an inactive shell can offer improved intensity. However, if phosphor particles are intended to be used as labels in a resonance energy transfer system, the optically inactive shell layer can be a disadvantage because the minimum donor–acceptor distance is increased by the thickness of the shell layer. Actually, for applications utilizing the resonance energy transfer, an inactive core with a thin optically active layer could be an advantage if quenching by the surface groups could be minimized. The percentage of the luminescent ions within the range of the resonance energy transfer would be larger and the background emission due to the donor ions deep inside the core would be reduced.

We have synthesized, characterized and studied the luminescence properties of one homogeneous core and five different core–shell combinations of nanosized phosphor particles based on the $NaYF_4$ host material (publication **IV**). Our core–shell combinations include materials where optically active lanthanide ions reside in the core or shell or in both regions (Table 7, p. 71). The structure of the core material was hexagonal and the structure of the core–shell materials was a mixture of the cubic and hexagonal phases. The crystal sizes were estimated from X-ray powder diffraction data with the Scherrer formula and were approximately 100 nm and 150 nm for the cubic and hexagonal phases, respectively.[219] The up-conversion luminescence of the materials was measured with the up-conversion spectroluminometer and the time-domain luminometer described in Chapter 3.1. The emission spectra and decay profiles are presented in Figures 23 and 24, respectively. The integrated emission intensities, the calculated red–green ratio and the lifetime results of the materials are collected in Table 7.

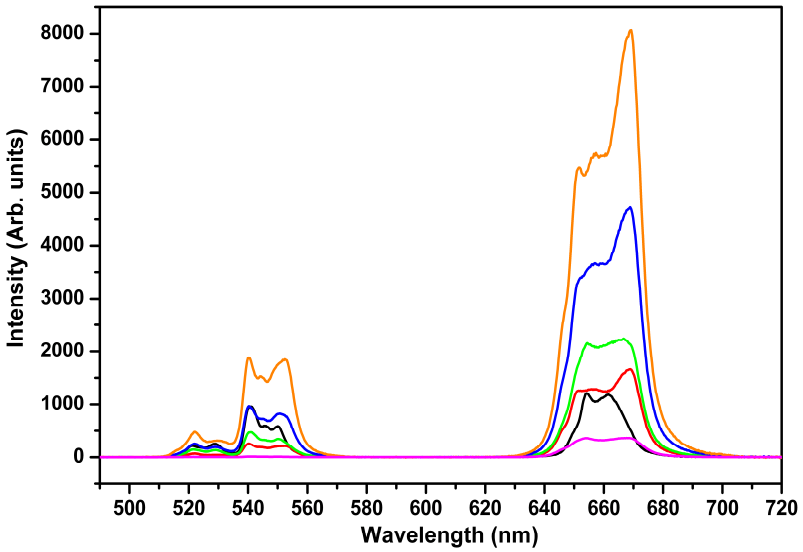

Figure 23. The up-conversion emission spectra of the $NaRF_4/NaR'F_4$ (R: Y, Yb, Er) materials (Table 7). Material **1** black line, **2** red, **3** green, **4** blue, **5** orange and **6** magenta. The excitation wavelength 970 nm.

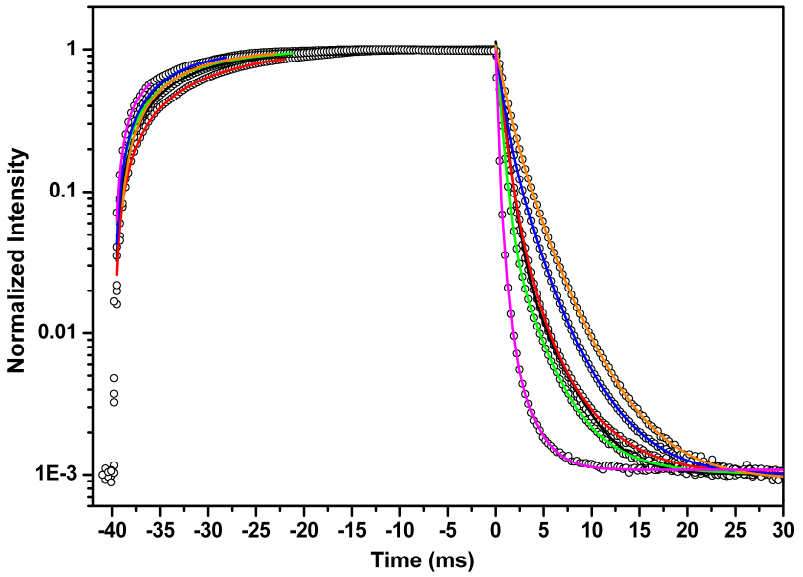

Figure 24. The up-conversion luminescence decay curves of the $NaRF_4/NaR'F_4$ phosphor materials (Table 7). The experimental results presented with open circles and the exponential fitting curves with coloured solid lines (material **1** black line, **2** red, **3** green, **4** blue, **5** orange and **6** magenta). The excitation wavelength 970 nm, the emission wavelength 650 nm. The excitation cycle profile: a 1 ms wait period, a 40 ms excitation pulse and a 60 ms decay period after the pulse. Only part of the decay period is shown. A single measurement consists of 2000 wait-pulse-decay cycles. For visual clarity, only every twentieth point of the experimental data is shown. The rise period of all the sample curves fitted with one exponential time constant. The decay period of the samples 1 to 5 fitted with three exponential time constants and sample 6 with two exponential time constants.

Table 7. The up-conversion luminescence properties of the $NaRF_4/NaR'F_4$ (R: Y, Yb, Er) nanoparticles.

#[a]	Core / Shell[b]	I_{Green}[c]	I_{Red}[d]	I_{Red}/I_{Green}[e]	Lifetimes (ms)[f]			
					τ_R	τ_1	τ_2	τ_3
1	$Na(Y,Yb,Er)F_4$	1	1.61	1.6	7.42	0.70 (95)	2.82 (5)	
2	$Na(Y,Yb,Er)F_4$ / $NaYF_4$	0.35	2.87	8.3	10.41	0.59 (78)	1.41 (21)	4.08 (2)
3	$5Na(Y,Yb)F_4$ / $Na(Yb,Er)F_4$	0.61	4.20	6.9	6.67	0.47 (92)	1.76 (7)	4.12 (1)
4	$4NaYF_4$ / $Na(Yb,Er)F_4$	1.36	8.20	6.0	5.69	0.60 (57)	1.63 (38)	3.77 (5)
5	$32Na(Y,Yb)F_4$ / $NaErF_4$	2.86	13.40	4.7	6.23	0.96 (57)	2.15 (39)	4.34 (4)
6	$6NaYbF_4$ / $NaErF_4$	0.02	0.72	39.9	3.12	0.15 (77)	0.47 (22)	1.79 (1)

[a] The phosphor material numbering used in Figures 23 and 24.
[b] The core–shell structures presented with the ideal molar ratios based on the amounts of the starting materials in the synthesis.
[c] The integrated intensity of the green emission (500–580 nm, Figure 23) relative to the green emission intensity of the core material $Na(Y,Yb,Er)F_4$.
[d] The integrated intensity of the red emission (620–720 nm, Figure 23) relative to the green emission intensity of the core material $Na(Y,Yb,Er)F_4$
[e] The ratio of the integrated red and green emission intensities.
[f] The calculated lifetimes of the experimental data in Figure 24 in milliseconds and the corresponding relative amplitude percentages in parenthesis.

The intensity of the red luminescence was stronger compared to the intensity of the green luminescence with every phosphor material. The red emission is favoured when the non-radiative relaxation and the cross-relaxation processes feed the red emitting level at the expense of the green emitting levels (Figures 6 and 22, pp. 22 and 67).[127,131,136,221,222] In the case of the phosphors **3** to **6** (Table 7) the erbium concentration in the shell is high. The high erbium concentration promotes the cross-relaxation since the Er(III) ions are located close to each other.[132] In the case of the $Na(Y,Yb,Er)F_4$ material it has been reported that the inactive shell on top of the optically active core favours the green emission.[227] The effect has been credited to the reduced influence of the surface defect and the impurities on the non-radiative relaxation of the green emitting levels. However, in our case the red–green emission ratio of the material with the inactive shell ($Na(Y,Yb,Er)F_4/NaYF_4$) was larger compared to the red–green ratio of the core material ($Na(Y,Yb,Er)F_4$). This can be explained by the crystal structure of the materials. The crystal structure of the core material was pure hexagonal, whereas the structure of the core–shell materials was a mixture of the cubic and hexagonal phases. Based on the X-ray powder diffraction results it was deduced that the structure of the core was mainly cubic and the shell hexagonal (publication **IV**). The red–green ratio of the cubic $Na(Y,Yb,Er)F_4$ phosphor material is larger compared to the hexagonal phosphor material.[128]

The most intense up-conversion luminescence at both the green and red wavelengths was obtained with the $32Na(Y,Yb)F_4/NaErF_4$ phosphor material. This was somewhat unexpected because the high concentration of the Er(III) ions should cause self-quenching by cross-relaxation.[132] The second best intensity was obtained with the $4NaYF_4/Na(Yb,Er)F_4$ material. The difference between the two materials is the location of the Yb(III) ions. In the shell the Yb(III) ions are subjected to quenching by impurities (e.g. CO_3^{2-} and OH^-).[131] Moreover, the local concentration of the Yb(III)

ions is higher in the second material and can lead to the Er(III)→Yb(III) back-transfer and to the self-quenching of Yb(III).[132,230] The explanation for the intense up-conversion luminescence of these two materials may be a favourable microdomain of the Er(III) ions. Due to the closeness of the surface the surroundings of the Er(III) ions in the shell layer are probably more distorted compared to the ions in the core.[231,232] The asymmetry of the crystal site increases the probability of the 4f→4f transitions. The similar microdomain of these two materials is evidenced by the similar shapes of the emission spectra (Figure 23, p. 70). However, this is in conflict with the long lifetimes of the $32Na(Y,Yb)F_4/NaErF_4$ phosphor material. The self-quenching due to a high Yb(III) concentration is supported by the low intensity of the $6NaYbF_4/NaErF_4$ material. The intensity of the core material compared to the best core–shell materials was unexpectedly low. This might be due to an aggregation of the optically active ions in the core–shell boundary or in the shell of the $32Na(Y,Yb)F_4/NaErF_4$ and $4NaYF_4/Na(Yb,Er)F_4$ materials, respectively. The aggregation might result in a favourable situation in which the Er(III) ions are surrounded by the Yb(III) ions and the energy transfer is very efficient.[104] In the case of the homogenous core material there is no concentration gradient which would induce aggregation. The lack of aggregation is supported by the lowest red–green ratio which is due to evenly distributed Er(III) ions with a low cross-relaxation probability.

The up-conversion luminescence rise and decay profiles of the $NaRF_4/NaR'F_4$ (R: Y, Yb, Er) materials are presented in Figure 24 (p. 70). The excitation wavelength was 970 nm and the emission wavelength was 650 nm. The rise and decay parts of the profiles were fit with exponential curves. The fitting results are collected in Table 7 (p. 71). The rise times were several milliseconds long. The $Na(Y,Yb,Er)F_4/NaYF_4$ and $Na(Y,Yb,Er)F_4$ materials had the longest rise times (10.41 ms and 7.42 respectively). The two materials have the same core composition with the optically active ions located in the core and a high Y(III) concentration. Inside the core the optically active ions are protected from the defects and the impurities of the surface which may reduce the lifetimes of the intermediate levels due to non-radiative relaxation processes. Other materials have Er(III) ions in the shell. Hence, the intermediate levels $^4I_{11/2}$ and $^4I_{13/2}$ of Er(III) are prone to non-radiative relaxation. The shortest rise time was observed for the $6NaYbF_4/NaErF_4$ material. The probable explanation is that the lifetimes of the $^2F_{5/2}$ (Yb(III)) and $^4I_{11/2}$ (Er(III)) levels are reduced by efficient self-quenching due to high local concentrations of Yb(III) and Er(III) ions. Hence, only a fast two-photon excitation at the core–shell interface can populate the emitting levels of Er(III). However, since the longest lifetimes were obtained with the $32Na(Y,Yb)F_4/NaErF_4$ material it seems that the self-quenching of Yb(III) is more crucial than the self-quenching of Er(III).

The decay profiles of all the core–shell materials were best fit with three lifetime components while two lifetimes were sufficient for the core material. In literature multiexponential decay profiles have been explained by surface effects, multiple sites and variations in the local doping concentrations.[223–225] With our materials all of these factors may be present. With small particles the surface area is large. In the cubic phase there is only a single cation site but in the hexagonal

phase there are three different cation sites.[233] The local concentration may vary due to a possible diffusion towards the core–shell interface. With all materials the longest calculated lifetime was over 1.7 ms and the tail of the decay extended to 20 ms at its best. The origin of this long lifetime might be the trapping of the energy in the cation vacancies in the lattice. Cation vacancies can be created by an excess of the trivalent ions in the lattice.[104] This kind of "persistent up-conversion" luminescence could provide new applications. However, in the current materials the fraction of "persistent up-conversion" is too low (1–2%) and the time frame too short for its utilization in any practical applications. The other two lifetimes are probably due to the Er(III) ions in different cation sites or the surface effects.

The experimental methods used did not provide direct evidence of the core–shell structures. However, some deductions can be made that suggest that the core–shell structure has indeed been formed. Firstly, the synthesis conditions at room temperature are rather mild. Hence, it is improbable that core particles would decompose during the deposition of the shell and form homogeneous particles with the source materials of the shell. However, the extent of the mixing of the core–shell structures during the annealing process (600^{o}C) is unknown. Another possibility is that new particles instead of the shell layer were formed during the deposition of the shell. Then in the case of the 32Na(Y,Yb)F_4/NaErF_4 phosphor material the Yb(III) and Er(III) ions would reside in separate particles. However, the absorption cross-section of the Er(III) ion is notably smaller compared to the Yb(III) ion, and the amount of the shell material in the 32Na(Y,Yb)F_4/NaErF_4 phosphor is small. Hence, it is unlikely that a rather intense up-conversion luminescence obtained with the 32Na(Y,Yb)F_4/NaErF_4 material would be induced by a two-steps absorption or an ETU process involving only Er(III) ions. The resonance energy transfer experiments with phosphor nanoparticles as the donor labels could provide an additional proof of the core–shell structure. In the case of the materials with the Er(III) ions in thin shell layers, the fraction of the donors unable to participate in the resonance energy transfer would be smaller compared to the material with the Er(III) ions in the core. The high luminescence intensity of the core–shell material obtained might be due to the aggregation of the optically active ions in the core–shell interface and the asymmetric microdomains of the Ln(III) ions which increase the probability of the 4f→4f transitions. A further optimization of the dopant concentrations and the thickness of the shell layer might provide a synthesis route for efficient phosphor materials, especially for the resonance energy transfer applications.

4.4 Lanthanide UCP Particles as Donors in LRET Assays

The UCP particles offer attractive features for bioanalytical assay applications. The general properties of lanthanides, the long lifetimes and the intense narrow-banded emission spectra, are effective with UCPs. In addition, the near-infrared excitation and the large anti-Stokes' shifts result in a total elimination of the autofluorescence and prevent the direct excitation of the acceptors. The NIR excitation and the possibility of the detection at far-red and NIR wavelengths (>650 nm)

enable the measurement of optically challenging samples such as plasma and whole blood which are practically transparent above 650 nm.[234] The first bioanalytical applications utilizing UCP particles were published in the 1990s.[235] The first reports demonstrating the RET based homogeneous bioaffinity assays with UCP donors were published in 2005.[27,28] Since then, several papers describing homogeneous assays combining up-converting material and energy transfer have been published.[29,173,174,234,236–241] In these reports the property detected was either the decrease of the donor emission intensity or the appearance and the increase of the sensitized acceptor emission. Both the resonance and the reabsorption energy transfer processes result in aforementioned changes in the emission intensity. However, the signal dependence on the proximity of the labels was regarded as an indication of the resonance energy transfer process. The definitive evidence for the presence of the RET process would be a decrease of the donor lifetime in the presence of the acceptor. There are few publications where the resonance energy transfer from UCP donors to acceptors is detected as a decrease of donor lifetime.[242,243] Sun et al. have studied the energy transfer between the rod-shaped hexagonal $NaYF_4$:Yb,Er donor (rod width tens of nanometers and rod length a few micrometers) and the tetramethylrhodamine isothiocyanate (TRITC) acceptor.[242] They used solid state samples prepared by dropping 40 µl of dilute TRITC solution onto UCP powder. The proximity of the donor and the acceptor was relied on the electrostatic interaction between the species. Sun et al. detected sensitized acceptor emission under both the 980 nm and the 488 nm excitation. However, they studied the decrease in the donor lifetime only with the 488 nm excitation. Under the 488 nm excitation the original lifetimes (94 and 232 µs) of the donor were decreased (84% and 44%, respectively) in the presence of the acceptor. Simultaneously the lifetime of the sensitized acceptor emission was elongated. However, the lifetime of the TRITC molecule alone was reported to be several microseconds long. This result disagrees with the generally known nanosecond time scale lifetime of rhodamine dyes.[244] Also the control measurements with samples including both the donor and the acceptor but not in close proximity were absent. Bednarkiewicz et al. used cubic $NaYF_4$:Yb,Er nanoparticles (diameter ca. 30 nm) as donors and CdSe quantum dots as acceptors.[243] They dispersed both particles in chloroform and placed a single drop of the particle suspension mixture on a quartz slide and let the chloroform vaporize in room temperature. The result was a solid mixture of the donor and acceptor particles. The relative concentration of the acceptor particles was controlled by the relative proportion of the quantum dot suspension in the mixture. Bednarkiewicz et al. reported an average lifetime of 153 µs for the $NaYF_4$:Yb,Er particles which was diminished to 130 µs (decrease 14 %) in the presence of quantum dots. The sensitized emission lifetime of the quantum dots was 82 µs which is in the same time scale as the donor lifetime and significantly greater than the nanosecond lifetimes of pristine quantum dots. Since the particle size was greater than the calculated Förster distance (ca. 15 Å), part of the energy transfer was credited to the reabsorption of the donor emission.

In both publications[242,243] discussed above, the measurements were performed with solid-state samples and without a controlled donor–acceptor proximity. In publication **V** we studied changes

in the luminescence lifetime of the UCP donor in aqueous solutions which are the fundamental environment for bioanalytical assays. The donor material was $NaYF_4$:Yb,Er synthesized with a co-precipitation method.[245] The average diameter of the UCP particles was 110 nm. Three different acceptors were used to confirm the results. A relatively large fluorescent protein (BPE, B-phycoerythrin) was chosen for its intense emission. Two other acceptors were small organic fluorophores ATTO565 and DY556. The excitation spectra of all three acceptors overlapped with the green emission ($^2H_{11/2}$ / $^4S_{3/2} \rightarrow {}^4I_{15/2}$) of the UCP donor (Figure 1. in publication **V**). The surface of the UCP particles was functionalized by the adsorption of poly(acrylic acid) for a conjugation with the amino-modified acceptors or with a non-fluorescent bovine serum albumin (BSA). The acronyms 'D' and 'A' were used for the donor and the acceptor respectively for naming different samples. In the 'D→A' samples acceptors were conjugated to the surface of the functionalized donor particles to generate a close proximity between the donor and the acceptor. The amount of the acceptors bound on the UCP particles was optimized for the maximum density of the acceptor molecules which did not inflict self-quenching. In the 'D only' and 'D+A' samples the surface of UCPs was blocked totally with BSA to prevent the binding of any other molecules. In the 'D only' sample no acceptor was added. In the 'D+A' samples the BSA-blocked UCP particles were mixed with same amount of the free acceptor molecules as was bound on the UCP surface in the corresponding 'D→A' sample. The blocked UCP surface resulted in an undefined diffusion-controlled donor–acceptor distance and samples capable only for radiative energy transfer. To confirm the luminescence lifetime results and their independence on the concentrations, the 'D+(5x)A' samples were prepared. The 'D+(5x)A' samples were similar to the 'D+A' samples but with a five-fold acceptor concentrations. The 'A only' samples were pure acceptor solutions without donor particles and were used to ensure that the acceptors were not directly excited by the NIR radiation. Although the previous measurements were done by using the wide-pulse excitation, the stricter requirements for the accuracy necessitated the use of the FD methods. The lifetimes were measured with the modular FD luminometer described in Chapter 3.1. The excitation source was a NIR laser diode with the central wavelength at 976 nm. The donor emission was collected at 544 nm and 650 nm, and the acceptor emission at 600 nm. Only the out-of-phase signals were used in the fitting. The data were compensated for instrumental deviations before fitting. The acceptor emission signals were fitted together with the donor emission signal and the sum of the sum of squares was minimized.

$$\chi^2(total) = \chi^2(donor) + \chi^2(acceptor) \qquad (33)$$

Here χ^2 are the sum of squares of the out-of-phase signals (Eq. 28, p. 49). The values of the relative amplitude (A_k) and the relative sum of amplitude factors (ρ) were calculated from the amplitude factors (h_k) and the corresponding lifetimes (τ_k) by using Equations 34 and 35, respectively. The goodness of fit was estimated by the value of the reduced chi-squared parameter (χ_R^2), the value of the relative sum of amplitude factors and the randomness of the lag plot.

$$A_k = 100 \frac{h_k \tau_k}{\sum_{i=1}^{N} h_i \tau_i} \qquad (34)$$

$$\rho = 100 \frac{\sum_{k=1}^{N} h_k}{\sum_{k=1}^{N} |h_k|} \qquad (35)$$

No significant changes in the luminescence lifetimes were observed at 544 nm. The finding can be explained by the large size (ca. 110 nm) of the UCP particles. The majority of the donor ions reside in the core parts of the particles and the distance to the acceptors on the surface is many times larger than the Förster distance. Hence, these internal donor ions do not participate in the energy transfer at all or transfer energy by reabsorption. Either way, the luminescence lifetime is not affected. Only the near-surface donor ions are able to contribute to the resonance energy transfer. As a result, the detection of the possible decreased lifetime caused by the resonance energy transfer is difficult due to a weakness of the signal compared to the intense signal from the donor ions in the core of the particles. Fortunately, in the case of long-lived lanthanide donors and short-lived organic acceptors, the lifetime of the sensitized acceptor emission mirrors the lifetime of the donor.[149,150] Hence, the decrease in the donor's lifetime can be calculated from the acceptor emission detected at 600 nm. At 600 nm all emission is due to the energy transfer (either non-radiative or radiative) because the acceptors are not directly excited by the NIR radiation.

The out-of-phase signals of the 'D only' sample at 544 nm and of the 'D→A' and 'D+A' samples containing the ATTO565 acceptor at 600 nm are presented in Figure 25. The calculated luminescence lifetimes of the same samples and the corresponding 'D+(5x)A' sample are presented in Table 8. The 'D only' sample data collected at 544 nm (Figure 25 (a)) was best fitted with three lifetimes. The calculated lifetimes τ_1 and τ_2 of the 'D only' sample at green (57 and 310 μs at 544 nm) and also at red (181 and 489 μs at 650 nm) wavelengths agreed with the values reported by Lin et al. for hexagonal $NaYF_4$:Yb,Er material.[246] The absence of the longest lifetime τ_3 in the report of Lin et al. may be due to a different method (time-domain instead of frequency-domain) used in their studies. Based on the congruence between our and Lin et al.'s results, the operation of the FD luminometer was considered to be valid and the results reliable.

The method of choice for the data analysis was to fit the signals of the acceptor ('D→A' or 'D+A' at 600 nm) and the donor ('D only' at 544 nm) samples together. As a result, both samples attain the same set of the lifetime values but different values for the relative amplitudes and for the relative sums of amplitude factors. The idea was to show that with the 'D+A' acceptor sample the amplitudes of the acceptor and donor signals are almost equal and the lifetimes are unchanged

compared to the values obtained when fitting the 'D only' sample alone. And, on the other hand, that in the case of the 'D→A' acceptor sample, a good fit requires an additional lifetime which has a negligible amplitude for the 'D only' sample and a relatively strong amplitude for the 'D→A' sample. The results support the presented hypothesis (Figure 25 and Table 8).

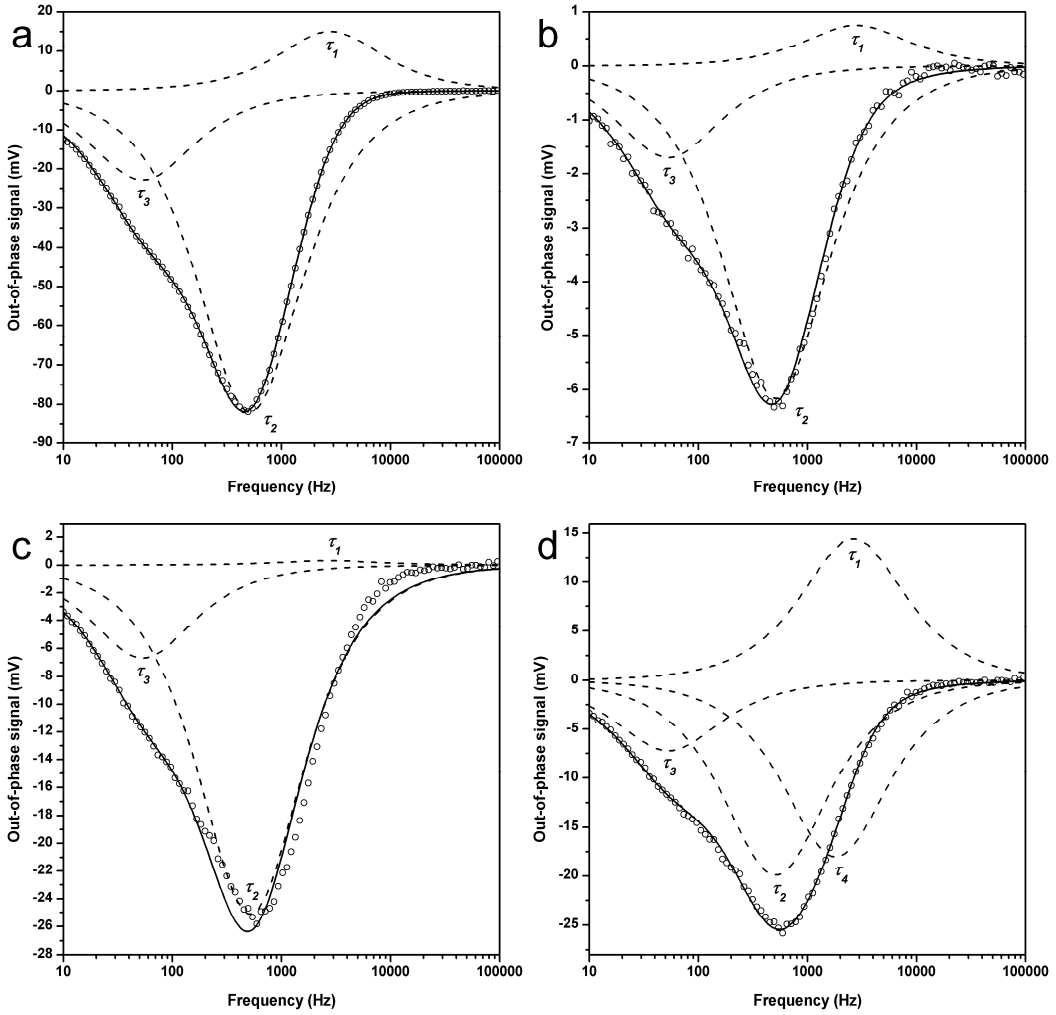

Figure 25. The experimental out-of-phase signals (circle), and the calculated fitting sum curves (solid line) and the individual lifetime components of the fit (dashed lines) of the selected samples with the ATTO565 acceptor. For visual clarity, only every second data point of the experimental signal is shown. (a) The 'D only' sample data collected at 544 nm and fitted alone to three lifetimes. (b) The 'D+A' sample data collected at 600 nm and fitted to three lifetimes, (c) and (d) the 'D→A' sample data collected at 600 nm and fitted to three or four lifetimes, respectively. The data in (b), (c) and (d) were fitted simultaneously with the 'D only' sample measured at 544 nm. The lifetime component curves are denoted with the same τ_x symbols as used in Table 8.

Table 8. The calculated luminescence lifetimes of the selected samples. The acceptor in the 'D+A', 'D+(5x)A' and 'D→A' samples was ATTO565. The acceptor sample data (600 nm) were fitted together with the 'D only' sample data (544 nm). The 'D only' sample was fitted also alone.

Sample		Lifetimes τ (μs)			'D only' at 544 nm A_k (%)	ρ (%)	Acceptor sample at 600 nm A_k (%)	ρ (%)	χ_R^2
D only	τ_1	57	±	0.33	-17	1.36	-	-	17.1
	τ_2	310	±	1.1	91		-		
	τ_3	3007	±	25	25		-		
D+A	τ_1	57	±	0.32	-17	1.37	-11	21.1	9.4
	τ_2	309	±	1.1	91		87		
	τ_3	3005	±	25	25		24		
D+(5x)A	τ_1	57	±	0.32	-17	1.36	-14	8.2	9.3
	τ_2	310	±	1.1	91		90		
	τ_3	3007	±	24	25		24		
D→A	τ_1	58	±	0.32	-17	1.53	-1	88.0	23.9
	τ_2	307	±	1.1	91		80		
	τ_3	2987	±	24	26		21		
D→A	τ_1	60	±	2.0	-21	1.30	-47	6.5	9.0
	τ_2	312	±	3.0	90		65		
	τ_3	2998	±	22	25		23		
	τ_4	88	±	7.0	6		59		

The 'D+A' sample was well-fit with three lifetimes (Figure 25 (b)). The values of the lifetimes were within the experimental error to the values obtained for the 'D only' sample alone. Likewise, the values of the relative amplitudes of the lifetime components were close to the values of the 'D only' sample alone. The results of the 'D+(5x)A' sample were similar to the results of the 'D+A' sample. For the fitting of the 'D→A' sample, three lifetimes were clearly inadequate (Figure 25 (c)) but four lifetimes were sufficient for a good fit (Figure 25 (d)). The improvement in the fit is also seen as an improvement of the values of ρ and χ_R^2 (Table 8). Of the four lifetimes, three were almost equal to the three lifetimes of the 'D only' sample alone. The fourth lifetime, τ_4 (88 μs), was attributed to the presence of the resonance energy transfer. The relative amplitude of the τ_4 component for the 'D only' sample was only 6% whereas it was 59% for the 'D→A' sample. The relative amplitude of the τ_2 component decreased from 90% ('D only') to 65% ('D→A') while the relative amplitude of τ_3 component remained virtually unchanged. Hence, the reduction of the lifetime ($\Delta\tau$) due to the resonance energy transfer was calculated as a difference between the values of τ_2 and τ_4. In the case of ATTO565 the reduction was −224 μs (−72%).

Even in the 'D→A' samples the dominant component was τ_2. The origin of this unchanged lifetime at 600 nm is mainly the radiative energy transfer. Another source is the donor emission passing through the bandpass filter. A weak signal at 600 nm was detected with the 'D only' sample

(Figure S4 in the supporting information of publication **V**). The 'A only' samples did not produce a detectable signal within the used frequency range (Figure S4). The standard deviations of the luminescence lifetimes were slightly higher for the 'D→A' sample compared to the 'D+A' and 'D+(5x)A' samples (Table 8). In the case of the donor particles larger than the Förster distance, the donor–acceptor distance increases as the distance of the donor ions to the surface increases. Hence, instead of one precise donor–acceptor distance and a corresponding lifetime there is a continuum of distances and lifetimes. Therefore, the calculated lifetimes τ_4 are actually average lifetimes and the elevated standard deviation reflects a distribution of lifetimes.

The results with the two other acceptor molecules BPE and DY556 were similar to the result with ATTO565 (publication **V**). The reduction of the lifetime was −202 μs (−64%) with BPE and −220 μs (−71%) with DY556. The reduction of the luminescence lifetimes observed only with the 'D→A' samples was considered as a definite evidence of the resonance energy transfer with the UCP donors in the aqueous environment. Our UCP particles were large compared to the Förster distance. With smaller UCP particles a larger part of the donor ions could participate in the resonance energy transfer. However, as the particle size decreases the surface area and the quenching by the surface effects are increased.[131] The solution could be a protective coating or core–shell particles.

5 Summary

The subject of this thesis was the lanthanide luminescence and the lanthanide-based resonance energy transfer. In addition to the research of the luminescence phenomena, the development of the modular frequency-domain and time-domain luminometers had an essential role in the study. Novel theoretical and instrumental aspects were presented for the FD luminometer operating in the low frequency domain and utilizing the dual-phase lock-in detection of the luminescence. The approach with the TD luminometer was more conventional as the measurement was based on the established time-gated detection and commercial software was used for fitting. However, the wide-pulse excitation and a very fast measurements were the assets of our TD instrument. The FD and TD methods have their own strengths which were successfully exploited in this research.

An anti-Stokes resonance energy transfer phenomenon was discovered recently and termed non-overlapping fluorescence resonance energy transfer. We studied the distance and temperature dependencies of the non-overlapping and the conventional resonance energy transfer. The behaviour of the nFRET process deviated from the Förster theory. A clear temperature dependence was observed with the nFRET samples whereas the FRET process was completely independent of the temperature. Two alternative temperature dependent routes for the nFRET process were proposed utilizing either the high excited states of the lanthanide ion or the ligand-to-metal charge-transfer states. Further studies with other lanthanide chelates and with the donor–acceptor distance series optimized for the short range of the nFRET phenomenon could provide answers for the open questions of the nFRET mechanism.

The UCP particles provide attractive benefits for binding assay applications. The near-infrared (NIR) excitation and the large anti-Stokes' shift result in a complete elimination of the autofluorescence and prevent the direct excitation of acceptors. In addition, the NIR excitation and the emission at red wavelength range are benefits in RET assays involving plasma and whole blood samples which have high absorbance below 650 nm. Indeed, several papers involving homogeneous assays combining up-converting material and energy transfer have been published. However, definite proof about the non-radiative nature of the energy transfer in aqueous solutions has been missing. We presented the lacking evidence as the decrease of the UCP donor lifetime was observed for the first time in aqueous solutions and with a controlled donor–acceptor distance. New UCP materials based on the Yb–Er up-conversion system were synthesized. The main aim was to develop UCP nanoparticles with appropriate properties to be used as donor labels in RET-based assays technology. The effect of the dopant concentrations on the total up-conversion luminescence intensity, the red–green emission ratio and the lifetime of the luminescence were measured with the ZrO_2:Y,Yb,Er material. The red Er(III) emission was dominant with all the synthesized ZrO_2 based materials. The properties of the core–shell phosphor particles were studied with the $NaRF_4/NaR'F_4$ (R: Y, Yb, Er) materials. The highest intensity was obtained with the material in which all Er(III) ions resided in the shell. The UCP particle synthesis research has continued in our laboratory with the target on decreasing the particle size.

6 References

[1] Hovinen, J.; Guy, P. M. *Bioconjugate Chem.* **2009**, *20*, 404–421.

[2] Blasse, G.; Grabmaier, B. C. *Luminescent Materials*, Springer–Verlag, Berlin, **1994**.

[3] Verstegen, J. M. P. J.; Radielovic, D.; Vrenken, L. E. *J. Electrochem. Soc.* **1974**, *121*, 1627–1631.

[4] Ronda, C. R.; Jüstel, T.; Nikol, H. *J. Alloys Compd.* **1998**, *275–277*, 669–676.

[5] Kim, C.-H.; Kwon, I.-E.; Park, C.-H.; Hwang, Y.-J.; Bae, H.-S.; Yu, B.-Y.; Pyun, C.-H.; Hong, G.-Y. *J. Alloys Compd.* **2000**, *311*, 33–39.

[6] Rao, R. P.; Devine, J. D. *J. Lumin.* **2000**, *87–89*, 1260–1263.

[7] Desurvire, E. *Phys. Today* **1994**, *47*, 20–27.

[8] Mears, R. J.; Reekie, R.; Jauncey, I. M.; Payne, D. N. *Electron. Lett.* **1987**, *23*, 1026–1028.

[9] Xin, H.; Li, F. Y.; Guan, M.; Huang, C. H.; Sun, M.; Wang, K. Z.; Zhang, Y. A.; Jin, L. P. *J. Appl. Phys.* **2003**, *94*, 4729–4731.

[10] Johnson, L. F.; Guggenheim, G. J. *Appl. Phys. Lett.* **1971**, *19*, 44–47.

[11] Allain, J. Y.; Monerie, M.; Poignant, H. *Electron. Lett.* **1990**, *26*, 261–263.

[12] Gustafson, K.; Finkel, J.; Jacobs, P.; Green, W. *US Patent* 4,738,901, **1988.**

[13] Gutmann, R.; Ahlers, B.; Kappe, F.; Paugstadt, R.; Franz-Burgholz, A. *US Patent* 6,234,537, **2001.**

[14] Suyver, F.; Meijerink, A. *Chemisch 2 Weekblad* **2002**, *98*, 12–13.

[15] Richards, B. S.; Shalav, A. *IEEE Trans. Electron. Devices* **2007**, *54*, 2679–2684.

[16] Soini, E.; Lövgren, T. *Crit. Rev. Anal. Chem.* **1987**, *18*, 105–154.

[17] Dickson, E. F. G.; Pollak, A.; Diamandis, E. P. *J. Photochem. Photobiol. B* **1995**, *27*, 3–19.

[18] Hemmilä, I. A. *Applications of Fluorescence in Immunoassays*, Winefordner, J. D. and Kolfhoff, I. M., (eds); Wiley and Sons, New York, **2004**.

[19] Hemmilä, I.; Laitala, V. *J. Fluoresc.* **2005**, *15*, 529–542.

[20] Selvin, P. R. *Annu. Rev. Biophys. Biomol. Struct.* **2002**, *31*, 275–302.

[21] Bergendahl, V.; Heyduk, T.; Burgess, R. R. *Appl. Environ. Microbiol.* **2003**, *69*, 1492–1498.

[22] Werts, M. H. V.; Hofstraat, J. W.; Geurts, F. A. J.; Verhoeven, J. W. *Chem. Phys. Lett.* **1997**, *276*, 196–201.

[23] Werts, M. H. V.; Woudenberg, R. H.; Emmerink, P. G.; van Gassel, R.; Hofstraat, J. W.; Verhoeven, J. W. *Angew. Chem. Int. Ed.* **2000**, *39*, 4542–4544.

[24] Laitala, V.; Hemmilä, I. *Anal. Chem.* **2005**, *77*, 1483–1487.

[25] Laitala, V.; Hemmilä, I. *Anal. Chim. Acta* **2005**, *551*, 73–78.

[26] Vuojola, J.; Lamminmäki, U.; Soukka, T. *Anal. Chem.* **2009**, *81*, 5033–5038.

[27] Wang, L.; Yan, R.; Huo, Z.; Wang, L.; Zeng, J.; Bao, J.; Wang, X.; Peng, Q; Li, Y. *Angew. Chem. Int. Ed.* **2005**, *44*, 6054–6057.

[28] Kuningas, K.; Rantanen, T.; Ukonaho, T.; Lövgren, T.; Soukka, T. *Anal. Chem.* **2005**, *77*, 7348–7355.

[29] Rantanen, T.; Päkkilä, H.; Jämsen, L.; Kuningas, K.; Ukonaho, T.; Lövgren, T.; Soukka, T. *Anal. Chem.* **2007**, *79*, 6312–6318.

[30] Connelly, N. G.; Damhus, T.; Hartshorn, R. M.; Hutton, A. T. *Nomenclature of Inorganic Chemistry: IUPAC Recommendations 2005*, RSC Publishing, Cambridge, **2005**.

[31] Carnall, W. T. in *Handbook on the Physics and Chemistry of Rare Earth*, Gschneidner, K, A. Jr. and Eyring L. (eds), North-Holland Publishing Company, Amsterdam, **1979**, *Vol. 3*, Chapter 24, pp. 171–208.

[32] Blasse, G. *J. Lumin.* **1970**, *1–2*, 766–777.

[33] Struck, C. W.; Fonger, W. H. *J. Lumin.* **1970**, *1–2*, 456–469.

[34] Hoffman, M. V. *J. Electrochem. Soc.* **1971**, *118*, 933–937.

[35] Blasse, G. *Phys. Status Solidi B* **1973**, *55*, K131–K134.

[36] Liu, G. in *Spectroscopic Properties of Rare Earths in Optical Materials*, Liu, G. and Jacquier, B. (eds), Springer, Heidelberg, **2005**, Chapter 1, pp. 1–94.

[37] Carnall, W. T.; Fields, P. R.; Rajnak, K. *J. Chem. Phys.* **1968**, *49*, 4424–4442.

[38] Blasse, G.; Bril, A.; Nieuwpoort, W. C. *J. Phys. Chem. Solids* **1966**, *27*, 1587–1592.

[39] Carnall, W. T.; Fields, P. R.; Rajnak, K. *J. Chem. Phys.* **1968**, *49*, 4447–4449.

[40] Carnall, W. T.; Fields, P. R.; Rajnak, K. *J. Chem. Phys.* **1968**, *49*, 4450–4455.

[41] Carnall, W. T.; Goodman, G. L.; Rajnak, K.; Rana, R. S. *J. Chem. Phys.* **1989**, *90*, 3443–3457.

[42] Horrocks, W. DeW. Jr.; Schmidt, G. F.; Sudnick, D. R.; Kittrell, C.; Bernheim, R. A. *J. Am. Chem. Soc.* **1977**, *99*, 2378–2380.

[43] Horrocks, W. DeW. Jr.; Sudnick, D. R. *J. Am. Chem. Soc.* **1979**, *101*, 334–340.

[44] Latva, M.; Takalo, H.; Mukkala, V.-M.; Matachescu, C.; Rodriguez-Ubis, J. C.; Kankare, J. *J. Lumin.* **1997**, *75*, 149–169.

[45] Wolbers, M. P. O.; van Veggel, C. J. M.; Snellink-Ruël, B. H. M.; Hofstraat, J. W.; Geurts, F. A. J.; Reinhoudt, D. N. *J. Am. Chem. Soc.* **1997**, *119*, 138–144.

[46] Li, M.; Selvin, P. R. *J. Am. Chem. Soc.* **1995**, *117*, 8132–8138.

[47] Weissman, S. L. *J. Chem. Phys.* **1942**, *10*, 214–217.

[48] Buono-Core, G.; Li, H. *Coord. Chem. Rev.* **1990**, *99*, 55–87.

[49] Crosby, G. A.; Whan, R. E.; Alire, R. M. *J. Chem. Phys.* **1961**, *34*, 743–748.

[50] Crosby, G. A.; Whan, R. E.; Freeman, J. J. *J. Phys. Chem.* **1962**, *66*, 2493–2499.

[51] Kleinerman, M. *J. Chem. Phys.* **1969**, *51*, 2370–2381.

[52] Bhaumik, M. L.; El-Sayed, M. A. *J. Chem. Phys.* **1965**, *42*, 787–788.

[53] Tanaka, M.; Yamaguchi, G.; Shiokawa, J.; Yamanaka, C. *Bull. Chem. Soc. Jpn.* **1970**, *43*, 549–550.

[54] Sato, S.; Wada, M. *Bull. Chem. Soc. Jpn.* **1970**, *43*, 1955–1962.

[55] Watson, W. M.; Zerger, R. P.; Yardley, J. T.; Stucky, G. D. *Inorg. Chem.* **1975**, *14*, 2675–2680.

[56] Hayes, A. V.; Drickamer, H. G. *J. Chem. Phys.* **1982**, *76*, 114–125.

[57] Bhaumik, M. L.; El-Sayed, M. A. *J. Phys. Chem.* **1965**, *69*, 275–280.

[58] Matsuda, Y.; Makishima, S.; Shionoya, S. *Bull. Chem. Soc. Jpn.* **1968**, *41*, 1513–1518.

[59] Kleinerman, M. *Bull. Am. Phys. Soc.* **1964**, *9*, 265.

[60] Zhang, L.; Li, B. *J. Lumin.* **2009**, *129*, 1304–1308.

[61] Dexter, D. L. *J. Chem. Phys.* **1953**, *21*, 836–850.

[62] Marshall, E. J.; Pilling, M. J. *J. Chem. Soc., Faraday Trans.* **1978**, *74*, 579–590.

[63] Brown, A.; Wilkinson, F. *J. Chem. Soc., Faraday Trans. 2* **1979**, *75*, 880–895.

[64] Samanta, S.; Pal, A.; Roy, M. B.; Ghosh, S. *J. Lumin.* **2008**, *128*, 1689–1700.

[65] Brown, T. D.; Shepherd, T. M. *J. Chem. Soc. Dalton Trans.***1973**, 336–341.

[66] Sabbatini, N.; Mecati, A.; Guardigli, M.; Balzani, V.; Lehn, J.-M.; Zeissel, R.; Ungaro, R. *J. Lumin.* **1991**, *48–49*, 463–468.

[67] Blasse, G.; Dirksen, G. J.; Van der Voort, D.; Sabbatini, N.; Perathoner, S.; Lehn, J.-M.; Alpha, B. *Chem. Phys. Lett.* **1988**, *146*, 347–351.

[68] Shi, M.; Li, F.; Yi, T.; Zhang, D.; Hu, H.; Huang, C. *Inorg. Chem.* **2005**, *44*, 8929–8936.

[69] Crosby, G. A.; Kasha, M. *Spectrochim. Acta* **1958**, *10*, 377–382.

[70] Whan, R. E.; Crosby, G. A. *J. Mol. Spectrosc.* **1962**, *8*, 315–327.

[71] Carnall, W. T.; Fields, P. R.; Rajnak, K. *J. Chem. Phys.* **1968**, *49*, 4443–4446.

[72] Voloshin, A. I.; Shavaleev, N. M.; Kazakov, V. P. *J. Lumin.* **2001**, *93*, 115–118.

[73] Beeby, A.; Dickins, R. S.; Faulkner, S.; Parker, D.; Williams, J. A. G. *Chem. Commun.* **1997**, 1401–1402.

[74] Kropp, J. L.; Windsor, M. W. *J. Chem. Phys.* **1963**, *39*, 2769–2770.

[75] Kropp, J. L.; Windsor, M. W. *J. Chem. Phys.* **1965**, *42*, 1599–1608.

[76] Heller, A. *J. Am. Chem. Soc.* **1966**, *88*, 2058–2059.

[77] Haas, Y.; Stein, G. *J. Phys. Chem.* **1971**, *75*, 3677–3681.

[78] Haas, Y.; Stein, G. *Chem. Phys. Lett.* **1972**, *15*, 12–16.

[79] von Lode, P.; Rosenberg, J.; Pettersson, K.; Takalo, H. *Anal. Chem.* **2003**, *75*, 3193–3201.

[80] Salama, S.; Richardson, F. S. *J. Phys. Chem.* **1980**, *84*, 512–517.

[81] Hemmilä, I.; Mukkala, V.-M.; Takalo, H. *J. Fluoresc.* **1995**, *5*, 159–163.

[82] Beeby, A.; Clarkson, I. M.; Dickins, R. S.; Faulkner, S.; Parker, D.; Royle, L.; de Sousa, A. S.; Williams, J. A. G.; Woods, M. *J. Chem. Soc., Perkin Trans. 2* **1999**, 493–503.

[83] Dickins, R. S.; Parker, D.; Desousa, A. S.; Williams, J. A. G. *Chem. Commun.* **1996**, *6*, 697–698.

[84] Klink, S. I.; Hebbink, G. A.; Grave, L.; Peters, F. G. A.; Van Veggel, F. C. J. M.; Reinhoudt, D. N.; Hofstraat, J. W. *Eur. J. Org. Chem.* **2000**, 1923–1931.

[85] Hasegawa, Y.; Ohkubo, T.; Sogabe, K.; Kawamura, Y.; Wada, Y.; Nakashima, N.; Yanagida, S. *Angew. Chem. Int. Ed.* **2000**, *39*, 357–360.

[86] Horrocks, W. D. Jr.; Sudnick, D. R. *Acc. Chem. Res.* **1981**, *14*, 384–392.

[87] Supkowski, R. M.; Horrocks, W. D. Jr. *Inorg. Chim. Acta* **2002**, *340*, 44–48.

[88] Takalo, H.; Mukkala, V.-M.; Mikkola, H.; Liitti, P.; Hemmilä, I. *Bioconjugate Chem.* **1994**, *5*, 278–282.

[89] Yuan, J.; Matsumoto, K. *Anal. Chem.* **1998**, *70*, 596–601.

[90] Mukkala, V.-M.; Helenius, M.; Hemmilä, I. K.; Kankare, J.; Takalo, H. *Helv. Chim. Acta.* **1993**, *76*, 1361–1378.

[91] Horrocks, W. D. Jr.; Holmquist, B.; Vallee, B. L. *Proc. Natl. Acad. Sci. U.S.A.* **1975**, *72*, 4764–4768.

[92] Härmä, H.; Soukka, T.; Lönnberg, S.; Paukkunen, J.; Tarkkinen, P.; Lövgren, T. *Luminescence* **2000**, *15*, 351–355.

[93] Härmä, H.; Soukka, T.; Lövgren, T. *Clin. Chem.* **2001**, *47*, 561–568.

[94] Soukka, T.; Härmä, H.; Paukkunen, J.; Lövgren, T. *Anal. Chem.* **2001**, *73*, 2254–2260.

[95] Soukka, T.; Paukkunen, J.; Härmä, H.; Lönnberg, S.; Lindroos, H.; Lövgren, T. *Clin. Chem.* **2001**, *47*, 1269–1278.

[96] Soukka, T.; Antonen, K.; Härmä, H.; Pelkkikangas, A.-M.; Huhtine, P.; Lövgren, T. *Clin. Chim. Acta* **2003**, *328*, 45–58.

[97] Härmä, H.; Pelkkikangas, A.-M.; Soukka, T.; Huhtinen, P.; Huopalahti, S.; Lövgren, T. *Anal. Chim. Acta* **2003**, *482*, 157–164.

[98] Huhtinen, P.; Soukka, T.; Lövgren, T.; Härmä, H. *J. Immunol. Method*s **2004**, *294*, 111–122.

[99] Kokko, L.; Sandberg, K.; Lövgren, T.; Soukka, T. *Anal. Chim. Acta* **2004**, *503*,155–162.

[100] Valanne, A.; Lindroos, H.; Lövgren, T.; Soukka, T. *Anal. Chim. Acta* **2005**, *539*, 251–256.

[101] Wang, L.; Jin, D.; Zhang, G.; Lv, G. *Inorg. Mater.* **2009**, *45*, 678–682.

[102] Zhang, W.-W.; Zhang, W.-P.; Xie, P.-B.; Yin, M.; Chen, H.-T.; Jing, L.; Zhang, Y.-S.; Lou, L.-R.; Xia, S.-D. *J. Colloid Interface Sci.* **2003**, *262*, 588–593.

[103] Page, R. H.; Schaffers, K. I.; Waide, P. A.; Tassano, J. B.; Payne, S. A.; Krupke, W. F. *J. Opt. Soc. Am.* **1998**, *B15*, 996–1008.

[104] Krämer, K. W.; Biner, D.; Frei, G.; Güdel, H. U.; Hehlen, M. P.; Lüthi, S. R. *Chem. Mater.* **2004**, *16*, 1244–1251.

[105] DeLuca, J. A. *J. Chem. Educ.* **1980**, *57*, 541–545.

[106] Lakowicz, J. R. in *Principles of Fluorescence Spectroscopy*, Second edition, Kluwer Academic Plenum Publishers, New York, **1999**.

[107] Auzel, F. *Chem. Rev.* **2004**, *104*, 139–173.

[108] Auzel, F. E. *Proc. IEEE* **1973**, *61*, 758–786.

[109] Yeh, D. C.; Sibley, W. A.; Suscavage, M.; Drexhage, M. G. *J. Appl. Phys.* **1987**, *62*, 266–275.

[110] Auzel, F. *J. Lumin.* **1990**, *45*, 341–345.

[111] Brown, M. R.; Shand, W. A.; *J. Phys. C: Solid State Phys.* **1971**, *4*, 83–92.

[112] Bloembergen, N. *Phys. Rev. Lett.* **1959**, *2*, 84–85.

[113] Chivian, J. S.; Case, W. E.; Eden, D. D.; *Appl. Phys. Lett.* **1979**, *35*, 124–125.

[114] Auzel, F. *C.R. Acad. Sci. Ser. B* **1966**, *262*, 1016–1019.

[115] Auzel, F. *C.R. Acad. Sci. Ser. B* **1966**, *263*, 819–821.

[116] Ovsyankin, V. V.; Feofilov, P. P. *Jetp. Lett.* **1966**, *4*, 317–318.

[117] Nakazawa, E.; Shionoya, S. *Phys. Rev. Lett.* **1970**, *25*, 1710–1712.

[118] Kleinman, D. A. *Phys. Rev.* **1962**, *128*, 1761–1775.

[119] Kaiser, W.; Garrett, C. G. B. *Phys. Rev. Lett.* **1961**, *7*, 229–231.

[120] Zou, X.; Izumitani, T. *J. Non-Cryst. Solids*, **1993**, *162*, 68–80.

[121] Rao, D. N.; Prasad, J.; Prasad, P. N. *Phys. Rev. B* **1983**, *28*, 20–23.

[122] Patra, A.; Friend, C. S.; Kapoor, R.; Prasad, P. N. *J. Phys. Chem. B* **2002**, *106*, 1909–1912.

[123] Salley, G. M.; Valiente, R.; Güdel, H. U. *J. Lumin.* **2001**, *94–95*, 305–309.

[124] Jacquier, B.; Linarès, C.; Mahiou, R.; Adam, J. L.; Dénoue, E.; Lucas, J. *J. Lumin.* **1994**, *60–61*, 175–178.

[125] Suyver, J. F.; Aebischer, A.; Biner, D.; Gerner, P.; Grimm, J.; Heer, S.; Krämer, K. W.; Reinhard, C.; Güdel, H. U. *Opt. Mater.* **2005**, *27*, 1111–1130.

[126] Gamelin, D. R.; Güdel, H. U. *Top. Curr. Chem.* **2001**, *214*, 1–56.

[127] Wittke, J. P.; Ladany, I.; Yocom, P. N.; *J. Appl. Phys.* **1972**, *43*, 595–600.

[128] Sommerdijk, J. L. *J. Lumin.* **1973**, *6*, 61–67.

[129] Sommerdijk, J. L. *J. Lumin.* **1973**, *8*, 126–130.

[130] Golding, P. S.; Jackson, S. D.; King, T. A.; Pollnau, M. *Phys. Rev. B* **2000**, *62*, 856–864.

[131] Vetrone, F.; Boyer, J.-C.; Capobianco, J. A.; Speghini, A.; Bettinelli, M. *Chem. Mater.* **2003**, *15*, 2737–2743.

[132] Vetrone, F.; Boyer, J.-C.; Capobianco, J. A.; Speghini, A.; Bettinelli, M. *J. Appl. Phys.* **2004**, *96*, 661–667.

[133] Vetrone, F.; Boyer, J. C.; Capobianco, J. A.; Speghini, A.; Bettinelli, M. *J. Phys. Chem. B* **2002**, *106*, 5622–5628.

[134] Vetrone, F.; Boyer, J. C.; Capobianco, J. A.; Speghini, A.; Bettinelli, M. *J. Phys. Chem. B* **2003**, *107*, 1107–1112.

[135] Suyver, J. F.; Grimm, J.; Krämer, K. W.; Güdel, H. U. *J. Lumin.* **2005**, *114*, 53–59.

[136] Sommerdijk, J. L. *J. Lumin.* **1971**, *4*, 441–449.

[137] Suyver, J. F.; Grimm, J.; van Veen, M. K.; Biner, D.; Krämer, K. W.; Güdel, H. U. *J. Lumin.* **2006**, *117*, 1–12.

[138] Song, H.; Sun, B.; Wang, T.; Lu, S.; Yang, L.; Chen, B.; Wang, X.; Kong, X. *Solid State Commun.* **2004**, *132*, 409–413.

[139] Miller, S. A.; Rast, H. E.; Caspers, H. H. *J. Chem. Phys.* **1970**, *52*, 4172–4179.

[140] Díaz-Torres, A.; De la Rosa-Cruz, E.; Salas, P.; Angeles-Chavez, C. *J. Phys. D: Appl. Phys.* **2004**, *37*, 2489–2495.

[141] Auzel, F. *Rare-Earth Spectroscopy,* World Scientific, Singapore, **1985**, p. 502.

[142] Cheung, H. C. in *Topics in Fluorescence Spectroscopy, Vol 2: Principles*, Lakowicz, J. R. (ed.), Plenum Press, New York, **1991**, Chapter 3, pp. 127–176.

[143] Förster, T. *Ann. Phys.* **1948**, *2*, 55–75.

[144] Förster, T. *Discuss. Faraday Soc.* **1959,** *27*, 7–17.

[145] Selvin, P. R. *Methods Enzymol.* **1995**, *246*, 300–334.

[146] Cantor, C. R.; Schimmel, P. R. *Biophysical Chemistry*, Freeman, San Francisco, California, **1980**, Vo. 2, pp. 448–455.

[147] Braslavsky, S. E. *Pure Appl. Chem.* **2007**, *79*, 293–465.

[148] Clegg, R. M. *Methods Enzymol.* **1992**, *211*, 353–388.

[149] Morrison, L. E. *Anal. Biochem.* **1988**, *174*, 101–120.

[150] Mathis, G. *Clin. Chem.* **1993**, *39*, 1953–1959.

[151] Xiao, M.; Selvin, P. R. *J. Am. Chem. Soc.* **2001**, *123*, 7067–7073.

[152] Demas, J. N.; Crosby, G. A. *J. Phys. Chem.* **1971**, *75*, 991–1024.

[153] Williams, A. T. R.; Winfield, S. A.; Miller, J. N. *Analyst* **1983**, *108*, 1067–1071.

[154] Eaton, D. F. *J. Photochem. Photobiol. B* **1988**, *2*, 523–531.

[155] Lemmetyinen, H.; Vuorimaa, E.; Jutila, A.; Mukkala, V.-M.; Takalo, H.; Kankare, J. *Luminescence* **2000**, *15*, 341–350.

[156] Stryer, L.; Thomas, D. D.; Meares, C. F. *Ann. Rev. Biophys. Bioeng.* **1982**, *11*, 203–222.

[157] Selvin, P. R. *IEEE J. Sel. Top. Quantum Electron.* **1996**, *2*, 1077–1087.

[158] Stryer, L. *Annu. Rev. Biochem.* **1978**, *47*, 819–846.

[159] Steinberg, I. Z. *Annu. Rev. Biochem.* **1971**, *40*, 83–114.

[160] Eisinger, J.; Dale, R. E. *J. Mol. Biol.* **1974**, *84*, 643–647.

[161] Wu, C.-W.; Stryer, L. *Proc. Natl. Acad. Sci. U.S.A.* **1972**, *69*, 1104–1108.

[162] Fung, B. K.-K.; Stryer, L. *Biochemistry* **1978**, *17*, 5241–5248.

[163] Dale, R. F.; Eisinger, J.; Blumberg, W. *Biophys. J.* **1979**, *26*, 161–193.

[164] Ivanov, V.; Mizuuchi, K. *Biophys. J.* **2009**, *97*, 922–929.

[165] Haas, E.; Katchalski-Katzir, E., Steinberg, I. Z. *Biochemistry* **1978**, *17*, 5064–5070.

[166] Matsumoto, S.; Hammes, G. G. *Biochemistry* **1975**, *14*, 214–224.

[167] Hillel, Z.; Wu, C. W. *Biochemistry* **1976**, *15*, 2105–2113.

[168] Wu, P. G.; Brand, L. *Biochemistry* **1992**, *31*, 7939–7947.

[169] Selvin, P. R.; Rana, T. M.; Hearst, J. E. *J. Am. Chem. Soc.* **1994**, *116*, 6029–6030.

[170] Selvin, P. R.; Hearst, J. E. *Proc. Natl. Acad. Sci. U.S.A.* **1994,** *91*, 10024–10028.

[171] Stenroos, K.; Hurskainen, P.; Eriksson, S.; Hemmilä, I.; Blomberg, K.; Lindqvist, C. *Cytokine* **1998**, *10*, 495–499.

[172] Wang, G.; Yuan, J.; Matsumoto, K.; Hu, Z. *Talanta* **2001**, *55*, 1119–1125.

[173] Kuningas, K.; Ukonaho, T.; Päkkilä, H.; Rantanen, T.; Rosenberg, J.; Lövgren, T.; Soukka, T. *Anal. Chem.* **2006**, *78*, 4690–4696.

[174] Zhang, P.; Rogelj, S.; Nguyen, K.; Wheeler, D. *J. Am. Chem. Soc.* **2006**, *128*, 12410–12411.

[175] Heyduk, T.; Heyduk, E. *Anal. Biochem.* **2001**, *289*, 60–67.

[176] Görller-Walrand, C.; Hendrickx, I.; Fluyt, L. *Chem. Phys. Lett.* **1990**, *170*, 223–230.

[177] Vereb, G.; Jares-Erijman, E.; Selvin, P. R.; Jovin, T. M. *Biophys. J.* **1998**, *74*, 2210–2222.

[178] Reifenberger, J. G.; Snyder, G. E.; Baym, G.; Selvin, P. R. *J. Phys. Chem. B* **2003**, *107*, 12862–12873.

[179] Ylikoski, A.; Elomaa, A.; Ollikka, P.; Hakala, H.; Mukkala, V.-M.; Hovinen, J.; Hemmilä, I. *Clin. Chem.* **2004**, *50*, 1943–1947.

[180] Clegg, R. M.; Murchie, A. I. H.; Zechel, A.; Carlberg, C.; Diekmann, S.; Lilley, D. M. J. *Biochemistry* **1992**, *31*, 4846–4856.

[181] Dalbey, R. E.; Weiel, J.; Yount, G. *Biochemistry* **1983**, *22*, 4696–4706.

[182] Liu, J.; Lu, Y. *J. Am. Chem. Soc.* **2002**, *124*, 15208–15216.

[183] Stryer, L.; Haugland, R. P. *Proc. Natl. Acad. Sci. U.S.A.* **1967**, *58*, 719–726.

[184] Kane, S. A.; Fleener, C. A.; Zhang, Y. S.; Davis, L. J.; Musselman, A. L.; Huang, P. S. *Anal. Biochem.* **2000**, *278*, 29–38.

[185] Baur, J. W.; Rubner, M. F.; Reynolds, J. R.; Kim, S. *Langmuir* **1999**, *15*, 6460–6469.

[186] Lowman, G. M.; Daoud, N.; Case, R. M.; Carson, P. J.; Buratto, S. K. *Nano Lett.* **2001**, *1*, 677–682.

[187] Caruso, F.; Donath, E.; Möhwald, H. *J. Phys. Chem. B* **1998**, *102*, 2011–2016.

[188] Latt, S. A.; Cheung, H. T.; Bluot, E. R. *J. Am. Chem. Soc.* **1965**, *87*, 995–1003.

[189] Kaschak, D. M.; Mallouk, T. E. *J. Am. Chem. Soc.* **1996**, *118*, 4222–4223.

[190] Kerimo, J.; Adams, D. M.; Barbara, P. F.; Kaschak, D. M.; Mallouk, T. E. *J. Phys. Chem. B* **1998**, *102*, 9451–9460.

[191] Bücher, H.; Drexhage, K. H.; Fleck, M.; Kuhn, H.; Möbius, D.; Schäfer, F. P.; Sondermann, J.; Sperling, W.; Tillmann, P.; Wiegand, *J. Mol. Cryst.* **1967**, *2*, 199–230.

[192] Kuhn, H.; Möbius, D. *Angew. Chem. Int. Ed.* **1971**, *10*, 620–637.

[193] Cardullo, R. A.; Agrawal, S.; Flores, C.; Zamecnik, P. C.; Wolf, D. E. *Proc. Natl. Acad. Sci. U.S.A.* **1988**, *85*, 8790–8794.

[194] Wahlroos, R.; Toivonen, J.; Tirri, M.; Hänninen, P. *J. Fluoresc.* **2006**, *16*, 379–386.

[195] Kokko, L.; Kokko, T.; Lövgren, T.; Soukka, T. *Anal. Chim. Acta* **2008**, *606*, 72–79.

[196] Tsuji, A.; Sato, Y.; Hirano, M.; Suga, T.; Koshimoto, H.; Taguchi, T.; Ohsuka, S. *Biophys. J.* **2001**, *81*, 501–515.

[197] Clegg, R. M.; Murchie, A. I. H.; Zechel, A.; Lilley, D. M. J. *Proc. Natl. Acad. Sci. U.S.A.* **1993**, *90*, 2994–2998.

[198] Cooper, J. P.; Hagerman, P. J. *Biochemistry.* **1990**, *29*, 9261–9268.

[199] Wu, P.; Brand, L. *Anal. Biochem.* **1994**, *218*, 1–13.

[200] Epe, B.; Steinhäuser, K. G.; Woolley, P. *Proc. Natl. Acad. Sci. U.S.A.* **1983**, *80*, 2579–2583.

[201] Steinhäuser, K. G.; Woolley, P.; Epe, B.; Dijk, J. *Eur. J. Biochem.* **1982**, *127*, 587–595.

[202] Epe, B.; Woolley, P.; Steinhäuser, K. G.; Littlechild, J. A. *Eur. J. Biochem.* **1982**, *129*, 211–219.

[203] Valeur, B. in *Springer Series on Fluorescence, Volume 3, Fluorecence Spectroscopy in Biology*, Series editor: O. S. Wolfbeis, Volume editors: M. Hof, R. Hutterer, V. Fidler, Springer, Germany, **2005**, Chapter 2, pp. 30–48.

[204] Tkachenko, N. V. and Lemmetyinen, H. in *Springer Serier on Fluorescence, Volume 5, Standardization and Quality Assurance in Fluorescence Measurements I*, Series editor: O. S. Wolfbeis, Volume editor: U. Resch-Genger, Springer–Verlag, Germany, **2008**, pp. 195–214.

[205] Laczko, G.; Gryczynski, I.; Gryczynski, Z; Wiczk, W.; Malak, H.; Lakowicz, J. R. *Rev. Sci. Instrum.* **1990**, *61*, 2331–2337.

[206] Kankare, J.; Hyppänen, I. *Lanthanide Luminescence: Photophysical, Analytical and Biological Aspects, Springer Series on Fluorescence, Vol. 7.* Hänninen, P. and Härmä, H. (eds); Springer Verlag, Berlin, **2011**, Chapter 10, pp. 279–312.

[207] Lakowicz, J. R. and Gryczynski, I. in *Topics in Fluorescence Spectroscopy, Volume 1, Techniques* Lakowicz, J. R. (ed.), Kluwer Academic / Plenum Publishers, New York, **1999**, Chapter 5, pp. 293–335.

[208] Lakowicz, J. R.; Laczko, G.; Cherek, H.; Gratton, E.; Limkeman, M. *Biophys. J.* **1984**, *46*, 463–477.

[209] Gratton, E.; Limkeman, M.; Lakowicz, J. R.; Maliwal, B.; Cherek, H.; Laczko, G. *Biophys. J.* **1984**, *46*, 479–486.

[210] Gamelin, D. R.; Güdel, H. U. *Top. Curr. Chem.* **2001**, 214, 1–56.

[211] Kankare, J.; Latva, M.; Takalo, H. *Eur. J. Solid State Inorg. Chem* **1991**, *28*, 183–186.

[212] Yi, G.; Lu, H.; Zhao, S.; Ge, Y.; Yang, W.; Chen, D.; Guo, L.-H. *Nano Lett.* **2004**, *4*, 2191–2196.

[213] Lucarini, V.; Saarinen, J. J.; Peiponen, K.-E.; Vartiainen, E. M. *Kramers–Kronig Reations in Optical Materials Research*; Springer–Verlag: Heidelberg, **2005**.

[214] Kropp, J. L.; Dawson, W. R. *J. Chem. Phys.* **1966**, *45*, 2419–2420.

[215] Haas, Y.; Stein, G. *Chem. Phys. Lett.* **1971**, *8*, 366–368.

[216] Berry, M. T.; May, P. S.; Xu, H. *J. Phys. Chem.* **1996**, *100*, 9216–9222.

[217] An, Y.; Schramm, G. E.; Berry, M. T. *J. Lumin.* **2002**, *97*, 7–12.

[218] Dexpert-Ghys, J.; Faucher, M.; Caro, P. *J. Solid State Chem.* **1984**, *54*, 179–192.

[219] Klug, H. P.; Alexander, L. E. *X-ray Powder Diffraction Procedures*, Wiley, New York, **1959**, p. 491.

[220] Tuilier, M. H.; Dexpert-Ghys, J.; Dexpert, H.; Lagarde, P. *J. Solid State Chem.* **1987**, *69*, 153–161.

[221] Kozhan, T. M.; Kuznetsova, V. V.; Sergeev, I. I.; Timofeev, Y. P.; Khomenko, V. S.; Chau, M. *J. Appl. Spectrosc.* **1994**, *61*, 500–504.

[222] Patra, A.; Friend, C. S.; Kapoor, R.; Prasad, P. N. *Appl. Phys. Lett.* **2003**, *83*, 284–286.

[223] Stouwdam, J. W.; van Veggel, F. C. J. M. *Nano Lett.* **2002**, *2*, 733–737.

[224] Zhang, Q.; Zhang, Q.-M. *Mater. Lett.* **2009**, *63*, 376–378.

[225] Tian, L. J.; Sun, Y. J.; Yu, Y.; Kong, X. G.; Zhang, H. *Chem. Phys. Lett.* **2008**, *452*, 188–192.

[226] Yi, G.-S.; Chow, G.-M. *Chem. Mater.* **2007**, *19*, 341–343.

[227] Mai, H.-X.; Zhang, Y.-W.; Sun, L.-D.; Yan, C.-H. *J. Phys. Chem. C* **2007**, *111*, 13721–13729.

[228] Wang, Y.; Tu, L.; Zhao, J.; Sun, Y.; Kong, X.; Zhang, H. *J. Phys.Chem. C* **2009**, *113*, 7164–7169.

[229] Xie, M.-Y.; Yu, L.; He, H.; Yu, X.-F. *J. Solid State Chem.* **2009**, *182*, 597–601.

[230] Auzel, F.; Baldacchini, G.; Laversenne, L.; Boulon, G. *Opt. Mater.* **2003**, *24*, 103–109.

[231] Song, H.; Wang, J.; Chen, B.; Peng, H.; Lu, S. *Chem. Phys. Lett.* **2003**, *376*, 1–5.

[232] Sudarsan, V.; van Veggel, F. C. J. M.; Herring, R. A.; Raudsepp, M. *J. Mater. Chem.* **2005**, *15*, 1332–1342.

[233] Liang, X.; Wang, X.; Zhuang, J.; Peng, Q.; Li, Y. *Adv. Funct. Mater.* **2007**, *17*, 2757–2765.

[234] Kuningas, K.; Päkkilä, H.; Ukonaho, T.; Rantanen, T.; Lövgren, T.; Soukka, T. *Clin. Chem.* **2007**, *53*, 145–146.

[235] Zarling, D. A.; Rossi, M. J.; Peppers, N. A.; Kane, J.; Faris, G. W.; Dyer, M. J. *WO* 94/07142 A1, **1994**.

[236] Chen, Z.; Chen, H.; Hu, H.; Yu, M.; Li, F.; Zhang, Q.; Zhou, Z.; Yi, T.; Huang, C. *J. Am. Chem. Soc.* **2008**, *130*, 3023–3029.

[237] Rantanen, T.; Järvenpää, M.-L.; Vuojola, J.; Kuningas, K.; Soukka, T. *Angew. Chem. Int. Ed.* **2008**, *47*, 3811–3813.

[238] Kumar, M.; Zhang, P. *Langmuir* **2009**, *25*, 6024–6027.

[239] Wang, M.; Hou, W.; Mi, C.-C.; Wang, W.-X.; Xu, Z.-R.; Teng, H.-H.; Mao, C.-B.; Xu, S.-K. *Anal. Chem.* **2009**, *81*, 8783–8789.

[240] Rantanen, T.; Järvenpää, M.-L.; Vuojola, J.; Arppe, R.; Kuningas, K.; Soukka, T. *Analyst* **2009**, *134*, 1713–1716.

[241] Bogdan, N.; Vetrone, F.; Roy, R.; Capobianco, J. A. *J. Mater. Chem.* **2010**, *20*, 7543–7550.

[242] Sun, L. D.; Gu, J. Q.; Zhang, S. Z.; Zhang, Y. W.; Yan, G. H. *Sci. China Ser. B Chem.* **2009**, *52*, 1590–1595.

[243] Bednarkiewicz, A.; Nyk, M.; Samoc, M.; Strek, W. *J. Phys. Chem. C* **2010**, *114*, 17535–17541.

[244] Brismar, H.; Trepte, O.; Ulfhake, B. *J. Histochem. Cytochem.* **1995**, *43*, 699–707.

[245] Hyppänen, I.; Hölsä, J.; Kankare, J.; Lastusaari, M.; Pihlgren, L.; Soukka, T. *Terra* Rarae **2009**, *16*, 1–6.

[246] Lin, C.; Berry, M. T.; Anderson, R.; Smith, S.; May, P. S. *Chem. Mater.* **2009**, *21*, 3406–3413.